Chapter 8

Bulk shell isotope analyses

Information about past climatic conditions can be obtained through proxies, which are geochemical or physical signals recorded in biological or geological structures that reflect an environmental signal (Dodd & Stanton, 1990; Gillikin, 2005; Brand et al., 2011). Properties of these biological or geological structures are dependent on the environment in which they were formed. Here I use stable isotope data from bivalve shells as a proxy to reconstruct the palaeoenvironmental conditions and the palaeoclimatic evolution during the Early Pleistocene in the Arda River section.

8.1 State of the art

The geochemical and isotope analyses of fossil shells have proven to be a very useful tool for the reconstruction of past climates since the milestones of the studies of Urey et al. (1951), Lowenstam (1954a,b) and Chave (1954), based on the assumption that these organisms fractionate stable isotopes in equilibrium with the seawater in which they live. In fact, aside from the environment, the physical chemistry and eventually diagenesis, physiology is the other factor that exerts a major control over the mode of how environmental changes are recorded in the shell (Dodd & Schopf, 1972; Dodd & Stanton, 1990). An important aspect of physiology is the so-called vital effect (e.g. Urey et al., 1951; Grossman, 1987), which refers to processes that modify the chemical composition of the carbonate-secreting fluid, and thus, the biogenic hard tissues, which are consequently not formed in isotopic equilibrium. Two main processes seem to be the causes of nonequilibrium precipitation (Grossman, 1984, 1987; McConnaughey, 1989a,b): 1) a kinetic effect, related to rapid calcification and thus lack

of time to attain equilibrium, and 2) a metabolic effect related to changes in dissolved inorganic carbon produced by respiration or photosynthesis.

Not all the fossil groups precipitate their skeletons in isotopic equilibrium, and corals and echinoderms represent an example of that (Dodd & Stanton, 1990 and references therein). It is thus important before interpreting past climate and environmental conditions preserved in the fossil record, to verify if these organisms precipitate their skeletons in isotopic equilibrium, if possible through a comparison with phylogenetically related recent specimens.

Bivalves, as brachiopods and foraminifera, are among the best tools for palaeoclimatic and palaeoenvironmental reconstructions because they precipitate their shells in isotopic equilibrium with the seawater in which they live (at least for oxygen isotopes, see discussion below), exerting no vital effect on isotopic fractionation during the biomineralization, as demonstrated by several studies on fossil and recent faunas (e.g. Epstein et al., 1953; Grossman & Ku, 1986; Lécuyer et al., 2004; Schone et al., 2005a; Johnson et al., 2009; Ivany & Runnegar, 2010; Brand et al., 2011).

For those taxa that are known to lack a vital effect, in this case bivalves, and are deemed to be pristine (see Chapter 7 for the screening tests to exclude diagenetic alteration), environmental data can be extracted both from bivalve geochemistry (stable isotopes and elemental composition) and from sclerochronological studies based on growth lines (see Chapter 9 for a detailed treatment of sclerochronology).

Several studies have confirmed that carbonate secretion in the three genera here selected for geochemical analyses is not influenced by vital effects: *Glycymeris* (Brocas et al., 2013; Royer et al., 2013; Bušelić et al., 2015), *Aequipecten* (Hickson et al., 1999, 2000) and *Arctica* (e.g. Schöne, 2013).

8.2 Stable oxygen isotopes

The stable oxygen isotope ratio in well preserved biogenic carbonates is one of the most used and studied indicators of palaeotemperature. McCrea (1950), Epstein et al. (1953) and Emiliani (1966), were the first to show that during calcium carbonate secretion of biogenic carbonates, an isotopic fractionation (i.e. the physico-chemical phenomenon that causes changes in the relative abundance of isotopes because of their mass differences) occurs between ^{18}O and ^{16}O.

Variation of the isotopic ratio $^{18}O/^{16}O$ are reported in per mil (‰) deviations relative to a standard [Vienna-SMOW (Standard Mean Ocean Water) for water, Vienna-PDB (Pee-Dee Belemnite) for carbonates)], following this formula:

$$\delta^{18}O = \frac{^{18}O/^{16}O_{sample} - {}^{18}O/^{16}O_{standard}}{^{18}O/^{16}O_{standard}} \; x\,1000$$

$\delta^{18}O > 0$, sample enriched in heavy (^{18}O) isotopes relative to the standard
$\delta^{18}O < 0$, sample enriched in light (^{16}O) isotopes relative to the standard
V-SMOW and V-PDB are virtually identical to the SMOW and PDB standards.

The oxygen isotopic composition in carbonate shells has been shown to be a function of the temperature during carbonate deposition and of the isotopic compositions of the seawater ($\delta^{18}O_{sw}$) from which it precipitates (Epstein et al., 1953). In turn, $\delta^{18}O_{sw}$ covaries with salinity (Epstein et al., 1953), changes through time with fluctuations in global ice sheet volume (Shackleton & Opdyke, 1973) and change in the balance of hydrothermal circulation at mid-ocean ridges with continental weathering (Veizer et al., 1999). As bivalves have been proved to precipitate their shells in oxygen isotopic equilibrium with the surrounding seawater, the oxygen isotopic signatures of bivalve shells is a very powerful tool for the reconstruction of palaeotemperature, salinity and ice sheet volume variation.
In interpreting the oxygen isotopic data from bivalve shells I have mainly considered these factors affecting $\delta^{18}O_{sw}$ and thus $\delta^{18}O_{shell}$:

- Temperature (T) dependent fractionation. The fractionation is such that ^{18}O tends to concentrate in the carbonate relative to the water in which it forms. As temperature increases, there is less isotopic fractionation; this means that carbonates more readily incorporate ^{18}O at lower temperatures (McCrea, 1950). $\delta^{18}O_{carbonate}$ values are thus inversely related to temperature: higher $\delta^{18}O_{carbonate}$ values correspond to a decrease in temperature (cooling), whereas lower $\delta^{18}O_{carbonate}$ values correspond to an increase in temperature (warming).
- Ice sheets volume variation (ISVV); ice sheets mainly contain the light isotope ^{16}O; as $H_2{}^{16}O$ has a higher vapor pressure than $H_2{}^{18}O$, it tends to evaporate from the surface of the ocean more easily than $H_2{}^{18}O$, precipitating then as rain and snow depleted in heavy isotopes; during cold time intervals, the $H_2{}^{16}O$ is precipitated on polar ice sheets, isolating the isotopically lighter water from the ocean basins; as a consequence of this the ocean seawater is therefore enriched in ^{18}O. More positive $\delta^{18}O_{sw}$ values correspond to an increase in ice sheets volume, whereas more negative values correspond to a decrease in ice sheets volume (this is not valid in an ice-free world).
- Salinity (S); evaporation and dilution may cause local effect due to enrichment or depletion in ^{18}O in coastal area or isolated basins; evaporation led to an increase of salinity and cause a depletion in the lighter isotopes (^{16}O) in favor of the heavier one (^{18}O). An increase in $\delta^{18}O_{sw}$ corresponds thus to an increase in salinity, whereas a decrease corresponds to a decrease in

salinity (as fresh water is enriched in the light isotope ^{16}O). A marine basin which is inundated by freshwater from the continent will have seawater with more negative $\delta^{18}O_{sw}$ values.

As at least two factors (S, ISVV) affect the $\delta^{18}O_{sw}$, and as $\delta^{18}O_{carbonate}$ depends on $\delta^{18}O_{sw}$ and on the temperature at which fractionation takes place, the interpretation of the stable oxygen signal recorded in the shells has to take into account all these parameters which can act singularly, but usually operate jointly. This makes the palaeoenvironmental interpretation not an easy task.

8.2.1 Palaeotemperature equations

As it has been shown that the oxygen isotopic composition in carbonate shells is a function of temperature dependent fractionation, empirical palaeotemperature equations were developed, which were determined by sampling bivalves grown under different temperatures with known $\delta^{18}O_{sw}$ (Gillikin, 2005 and reference therein).

Bivalves are known to precipitate the two polymorphs of calcium carbonate, calcite or aragonite (or both) (Gillikin, 2005); for this reason two different palaeotemperature equations have been calculated, one for calcitic shells and one for aragonitic ones.

Calcite was shown to be depleted in ^{18}O relative to aragonite by 0.5‰ to 0.8‰ (e.g. Tarutani et al., 1969; Böhm et al., 2000). On the other hand, other studies suggest that calcite is ^{18}O-enriched with respect to aragonite from a few tenths of permil up to 4.5‰ (e.g. Epstein et al., 1953; Zhou & Zheng, 2003). Lécuyer et al. (2004) observed that, analyzing calcitic and aragonitic layers from the same bivalve shell, there is no evidence that oxygen isotope fractionation between aragonite and water differs from that between calcite and water. As there is no consensus about the direction and magnitude of the oxygen isotope fractionation between calcite and aragonite, here I prefer to use the two different equations when determining the palaeotemperature in calcitic (*Aequipecten*) or aragonitic shells (*Glycymeris* and *Arctica*).

For the reconstruction of temperatures from $\delta^{18}O$ of aragonitic shells, the palaeotemperature equation of Grossman & Ku (1986) is widely used. However, a small modification of their equation is required because they report $\delta^{18}O_{sw}$ values in SMOW – 0.27 ‰ (see Dettman et al., 1999):

$$T_{\delta^{18}O}\,(°C) = 20.60 - 4.34\,[\,\delta^{18}O_{aragonite} - (\delta^{18}O_{sw} - 0.27)\,]$$

where $\delta^{18}O_{aragonite}$ is measured relative to the V-PDB scale and $\delta^{18}O_{sw}$ is relative to the V-SMOW scale. Thus, assuming no change in the $\delta^{18}O_{sw}$, a shift in $\delta^{18}O_{aragonite}$ by 1‰ reflects a temperature change of 4.34 °C.

This equation has been used here to obtain palaeotemperatures from oxygen data from both *Arctica* and *Glycymeris* shells, as they are both composed of aragonite; previous studies support the use of this equation in these two genera (e.g. Schöne, 2013; Bušelić et al., 2015).
The equation of O'Neil et al. (1969) was used in previous works on *A. opercularis* calcitic shells (Hickson et al., 1999, 2000; Johnson et al., 2009) with a 0.26‰ subtracted from the water composition ($\delta^{18}O_{sw}$; measured versus V-SMOW) to compare with V-PDB (Coplen et al., 1983):

$$T\ _{\delta^{18}O}\ (°C) = 16.90 - 4.38\ (\delta^{18}O_{calcite} - \delta^{18}O_{sw}) + 0.10\ (\delta^{18}O_{calcite} - \delta^{18}O_{sw})^2$$

where $\delta^{18}O_{calcite}$ is measured relative to the V-PDB scale and $\delta^{18}O_{sw}$ is relative to the V-SMOW scale; a shift in $\delta^{18}O_{calcite}$ by 1‰ reflects a temperature change of the ambient seawater of ~4 °C.
In both the equation for aragonite shells and that for calcite shells, the $\delta^{18}O_{sw}$ must be assumed, as there are no $\delta^{18}O_{sw}$ data available for the Early Pleistocene of the Mediterranean area; also this was a time interval characterized by frequent climate oscillations and change in ice volumes (Ghinassi et al., 2004; Clark et al., 2006). $\delta^{18}O_{sw}$ values have been thus assumed in each stratigraphic level according to the correlation to the Marine Isotope Stages (MIS) explained below.

8.3 Stable carbon isotopes

During formation of biogenic carbonates, an isotopic fractionation occurs also between ^{13}C and ^{12}C. The variation of the isotopic ratio between $^{13}C/^{12}C$ is reported in per mil (‰) deviations relative to a standard (Vienna Pee-Dee Belemnite in carbonates), following this formula:

$$\delta^{13}C = \frac{^{13}C/^{12}C_{sample} - {}^{13}C/^{12}C_{standard}}{^{13}C/^{12}C_{standard}}\ x\ 1000$$

$\delta^{13}C > 0$, sample enriched in heavy (^{13}C) isotopes relative to the standard
$\delta^{13}C < 0$, sample enriched in light (^{12}C) isotopes relative to the standard

However, unlike the oxygen isotope ratio, the stable carbon isotope ratio in bivalve shells ($\delta^{13}C_{shell}$) represents an enigmatic geochemical archive whose interpretation is often complicated by variable and unpredictable vital effects which can influence the mix of metabolic and dissolved inorganic carbon (DIC) in the shell material (Butler et al., 2011).
Early works suggested that carbon in skeletal carbonates originates directly from dissolved inorganic carbon (DIC) in seawater (e.g. Mook & Vogel, 1968; Killingley & Berger, 1979). However, many

recently researches found that bivalves do not deposit in isotopic equilibrium with DIC and suggested that both kinetic and metabolic effects may play important roles (e.g. Tanaka et al., 1986; McConnaughey et al., 1997; Dettman et al., 1999; Lorrain et al., 2004; Gillikin et al., 2007).

Kinetic effects generally affect both $\delta^{18}O_{shell}$ and $\delta^{13}C_{shell}$ but, as bivalves generally precipitate in oxygen isotope equilibrium with the seawater, kinetic effects should be minimal and thus the disequilibrium should be mainly due to metabolic effects (Butler et al., 2011).

Metabolic effects are due to the introduction of ^{13}C-depleted respired carbon into the internal DIC pool of the bivalve. Tanaka et al. (1986) first suggested that up to 85% of the carbon in bivalve shells was metabolic in origin, but McConnaughey et al. (1997) have moderated this idea, suggesting that in aquatic invertebrates, the amount of metabolic C (respired CO_2) in the shell is typically less than 10%, although higher values have been found (5%–37%; Gillikin et al., 2009).

In marine mollusks, metabolic effects are thought to be the cause of ontogenetically decreasing in $\delta^{13}C_{shell}$ (Butler et al., 2011). Lorrain et al. (2004) suggest that the decrease of $\delta^{13}C_{shell}$ through ontogeny is actually caused by increasing utilization of metabolic C (respiratory CO_2, ^{13}C-depleted) to satisfy carbon requirements for calcification. The model of Lorrain et al. (2004) is based on the relationship between metabolic rate and body size: as bivalves grow and become older, their metabolism increases while shell growth slows; therefore, more metabolic CO_2 will be available, while the amount needed for shell growth is reduced, resulting in more metabolic carbon being incorporated into the shell. However, this is apparently species-specific: in fact although in some species a strong ontogenetic decrease in $\delta^{13}C_{shell}$ has been noted (e.g. Krantz et al., 1987; Keller et al., 2002; Lorrain et al., 2004), in others there is no discernable decrease (e.g. Gillikin et al., 2005).

More recently, Schöne et al. (2011a) and Butler et al. (2011) found that long-lived bivalves, as *Arctica islandica*, probably form their shells with a constant offset from expected equilibrium for $\delta^{13}C$; so, if the proportion of metabolic carbon can be determined and if it can be shown to remain stable during the mature lifetime of the animal, then the extent of disequilibrium can be accounted for and a systematic association can potentially be established between $\delta^{13}C_{shell}$ and $\delta^{13}C_{DIC}$.

Although metabolic carbon can make more complicate the $\delta^{13}C_{shell}$ data interpretation, $\delta^{13}C_{shell}$ is still a useful indicator of environmental conditions. If the metabolic effect can be determined, $\delta^{13}C$ from bivalve shells can be used as a proxy to investigate the $\delta^{13}C_{DIC}$ in ancient water, to obtain information about primary production, atmospheric CO_2 levels, salinity, anthropogenic carbon inputs, respiration, photosynthesis and carbonate dissolution/precipitation (e.g. Dettman et al., 1999; McConnaughey & Gillikin, 2008; Gillikin et al., 2009).

In particular, for the subsequent discussion of isotopic and sclerochemical results, I have considered mainly these factors affecting $\delta^{13}C_{DIC}$ and thus $\delta^{13}C_{shell}$:

- Primary productivity (PP); primary producers fractionate towards ^{12}C, and thus absorb large amounts of lighter isotopes (^{12}C) from the oceans during photosynthesis; this results in seawater being depleted in ^{12}C and enriched in ^{13}C. ^{12}C is then released in the ocean during the decomposition of the organic matter. In particular an increase in primary productivity causes a positive fluctuation in $\delta^{13}C_{DIC}$ and thus in $\delta^{13}C_{shell.}$
- Salinity (S); freshwater input is enriched in ^{12}C; therefore, a drop in salinity caused by freshwater from the continent will cause a decrease in $\delta^{13}C_{DIC}$ (Gillikin, 2005). Gillikin et al. (2006) found that $\delta^{13}C_{shell}$ of *Mytilus edulis* shifted to lower value when it was transplanted from marine into estuarine conditions, reflecting freshwater inputs to the ocean. It thus provides a proxy for salinity.

These topics are very interesting for the palaeoenvironmental and palaeoclimatic interpretation, however I want to stress that the calibration and interpretation of $\delta^{13}C_{shell}$ has to be approach with considerable caution (Butler et al., 2011), as metabolic effects may affect the $\delta^{13}C_{shell.}$

8.4 Material and methods

Species belonging to *Glycymeris, Aequipecten* and *Arctica* represent the most abundant and continuously occurring along the Arda succession; for these reasons they were selected and used for isotopic analyses. The use of seven species belonging to three genera allow to constrain and minimize the species-specific effect.

Two bivalve shells belonging to two different species of the three genera indicated above were selected, when present, from each fossiliferous bed. In total, 249 fossil specimens from 141 beds of the Arda section belonging to *Glycymeris glycymeris*, *Glycymeris insubrica*, *Glycymeris inflata*, *Glycymeris* sp., *Aequipecten opercularis*, *Aequipecten scabrella* and *Arctica islandica* have been selected and analyzed for stable carbon and oxygen isotopes. One valve of each specimen was cleaned, then longitudinally cut and half of the valve was crushed using a marble vase in order to obtain a fine powder.

Analysis of the powder samples for oxygen and carbon isotope ratios ($^{18}O/^{16}O$ and $^{13}C/^{12}C$) was undertaken using a GV IsoPrime dual inlet mass spectrometer plus Multiprep device at the NERC (Natural Environment Research Council) Laboratory of the British Geological Survey, Keyworth, UK under the supervision of Prof. M. Leng. Once placed in sample vials, the powder for each sample was dissolved in phosphoric acid (H_3PO_4) and vaporized. Isotope values ($\delta^{13}C$, $\delta^{18}O$) are reported as per

mil (‰) deviations of the isotopic ratios ($^{18}O/^{16}O$, $^{13}C/^{12}C$) calculated to the V-PDB scale using a within-run laboratory standard (KMC) calibrated against the international NBS standards (NBS18 and 19). Analytical reproducibility for these analyses was better than 0.1‰ for $\delta^{13}C$ and $\delta^{18}O$.
Shells which did not pass the preservation tests (nine shells belonging to *A. opercularis* and *A. scabrella;* see Chapter 7) were removed and not included in the results.

8.5 Results

8.5.1 Oxygen isotopes

Fig. 8.1 shows the results of the bulk shell oxygen isotope analysis performed on species of the genus *Glycymeris, Aequipecten* and *Arctica* from each stratigraphic bed of the Arda River succession. As these taxa are not always simultaneously present in each sampled bed, an additional oxygen curve has been produced using the average oxygen values (Fig. 8.1, $\delta^{18}O$ mean values curve). This curve has been calculated considering the different life habits of the three taxa: *Glycymeris* species live in shallow water, *A. islandica* is at greater depths and *Aequipecten* species usually live in intermediate water depths (see Chapter 3 for a detailed discussion of their palaeoecology). The differences existing between the oxygen isotopic values of *Aequipecten* and *Glycymeris*, *Arctica* and *Aequipecten* and, *Arctica* and *Glycymeris* respectively, have been calculated for each bed in which they occur together, in order to obtain three average values of their differences (Table 8.1). These difference average values were then added or subtracted to the oxygen isotope datum of each shells in each bed, taking into account the different living depths of the three genera. As an example, the difference average value between *Aequipecten* and *Glycymeris* is 0.65‰ and that between *Arctica* and *Aequipecten* is 1.56‰; in a bed in which only one *Aequipecten* shell occurs, 1.56‰ should be added to its oxygen isotope value to obtain the corresponding value for *Arctica* and 0.65‰ should be subtracted to obtain the corresponding value for *Glycymeris*. In each sampled bed I will thus have three values, one representing the original datum, obtained from the shell occurring in that bed, and two newly derived values corresponding to the other two taxa not present in the same bed. The average value of these three values (one original, the others derived based on the method described above) has then been calculated and plotted on the stratigraphic log to obtain the mean oxygen curve. This method, although complex, allows to minimize the effect of the different life habits of the analyzed taxa and also to have a more continuous oxygen isotope record along the overall section, also even in beds in which these genera do not occur together.

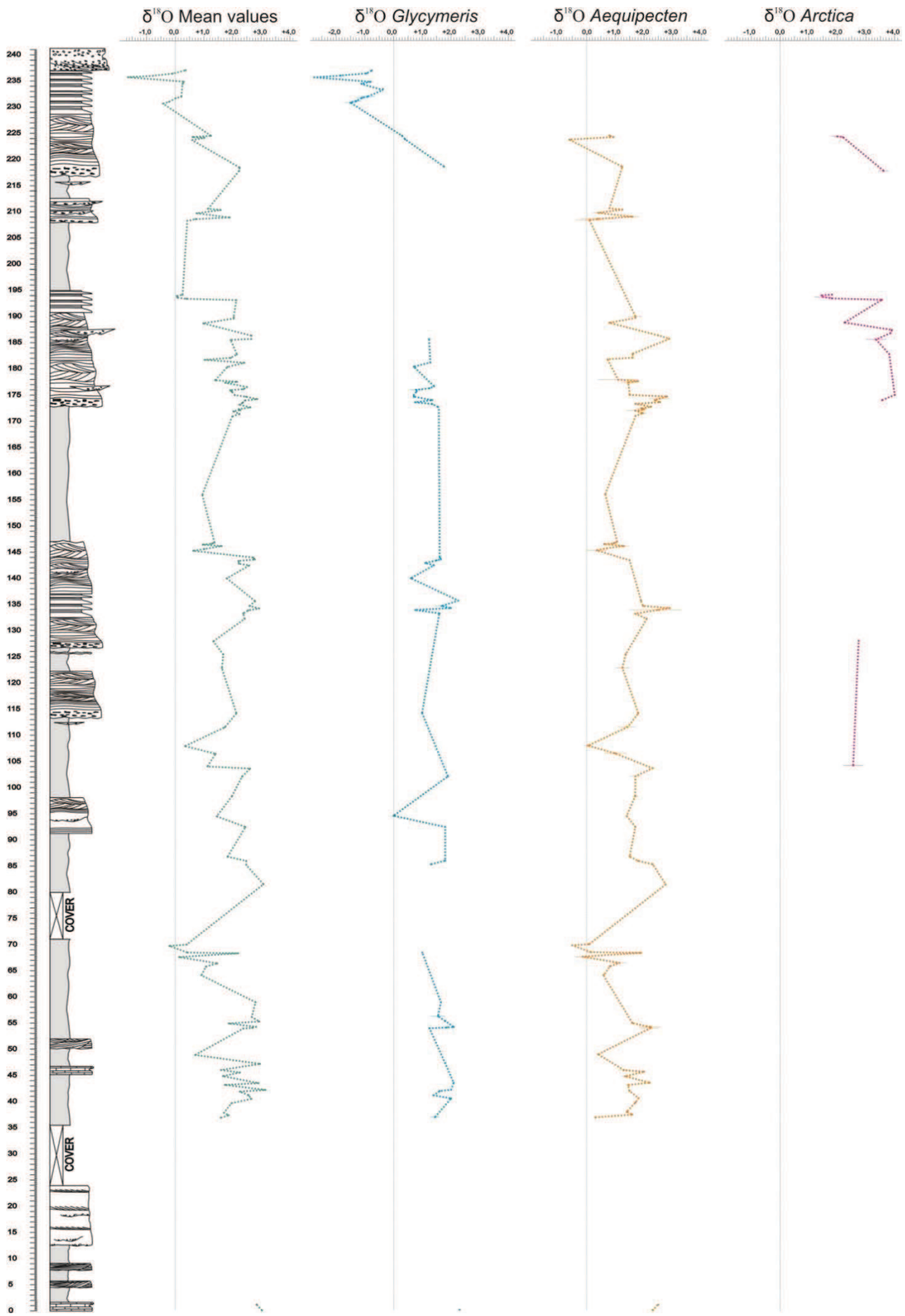

Fig. 8.1. Results of the bulk shell oxygen isotope analysis performed on species of the genus *Glycymeris, Aequipecten* and *Arctica* in each bed of the Arda River succession. The mean values curve has been obtained using average oxygen values.

	Diff.
Aequipecten-Glycymeris	0.65 ‰
Arctica-Aequipecten	1.56 ‰
Arctica-Glycymeris	2.71 ‰

Table 8.1. Average values of the difference of the oxygen isotope values between *Aequipecten* and *Glycymeris, Arctica* and *Aequipecten* and, *Arctica* and *Glycymeris*.

As it is not possible to know for each single stratigraphic bed the exact value of $\delta^{18}O_{sw}$, the maximum (T_{max}), minimum (T_{min}) and average (T_{av}) palaeotemperatures, based on $\delta^{18}O_{shell}$ from each taxon, have been calculated assuming two different values for $\delta^{18}O_{sw}$: +0‰, which is similar to average modern seawater and represents modern glacial-type conditions, and +1‰, which is the $\delta^{18}O_{sw}$ assumed for the last glacial maximum (Schrag et al., 2002).

The following observations have been deduced from bulk shell oxygen isotope analysis:

1) *Glycymeris.* The oxygen curve shows rather irregular low amplitude oscillations of $\delta^{18}O$ values from +0.07‰ to +2.30‰, except in the upper part of the section where $\delta^{18}O$ values are more negative (reaching -2.77‰), suggesting a warming trend in the upper seven metres. Here are the corresponding palaeotemperatures for the minimum, maximum and average values recorded:

V-SMOW	$\delta^{18}O_{max}$	T_{min}	$\delta^{18}O_{min}$	T_{max}	$\delta^{18}O_{av}$	T_{av}
+0‰	+2.30‰	9.4 °C	-2.77‰	31.4 °C	+0.70‰	16.4 °C
+1‰	+2.30‰	13.8 °C	-2.77‰	35.8 °C	+0.70‰	20.7 °C

2) *Aequipecten.* Also *Aequipecten* oxygen curve shows small oscillations of $\delta^{18}O$ value and a slightly warming trend in the upper part of the section. Here are the corresponding palaeotemperatures for the minimum, maximum and average values recorded:

V-SMOW	$\delta^{18}O_{max}$	T_{max}	$\delta^{18}O_{min}$	T_{min}	$\delta^{18}O_{av}$	T_{av}
+0‰	+2.87‰	4.2 °C	-0.62‰	18.5 °C	+1.40‰	9.9 °C
+1‰	+2.87‰	8.0 °C	-0.62‰	23.0 °C	+1.40‰	14.0 °C

3) *Arctica.* Notwithstanding the paucity of data relative to the other two genera the $\delta^{18}O$ curve does not show particular trend, keeping rather constant values. Here are the corresponding palaeotemperatures for the minimum, maximum and average values recorded:

V-SMOW	$\delta^{18}O_{max}$	T_{max}	$\delta^{18}O_{min}$	T_{min}	$\delta^{18}O_{av}$	T_{av}
+0‰	+4.03‰	2.0 °C	+1.48‰	13.0 °C	+2.71‰	7.6 °C
+1‰	+4.03‰	6.3 °C	+1.48‰	17.3 °C	+2.71‰	12.0 °C

4) Mean values curve. This curve represents the oxygen average values obtained from the three genera, as described above; the average $\delta^{18}O$ ($\delta^{18}O_{av}$) is 1.66‰. However, in this case, as *Glycymeris* and *Arctica* species have aragonitic shells, whereas *Aequipecten* species have calcitic ones, it has not been possible to calculate the corresponding palaeotemperatures due to the different temperature

palaeoequations used for aragonitic or calcitic shells. The oxygen isotope values remain in almost all the section above 0‰, except in the upper part where a warming trend is present reaching oxygen values as low as -1.80‰.

In the three separated curves it is clearly observable that species of *Glycymeris* have the lower average oxygen values (+0.70‰), followed by species of *Aequipecten* (+1.40‰) and by the higher average values of *Arctica islandica* (+2.71‰), which is the taxon living in deepest water.

8.5.1.1 Marine Isotope Stages correlation

The isotope data of the mean oxygen curve have been used to correlate the Arda River bulk shell oxygen values to the Atlantic Marine Isotope Stages (MIS) stack and to the Mediterranean stack using Analyseries 2.0 (Fig. 8.2). This analysis was performed by Dr. J. Hennissen from the British Geological Survey, Keyworth, UK. The three dates used to establish tie points used for the age model were obtained from nannoplankton biostratigraphy (see Chapter 4 for details).

Atlantic stack (LR04). The Atlantic stack is published by Lisiecki & Raymo (2005) and it is based on benthic foraminifera from 57 cores across a wide variety of latitudes (Fig. 8.2A).

Mediterranean stack correlation. The Mediterranean $\delta^{18}O$ data are taken from Lourens et al. (1996) and from Lourens (2004) as published in the supplementary information of Wang et al. (2010). This stack is based on $\delta^{18}O$ of planktic foraminifera in four Mediterranean boreholes (Fig. 8.2B).

Comparing these two stacks with the Arda bulk shell data, the best correlation seems to be with the Atlantic MIS curve rather than with the Mediterranean one.

8.5.2 Carbon isotopes

The carbon isotope curves obtained from carbon bulk shell analysis of species of *Glycymeris, Aequipecten* and *Arctica* show a similar trend (Fig. 8.3); carbon values remain rather constant in almost all the carbon curves, with an average value of +0.40‰ for *Glycymeris* shells, +0.30‰ for *Aequipecten* shells and +1.16‰ for *A. islandica* shells.

The *Glycymeris* curve, however, shows a trend towards lower values at the top of the section, reaching low carbon values of -1.00‰. In addition, the *Glycymeris* carbon curve has also the higher amplitude oscillations relative to the other two genera.

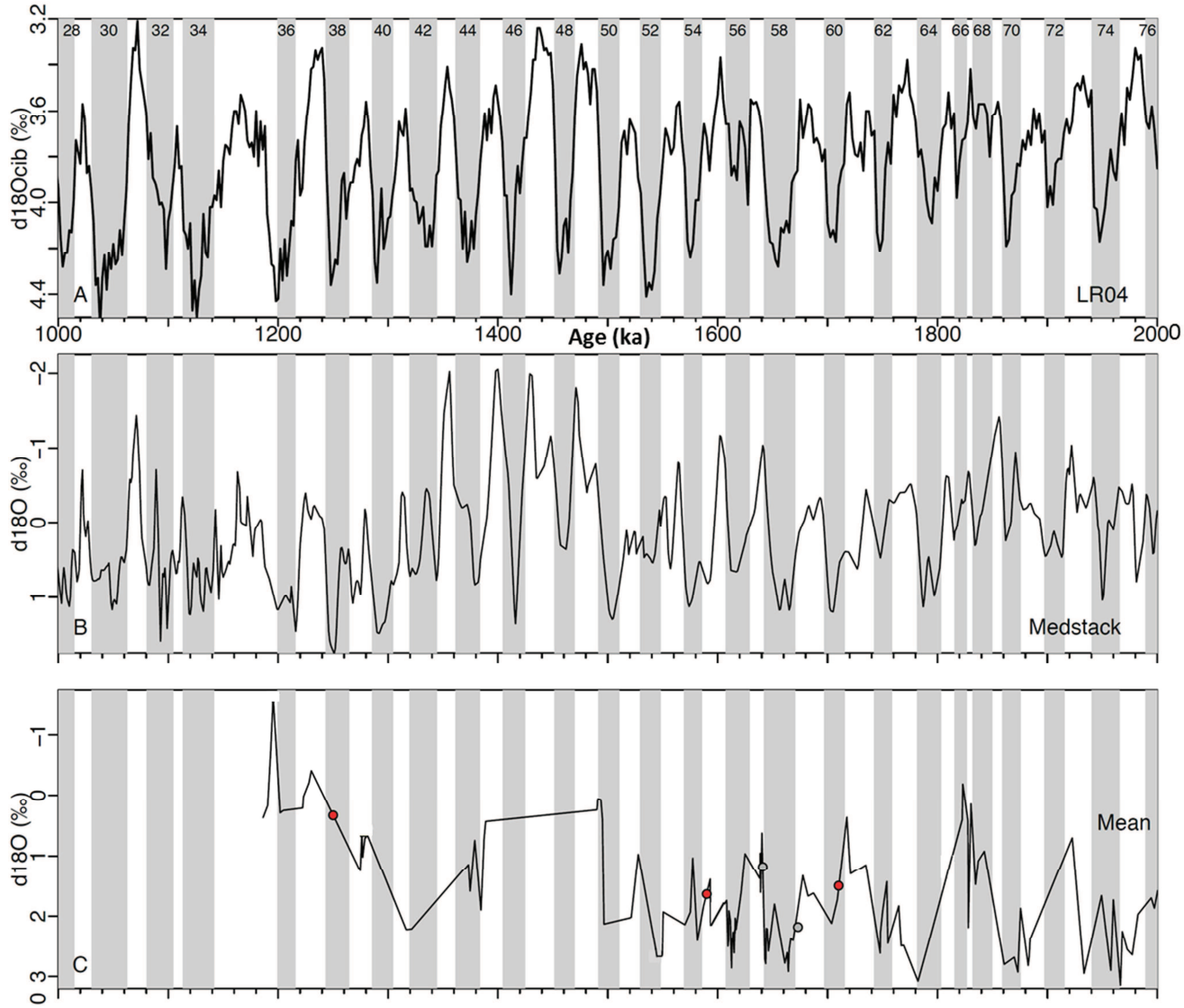

Fig. 8.2. Correlation of the Arda bulk shell mean oxygen curve (C) with the Atlantic MIS stack (A) and with the Mediterranean stack (B). Grey bands represent the cold stages; in red are the tie-points obtained from nannofossil biostratigraphy; in grey are added pointers.

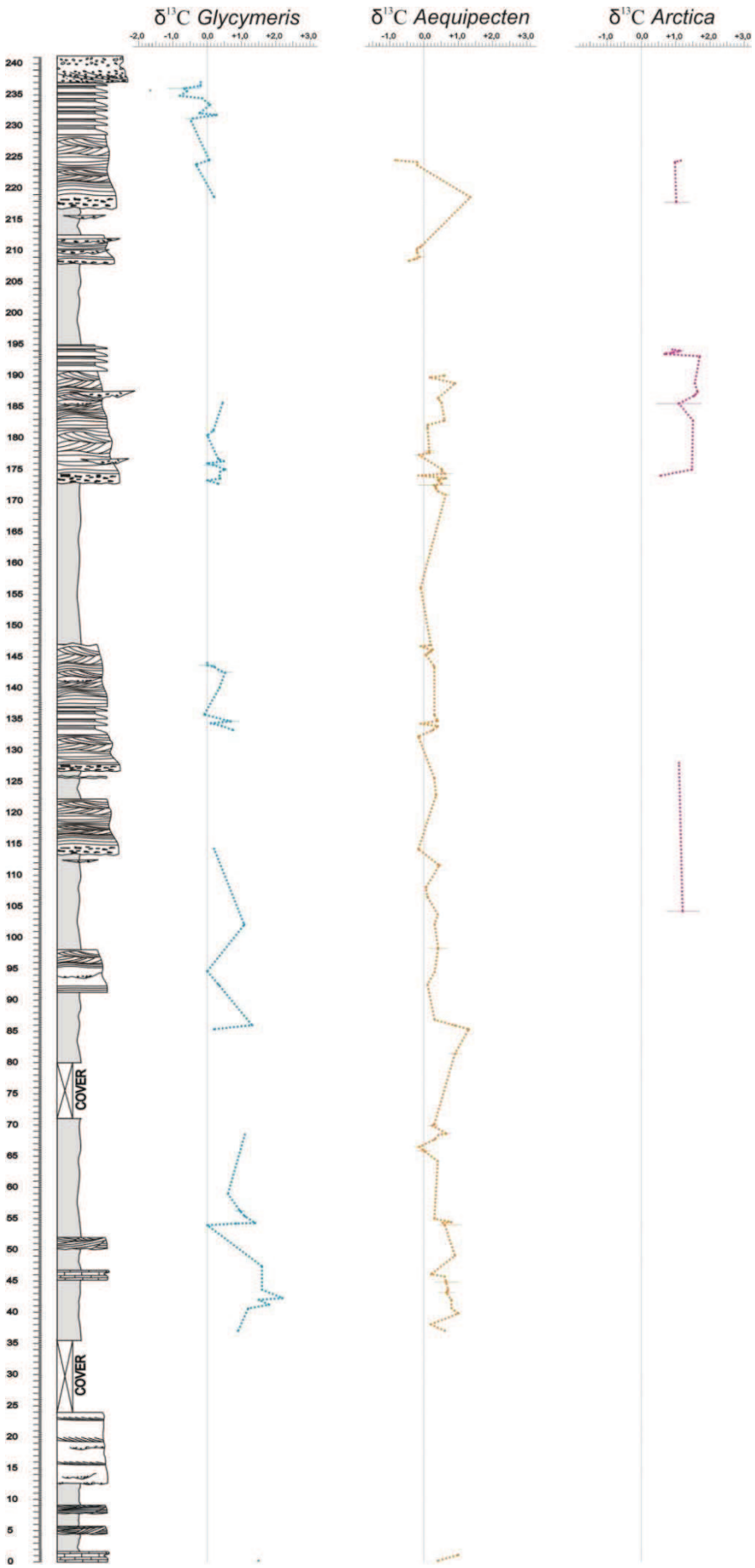

Fig. 8.3. Results of the bulk shell carbon isotope analysis performed on species of the genus *Glycymeris, Aequipecten* and *Arctica* in each bed of the Arda River succession.

8.6 Discussions

8.6.1 Oxygen isotopes

The bulk shell oxygen curves point out the presence of oscillations of variable amplitude not linked to facies variation; in fact several oscillations are also present within the same lithology. These oxygen variations are thus caused by $\delta^{18}O_{sw}$ changes and/or by temperature changes. In the tables above, I have reported the calculations assuming different $\delta^{18}O_{sw}$ values and these show that temperature change is the dominating factor in causing the recorded oscillations. The average temperature though remains rather constant along the overall succession, without showing any cooling in the seawater temperatures, as might be expected being close to the Middle Pleistocene Transition and the beginning of the continental glaciations; actually a slight warming trend is found. This warming at the top of the section is probably due to a shallowing in this part, but also to a major contribute of freshwater inputs (causing salinity variation) which act to lighten the oxygen isotope signal; in fact, the shells analyzed in the upper part of the section (from 230.80 m to the top) belong to *Glycymeris insubrica*, a species which tolerates salinity variations; sedimentological evidence in this part of the section also supports an increase in freshwater input. However, this trend to lower values is also seen in the *Aequipecten* oxygen curve; contrary to *Glycymeris*, species of *Aequipecten* are living in fully marine conditions, tolerating only very little changes in salinity (see Chapter 3). It could be that also *Aequipecten* shells record the change in salinity in the upper part of the section, but probably it was not so strong to prevent their survival; when salinity dilution became too high, they disappeared; in fact they are not present from 230.80 m to the top, where only specimens of *G. insubrica* are present and where freshwater inputs are higher. A combination of salinity decrease and a slight temperature increase due to shallowing is thus responsible for the observed trend, with salinity change being most important.

In the three separated oxygen curves it is clearly observable that species of *Glycymeris* have the lower average oxygen values (+0.70‰), follow by species of *Aequipecten* (+1.40‰) and by the higher average values of *Arctica islandica* (+2.71‰), which in terms of palaeotemperatures correspond to 16.4-20.0°C ($\delta^{18}O_{sw}$=0-1‰) for *Glycymeris*, 9.9-14.0°C ($\delta^{18}O_{sw}$=0-1‰) for *Aequipecten* and 7.6-12.0°C ($\delta^{18}O_{sw}$=0-1‰) for *Arctica*. These differences in oxygen isotope values and therefore in palaeotemperatures is explained with the different life habit depth of the species belonging to these genera. *Glycymeris* species being the shallower water taxa (see Chapter 3), record the highest palaeotemperatures and also the highest temperature variation (22.0°C); in fact major temperatures excursions are recorded in shallow water, where surface water temperatures are also affected by atmospheric variations, whereas they decrease in deep water. *Arctica islandica* represents the deeper

water taxon among the three and it shows the coldest palaeotemperatures and also the smallest temperature variation (11.0°C); *Aequipecten* species have intermediate palaeotemperatures and also record intermediate temperature excursions (14.6°C), thus confirming an intermediate living depth between *Glycymeris* and *Arctica*.

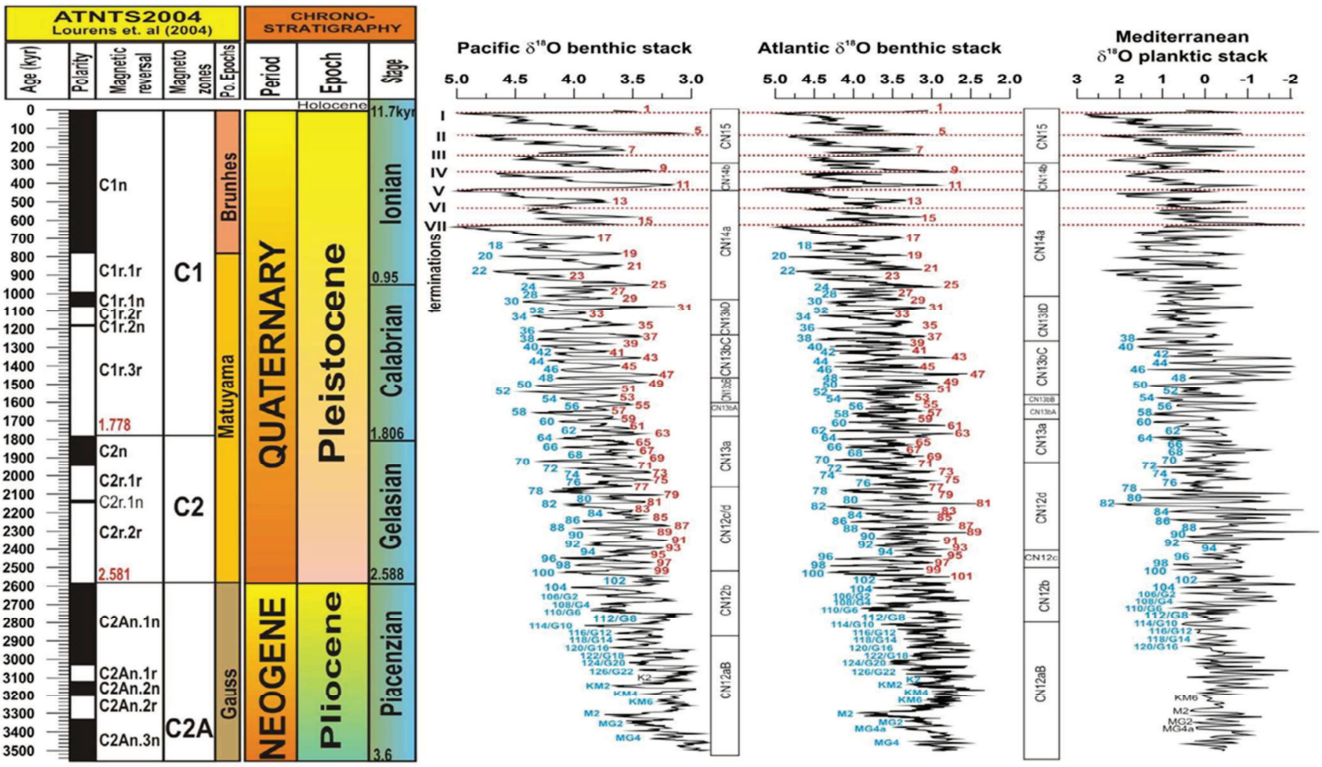

Fig. 8.4. Comparison of the Pacific, Atlantic and Mediterranean oxygen stacks (from Shackleton & Opdyke, 1976; Lisiecki & Raymo, 2005; Lourens, 2004)

It is interesting to note that comparing the different oxygen isotope stacks from foraminifera of the Pacific Ocean, the Atlantic Ocean and the Mediterranean Sea a cooling trend in seawater temperature from the Piacenzian to the end of the Calabrian is detectable in the first two stacks but not in the Mediterranean one (Fig. 8.4). In fact in the two oceanic stacks temperatures become colder toward the Middle Pleistocene Transition, reaching $\delta^{18}O$ values of +5‰. In the Mediterranean Sea, the temperature seems to be nearly constant and $\delta^{18}O$ is not so high as in the oceanic stacks, reaching a max of + 3‰. The oxygen isotope variation that I obtained from the analyses of bulk shell isotope data from the Arda specimens is in agreement with the trend recorded in the Mediterranean stack, as there is not an evident decrease in average seawater temperature during the Early Pleistocene. However, the pattern of cyclicity of the mean oxygen curve of the Arda shells better correlates with that of the Atlantic MIS stack, which is controlled by obliquity (Lisiecki & Raymo, 2005). It has to be taken into account that the bulk shell isotope record is discontinuous, due to the nature of the macrofossil preservation along the section; thus it is not possible to have a very good correlation between the

stacks and the curve from bulk shell data. However, the slightly better correlation between the Arda bulk shell mean curve and the Atlantic MIS stack may be due to the fact that both curves are based on benthic organisms, while the Mediterranean stack is based on planktic ones.

8.6.2 Carbon isotopes

The carbon isotope curves obtained from the shells of the species of *Glycymeris, Aequipecten* and *Arctica* show a similar trend (Fig. 8.3), with carbon values remaining rather constant in almost all the three curves. The *Glycymeris* curve, however, shows a lowering trend in $\delta^{13}C$ values towards the top of the section, reaching values of -1.00‰; this trend to low values can be explained as due to an increase in freshwater input due to a shallowing toward the top of the section, as described above. Freshwater is relatively depleted in ^{13}C (being enriched in ^{12}C derived from the decomposition of terrestrial plants) and therefore, a drop in salinity due to freshwater input will cause a decrease in $\delta^{13}C$ (Gillikin, 2005). *Glycymeris* shells from the upper part of the section (230.80 m-top) thus seem to record this dilution.
Also the shells of *Aequipecten* show lower $\delta^{13}C$ values toward the top of the succession, suggesting that also these specimens underwent the same salinity variation recorded by *Glycymeris* shells; however, in contrast to *Glycymeris* species, *Aequipecten* ones do not tolerate large salinity changes; in fact they disappear in the uppermost part of the section where only *G. insubrica* specimens are present (see previous paragraph for discussion on salinity influence on *Aequipecten* shells). The species of *Aequipecten* and *Glycymeris* lived above the thermocline, and thus they recorded a similar variation in nutrient input and salinity; in fact they have similar average values of carbon isotopes (+0.40‰ for *Glycymeris* shells, +0.30‰ for *Aequipecten* shells); *A. islandica* have, on the contrary, an higher carbon average value (+1.16‰). The different life habit depths account for the difference between the mean carbon values of *Glycymeris-Aequipecten* on one side and *Arctica islandica* on the other. *Arctica islandica* was living below the thermocline, thus it was not influenced by freshwater input; so a depletion in ^{13}C is not recorded in its carbon curve. The thermocline in the Northern Adriatic sea may be very shallow (15-30 m) (Artegiani et al., 1997), thus being consistent with the living depth of fossil *A. islandica*. Furthermore, according to Zavatarelli et al. (1998) during stratification periods (spring–summer) there is a strong nutrient increase in the bottom layers, as export organic matter sinks to the bottom; this situation is particularly evident on the western side of the Adriatic basin, the most affected by the river inputs, in agreement with the location of the Arda River marine succession. The highest mean carbon value observed in *A. islandica* may thus be explained with the lack of a salinity decrease, depth and with water stratification preventing mixing across the thermocline.

8.7 Conclusions

249 fossil shells from 141 stratigraphic beds of the Arda River marine succession belonging to the species *Glycymeris glycymeris*, *Glycymeris insubrica*, *Glycymeris inflata*, *Glycymeris* sp., *Aequipecten opercularis*, *Aequipecten scabrella* and *Arctica islandica* have been selected and analyzed for carbon and oxygen isotope analyses. The oxygen isotope data obtained from the analyzed taxa have been used to construct a mean $\delta^{18}O$ curve, which was then compared to the Atlantic and Mediterranean stacks, suggesting a better correlation with the Atlantic one, which is also obtained from benthic taxa.

Carbon and oxygen bulk shell isotope analyses allow to conclude that:

- Sea surface palaeotemperatures calculated from bulk shell $\delta^{18}O$ seem to remain rather constant during the deposition of the Arda marine succession and they do not suggest any significant cooling during Gelasian and Calabrian (Early Pleistocene), in agreement with the oxygen isotope record of the Mediterranean stack; actually a trend to lower values is observed, probably due to shallowing and fresh water influx with salinity decrease at the top of the section.
- The species of *Glycymeris* living in shallow water and tolerant of salinity variations, record the highest palaeotemperature variation (22.0°C); a salinity decrease at the top of the section is also recorded in these shells by both oxygen and carbon isotopes.
- The species of *Aequipecten* live at intermediate water depths; they record a palaeotemperature excursion of 14.6°C based on oxygen isotopes. The average $\delta^{13}C$ value is similar to that of the species of *Glycymeris*, suggesting a living depth for both genera above the thermocline, where they are affected by salinity and nutrient variations.
- The shells of *Arctica islandica* record the lowest palaeotemperature excursion (11.0°C) and the highest average $\delta^{13}C$ value, in agreement with a living depth below the thermocline.

The analysis of the isotope record of bivalve shells of genera with different palaeoecological behaviours allow to obtain a complete picture of the palaeoclimatic evolution and palaeoenvironmental conditions affecting the Arda succession during the Early Pleistocene. The interpretation of the oxygen and carbon isotope curves was not an easy task, as several factors affecting the signals had to be taken into account. Notwithstanding these difficulties, what is clearly recorded by the bivalve shells of the Arda marine succession is that the average seawater palaeotemperature remains rather constant during the Early Pleistocene, albeit a low amplitude cyclicity. This, however, is difficult to constrain due to the discontinuous stratigraphic record of the bivalve shells, but it may be consistent with the obliquity controlled cyclicity of the Atlantic stack in this time interval. The lack of a cooling trend seems to be typical of the Mediterranean region (Lourens et al., 1996; Lourens, 2004) and may be due to factors

related to its location surrounded by continental masses, such as local currents, uplift of the Apennines, and rates of continental weathering. This suggests that the Middle Pleistocene Transition was quite abrupt in this area.

Chapter 9
Sclerochemical analyses

Seasonality is a fundamental component of the climate system and has a strong influence on biotic distribution and evolution. Fossil shells are high-resolution archives which vary in response to growth and environmental conditions. During their life span they are potentially able to record the seasonal physical and chemical variations of the seawater in which they thrive. Sclerochronology and in particular isotope profiles across growth lines of ten bivalve shells, belonging to species of *Glycymeris* and *Arctica*, have been used to assess the variation in seasonality (meant as winter-summer seawater temperatures) during the deposition time of the Arda marine succession in order to understand if and how seasonality varies approaching the Middle Pleistocene Transition and the beginning of the continental glaciations (Crippa et al., in prep.).

9.1 What is sclerochronology?

According to Gröcke & Gillikin (2008, p. 265) sclerochronology is:

"the study of physical and chemical variations in the accretionary hard tissues of organisms, and the temporal context in which they formed. Sclerochronology focuses primarily upon growth patterns reflecting annual, monthly, fortnightly, tidal, daily, and sub-daily increments of time entrained by a host of environmental and astronomical pacemakers. Familiar examples include daily banding in reef coral skeletons or annual growth rings in mollusk shells. Sclerochronology is analogous to dendrochronology, the study of annual rings in trees, and equally seeks to deduce organismal life history traits as well as to reconstruct records of environmental and climatic change through space and time"

Bivalves form their external calcium carbonate skeletons episodically; this episodic growth produces incremental growth lines that offer a chronological record. Episodic growth patterns provide a sequential record of growth increments which can then be analyzed as a geochemical proxy for environmental conditions operating during growth of the shell or biomineral framework (Royer et al., 2013).

Several authors differentiate sclerochronology from sclerochemistry (e.g. Gröcke & Gillikin, 2008): the first term is used for studies of the physical structure of the hard tissues of organisms, even when combined with geochemistry (e.g. growth-line periodicity); the second one is a sub-discipline of sclerochronology, used to describe solely geochemical (isotopic or elemental) studies of the hard tissues of organisms. Here, I deal mainly with sclerochemistry.

9.2 State of the art

Since the growth rate of invertebrates is largely controlled by external factors (nutrients, food availability, temperature, salinity, light, pH), the relative changes in skeletal growth of these organisms can provide valuable information on the variability of these environmental variables (e.g. Kennish & Olsson, 1975).

Sclerochronological analyses have been carried out for numerous purposes and for a great ecological and taxonomic spectrum of recent and extinct animal groups including corals (Wilkinson & Ivany, 2002), brachiopods (Mii & Grossman, 1994; Angiolini et al., 2012), bivalves (e.g. Marchitto et al., 2000, Schöne et al., 2004; Ivany & Runnegar, 2010), gastropods (e.g. Schöne et al., 2007), amphibians (Steyer et al. 2004), sharks (McFadden et al. 2004), teleost fishes (Wilkinson & Ivany, 2002) and mammals (e.g. Wilkinson & Ivany, 2002).

Recently, shells of bivalve mollusks have been increasingly and successfully used for past and recent reconstructions of seawater temperature records (Schöne et al., 2011b), phytoplankton dynamics (Thébault et al., 2009a) and climatic oscillations (Schöne et al., 2003; Carré et al., 2005). Furthermore, it has been pointed out that they may also provide detailed biological information concerning the organism's lifespan (e.g. Wanamaker et al., 2008), metabolism (Chauvaud et al., 2011), calcification rate (Thébault et al., 2009b) and the length of the growing season (e.g. Ivany et al., 2003).

Also, bivalves show an extremely broad biogeographic distribution, occurring in shallow water and deep-sea environments, in freshwater, marine and brackish settings, near the poles and at the equator (Schöne et al., 2005a). Some species, as *A. islandica*, are extremely long-lived and thus are perfectly suited for long-term environmental reconstructions. Bivalves thus virtually combine all the requirements for being a perfect climate and environmental recorder.

9.3 Growth lines formation

Bivalve growth is costly and includes shell production, which involves calcification and the formation of the organic matrix (Palmer, 1992; Irie & Iwasa, 2005). When the physiological tolerance of an organism to environmental stressors (e.g. temperature) is exceeded, a growth line is formed, which represent a growth cessation. According to Wahl et al. (2011, p. 39), stress is defined as "the impact of any set of abiotic and/or biotic factors that adversely affects individual 'performance' and ultimately impairs population growth rate through reduced individual survival, growth and/or reproduction".

During periods of stress, the shell secreting mantle edges are withdrawn from the shell margins and shell deposition slows down or ceases. When conditions are again suitable for shell growth the mantle margins are extended so that old and new regions of the shell are no longer continuous and an obvious growth line results (Richardson in Gibson et al., 2001). These slower-growth portions of the shell are associated with a change in crystal habitus, size and orientation (Carter, 1990) and changes in crystallographic properties.

Notably, the formation of distinct growth lines requires a waning shell growth that precedes a complete stop of carbonate deposition. If shell growth stopped suddenly, or resumed with the same rate as before, growth lines would be difficult to recognize, or not visible at all (Schöne, 2008). A gradual slowdown of carbonate production increases the relative amount of organic material in the shell, as it is indicated by higher amounts of phosphorous and sulfur, i.e., major components of amino acids, at the growth lines (Tanabe, 1988), higher resistance against etching (e.g. Goodwin et al., 2001; Schöne et al., 2002; Dunca et al., 2005), and strong blue coloration when immersed in Mutvei's solution (Schöne et al., 2005b).

The physiologic mechanism by which the bivalve produces growth lines is not known but is related to variation in the relative rate of formation of organic matrix and calcium carbonate. There are two hypotheses proposed (Lutz & Rhoads, 1980; Dodd & Stanton, 1990):

1. The organic matrix may form at a relatively more constant rate than $CaCO_3$, so that at time when little or no $CaCO_3$ forms, as a results of a stress factor, an organic rich band occurs in the shell.

2. The banding may results from periodic solution at the shell surface. When the bivalve shell is closed, the animal respires anaerobically and produces acids that are neutralized by dissolution of shell calcium carbonate. The organic matrix associated with the dissolved carbonate is left, as it is insoluble, as a residue on the shell surface. When the valves are reopened and the animal resumes aerobic respiration, calcification is also renewed, and the organic matrix residue is incorporated within the new shell material, giving it a high organic content.

The principal difficulty encountered in employing growth lines on bivalve shells arises from a difficulty to distinguish between disturbance lines and those of annual origin. Disturbance lines are produced by various environmental irregularities such as storms, spawning, gales, displacement or anthropogenic disturbance. They are generally less prominent than annual growth lines and usually do not encircle the shell, tending to fade away at posterior and anterior shell margins.

9.4 Growth lines in species of *Glycymeris* and *Arctica*

For the successful development of a fossil sclerochronological archive it is necessary to reconstruct the periodicity of the growth increments that records the chronology and to assess if the shell precipitates in isotopic equilibrium with the surrounding seawater. This can be done analyzing the biomineralization processes of extant organisms.

Glycymeris – Brocas et al. (2013) and Royer et al. (2013), using live-collected specimens, demonstrated that both the widths of the growth increment and the geochemical composition of the shells of *Glycymeris* are sensitive to seawater temperature variability, which can thus be accurately estimated through sclerochronological and sclerochemical analyses of their shells. Several studies have confirmed that carbonate secretion in species of *Glycymeris* is not influenced by vital effects (Brocas et al., 2013; Royer et al., 2013; Bušelić et al., 2015).

Annual periodicity in *G. glycymeris* has been validated by means of stable isotope (Berthou et al., 1986) and radiocarbon analyses (Brocas et al., 2013). It has been demonstrated that the periodic growth increments in *G. glycymeris* are formed annually (Berthou et al., 1986; Brocas et al., 2013; Royer et al., 2013). Shell growth is apparently synchronized with the six warmest months of the year and growth lines correspond to winter growth cessation. Not only temperature affects shell growth but also other contributing factors such as low food abundance play a role in the formation of narrow annual growth increments (Brocas et al., 2013).

As for *G. glycymeris*, also *Glycymeris nummaria* (synonym of *Glycymeris insubrica*) forms a narrow growth line when seawater temperatures are at a minimum (late February) (Peharda et al., 2012). However, the timing and rate of shell growth can vary among different species of the genus *Glycymeris*: *Glycymeris bimaculata*, for example, forms a line at the beginning of spring when sea water temperatures start to increase (Bušelić et al., 2015).

Arctica – Of all long-lived bivalve mollusks, *Arctica islandica* is by far the most comprehensively studied species. In fact, aside from recording seasonal extremes (Schöne et al., 2005c), the exceptional lifespan of *A. islandica* (Butler et al., 2013) is what makes this species an outstanding palaeoclimatic archive.

A wide variety of methods have been used to establish that growth increment formation is annual, including stable isotope analyses (e.g. Schöne et al., 2004) and mark-recapture experiments (Ropes, 1988); these methods also allow to confirm that *A. islandica* incorporates the stable oxygen isotopes in equilibrium with ambient seawater (Schöne et al., 2005c).

A. islandica shells form growth lines about one month after the seasonal maximum temperature and before the winter minimum temperatures are attained (Schöne et al., 2005c).

Although there is still some debate about the exact environmental factors which lead to the formation of a growth line, most studies suggest that the growth line formation in *A. islandica* is related to reproduction (Jones, 1980). However the stimulus for spawning is poorly understood (Landers, 1976). Some authors consider a minimum temperature of 13.5°C as the critical factor (Loosanoff, 1953), while according to others a change in temperature in autumn, and the loss of stratification, is the key factor (Mann & Wolf, 1983). A firm link between growth line deposition and reproduction is not clear because immature *A. islandica* specimens also form such annual growth breaks at the exact same period of the year. According to Thompson et al. (1980), the bivalve mimics reproduction during pre-maturity.

9.5 Material and methods

I had the opportunity to learn the preparation techniques and the analytic method for sclerochronological analyses at the Earth Sciences Department of "Johannes Gutenberg" University of Mainz (Germany) under the supervision of Prof. B. Schöne. During this visit, I prepared and analyzed some of the specimens of species of *Glycymeris* and *Aequipecten* collected along the Arda River. I also studied some sections of the shells of *Arctica islandica* already prepared and under study by the German research group. Following this stage, I came to the conclusion that the best shells for sclerochemical purposes are the ones belonging to species of *Glycymeris* and *Arctica*, which have distinct growth lines in their outer shell layer; on the contrary growth lines of species of *Aequipecten* are clear only on the external shell surface, but they are not traceable inside the shell, thus making very difficult and uncertain the sampling for isotopic analysis. For these reasons sclerochemical analyses have been here undertaken only on shells belonging to species of the genera *Arctica* and *Glycymeris*. Some of the shells were also treated with Mutvei's solution and observed in fluorescence (Schöne et al., 2005b; Wanamaker et al., 2009); however the results were not successful at all, as fossil specimens have a low residual organic content and thus they do not respond well to these kind of analyses.

Ten fossil specimens were then selected for sclerochemical analyses: one specimen belonging to *Glycymeris inflata* (ACG29bis-33; 42 m[1]), four specimens belonging to *Glycymeris insubrica* (ACG200-8, 174 m; ACG252-1, 223.80 m; ACG261-1, 235.70 m; ACG261bis-1, 235.70 m) and five specimens belonging to *Arctica islandica* (ACG78-1, 103.70 m; ACG78-7; 103.70 m; ACG200-13, 174 m; ACG215-5, 185.70 m; ACG254-1, 224.30 m).

Valves were cut along the axis of maximum growth in order to obtain a 5mm-thick sections from each specimen; to facilitate the cutting and avoid shell breakage, valves of species of *Glycymeris* were embedded in a bicomponent metal epoxidic resin, whereas the more fragile valves of *A. islandica* were embedded in gypsum or in araldite, which are more resistant at cutting. The obtained sections were then mounted on glass slides, ground smoothed with 400 and 1000 SiC grit, polished with 1μm Al_2O_3 powder and cleaned.

Shell aragonite fractions were sampled from these thick sections using a microdrill (Dremel 3000) equipped with a 300-μm tungsten carbide drill bit at Dipartimento di Scienze della Terra 'A. Desio', Università di Milano. Between 3 and 15 carbonate fractions were collected from each annual growth increment of the outer layer corresponding to the ontogenetically youngest portions of the shells (from 16 to 66 total samples per shell). The powder obtained from the drilling was collected, labelled and stored separately in 0.5 ml tubes.

Aragonite samples were then acidified in 100% phosphoric acid and vaporized. Analysis of the powder samples for oxygen and carbon isotope ratios ($^{18}O/^{16}O$ and $^{13}C/^{12}C$) was undertaken using a GV IsoPrime dual inlet mass spectrometer plus Multiprep device at NERC Laboratory of the British Geological Survey under the supervision of Prof. M. Leng. Isotope values ($\delta^{13}C$, $\delta^{18}O$) are reported as per mil (‰) deviations of the isotopic ratios ($^{18}O/^{16}O$, $^{13}C/^{12}C$) calculated to the V-PDB scale using a within-run laboratory standard (KMC) calibrated against the international NBS standards (NBS18 and 19). Analytical reproducibility for these analyses was better than 0.1‰ for $\delta^{13}C$ and $\delta^{18}O$.

9.6 Results

9.6.1 Sclerochemical record in the species of *Glycymeris*

Five specimens belonging to *G. inflata* and *G. insubrica* have been sampled for oxygen and carbon isotope analyses; three specimens have been found articulated in life position (ACG29bis-33, ACG261-1 and ACG261bis-1), whereas the other two (ACG200-8 and ACG252-1) are disarticulated.

1. 42m from the base of the section. From this point on, all the metres values are referred from the base of the section.

The latter are part of a transported assemblage with well preserved specimens, which show no loss of shell ornamentation or breakage. The taphonomic signature and the biofabric suggest transport or winnowing but not over distance. Shells from transported assemblage prevent the determination of an accurate habitat depth; thus palaeodepths were supposed in each bed according to the faunal association and to the sedimentary structures occurring in the same bed.

Annual growth lines in section are well distinct; however supernumerary growth lines are also present in the shells, which may have induced small errors in the dating of annual increments.

Notwithstanding the analyzed specimens record several annual growth increments (AGI), only about 4 to 10 were easily discernible and subject to sampling (Fig. 9.1). As growth rate decreases during the lifespan of bivalve mollusks (e.g. Goodwin et al., 2003), shells were sampled only in the first years of growth in order to avoid overlap between closely spaced annual records.

9.6.1.1 Oxygen isotopes

$\delta^{18}O$ values in the species of *Glycymeris* show quite a regular cyclicity from low to high values and the position of the growth lines correlates well with the highest values of $\delta^{18}O$.

Analyzing the shells, from the base to the top of the section, in four different stratigraphic intervals I have observed the following changes (Figs. 9.1, 9.2):

1) an increase in the amplitude of the cycles from the base to the top of the section;

2) an increase in the excursion between $\delta^{18}O_{max}$ and $\delta^{18}O_{min}$ and, in consequence of that, an increase in the palaeotemperature excursions;

3) an overall decrease in the mean oxygen values.

To calculate the palaeotemperatures (Fig. 9.1) with the equations reported in Chapter 8, it is necessary to introduce a $\delta^{18}O_{sw}$ value. As it is not possible to know the exact $\delta^{18}O_{sw}$ value in each bed of the succession, this has been assumed for each shell, considering its position in the average oxygen curve correlated to the Atlantic MIS and Mediterranean stacks (Fig. 9.3; see also Chapter 8 for more details on this correlation):

1) a value of +0.8 ‰ for $\delta^{18}O_{sw}$ is used for *G. insubrica* collected at 174 m from the base of the section (C in Fig. 9.3); this value is in fact coherent with a cold interval, which is supported by: a) high bulk shell oxygen data from the same bed, thus indicating low palaeotemperatures; b) Atlantic MIS and Mediterranean stacks correlation with a cold stage; c) high $\delta^{18}O_{shell}$ values and thus low palaeotemperatures recorded by a specimen of *Arctica islandica* coming from the same bed (see next paragraph).

2) a value of -0.5 ‰ for $\delta^{18}O_{sw}$ is used for two specimens of *G. insubrica* (235.70 m; G in Fig. 9.3) in the upper part of the section. The use of this value is supported both by the correlation with a warm stage in the Atlantic MIS and Mediterranean stacks and by rather low bulk shell oxygen data from the same bed, thus indicating warmer palaeotemperatures.

3) a value of +0.0 ‰ for $\delta^{18}O_{sw}$ is used for *G. inflata* (42 m; A in Fig. 9.3) and *G. insubrica* (223.80 m; E in Fig. 9.3). The use of this value is compatible with a warmer time interval than the one in case 1), but colder than the one in case 2), as supported also by a correlation with intermediate stages in the Atlantic MIS and Mediterranean stacks.

a

Species	Sample number	Position	Mean	$\delta^{18}O_{min}$	$\delta^{18}O_{max}$
Glycymeris insubrica	ACG261bis-1	235.70 m	-2.26 ‰	-3.98 ‰	+0.40 ‰
Glycymeris insubrica	ACG261-1	235.70 m	-1.77 ‰	-2.94 ‰	+0.31 ‰
Glycymeris insubrica	ACG252-1	223.80 m	-0.46 ‰	-1.95 ‰	+0.80 ‰
Glycymeris insubrica	ACG200-8	174 m	+0.21 ‰	-0.64 ‰	+1.48 ‰
Glycymeris inflata	ACG29bis-33	42 m	+1.01 ‰	+0.33 ‰	+1.66 ‰

b

$\delta^{18}O_{max}$ - $\delta^{18}O_{min}$	Temperature	T excursion	Living depth	V-SMOW	AGI sampled
+4,38 ‰	15.5-34.5 °C	19.0 °C	5m	-0.5 ‰	10
+3,25 ‰	15.9-30.0 °C	14.1 °C	5m	-0.5 ‰	10
+2,75 ‰	15.9-27.9 °C	12.0 °C	10m	+0.0 ‰	10
+2,12 ‰	16.5-25.7 °C	9.2 °C	10m	+0.8 ‰	4
+1,33 ‰	12.3-18.0 °C	5.7 °C	20m	+0.0 ‰	6

Species	Sample number	Position	Mean	$\delta^{13}C_{min}$	$\delta^{13}C_{max}$	$\delta^{13}C_{max-min}$	Living depth
Glycymeris insubrica	ACG261bis-1	235.70 m	-0.10 ‰	-0.78 ‰	+0.72 ‰	+1.50 ‰	5m
Glycymeris insubrica	ACG261-1	235.70 m	+0.24 ‰	-1.16 ‰	+0.96 ‰	+2.12 ‰	5m
Glycymeris insubrica	ACG252-1	223.80 m	-0.43 ‰	-1.17 ‰	+0.12 ‰	+1.29 ‰	10m
Glycymeris insubrica	ACG200-8	174 m	-0.13 ‰	-0.71 ‰	+0.19 ‰	+0.90 ‰	10m
Glycymeris inflata	ACG29bis-33	42 m	+1.96 ‰	+0.79 ‰	+2.94 ‰	+2.15 ‰	20m

Fig. 9.1. Oxygen (in blue; part b is a continuation of part a) and carbon (in orange) isotope data of the five specimens of *G. inflata* and *G. insubrica*, analyzed for sclerochemistry. Aside from the max, min, max-min and mean values, the living depth and the number of annual growth increments (AGI) sampled is reported. For oxygen isotopes is also indicated the value of V-SMOW ($\delta^{18}O_{sw}$) used in each stratigraphic level and the palaeotemperatures calculated with the modified equation of Grossman & Ku (1986).

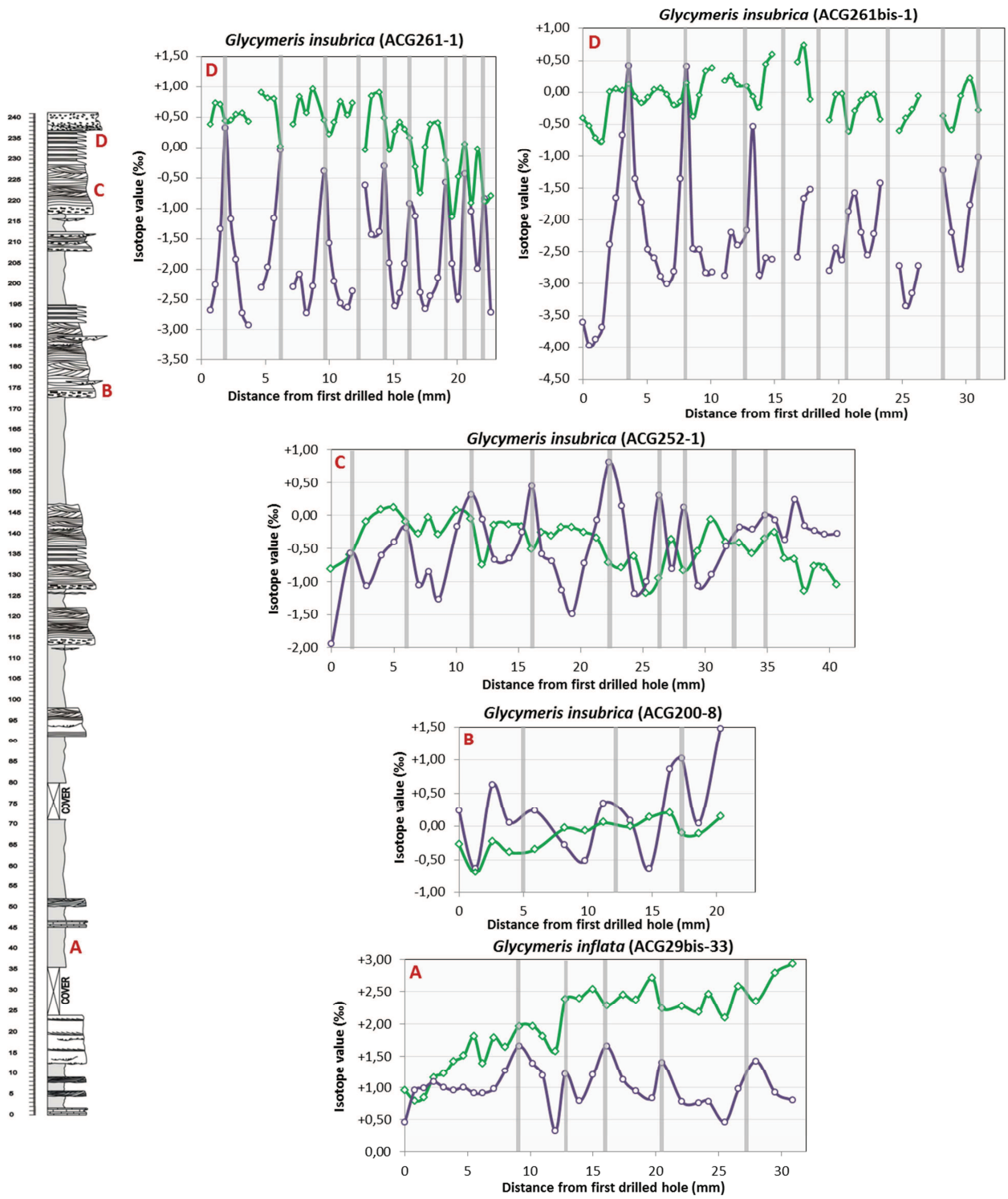

Fig. 9.2. Oxygen (in violet) and carbon (in green) stable isotope signals of *Glycymeris* shells from the base to the top of the section. The position of the growth lines is represented by vertical grey bands.

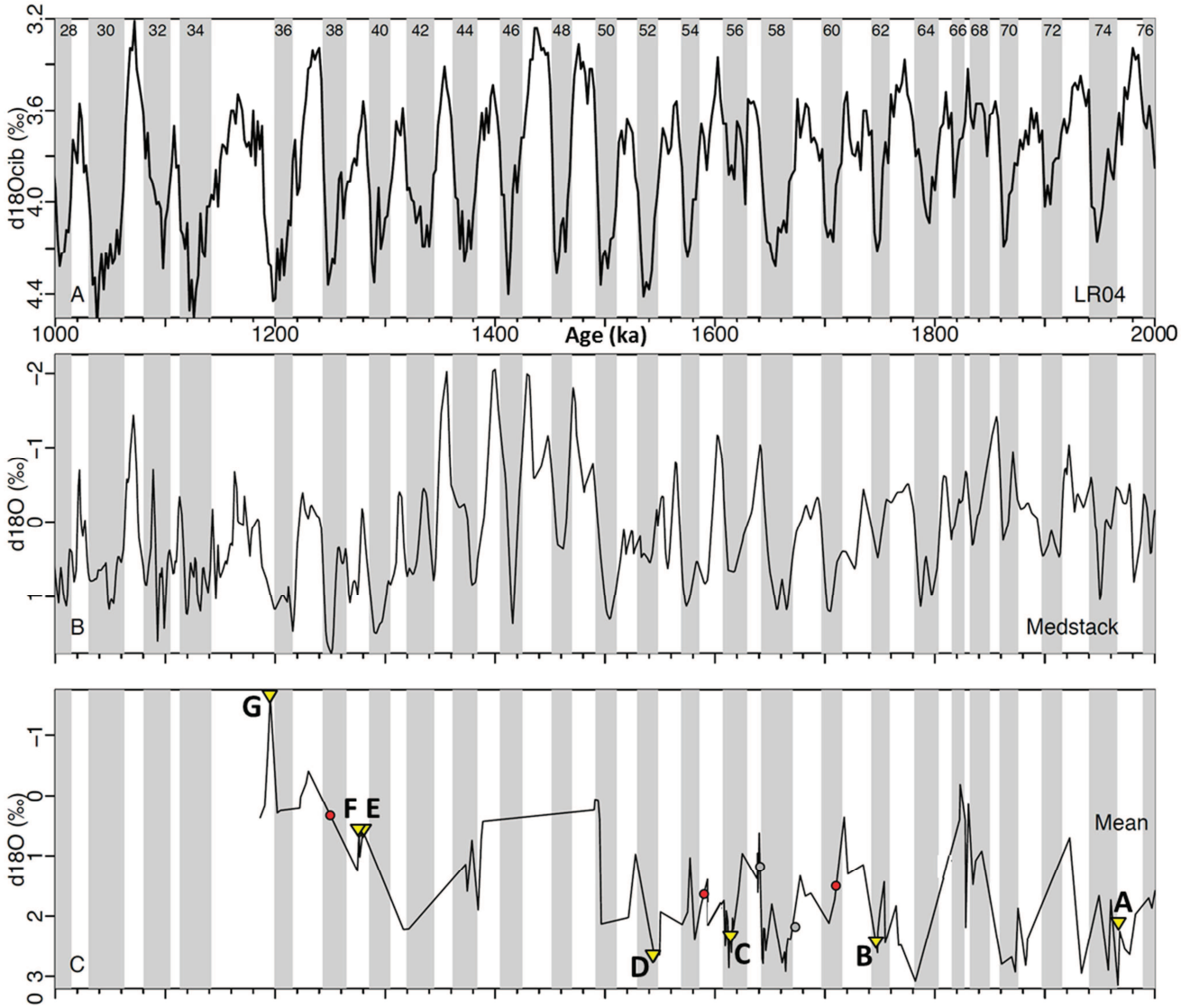

Fig. 9.3. Correlation of the Arda bulk shell mean oxygen curves (C) with the Atlantic MIS stack (A) and with the Mediterranean stack (B). Grey bands represent the cold stages; in red are the tie-points obtained from nannofossil biostratigraphy; in grey are added pointers. The base of the section is on the right, the top on the left of the figure.
Yellow triangles indicate the position of the shells analyzed for sclerochemistry. A: one specimen of *Glycymeris inflata*; B: two specimens of *Arctica islandica*; C: one specimen of *Glycymeris insubrica* and one of *Arctica islandica*; D: one specimen of *Arctica islandica*; E: one specimen of *Glycymeris insubrica*; F: one specimen of *Arctica islandica*; F: two specimens of *Glycymeris insubrica*.

9.6.1.2 Carbon isotopes.

The $\delta^{13}C$ signal registered in the shells of the species of *Glycymeris* does not show a characteristic cyclicity as observed in the oxygen ones, nor a particular trend toward the top of the section (Fig. 9.2). However, worthy of note is that generally the highest peaks of $\delta^{13}C$ slightly precede the highest peaks of $\delta^{18}O$ or they show a positive correlation (Fig. 9.2). Specimens belonging to *Glycymeris insubrica* have lower carbon values relative to *Glycymeris inflata* (Fig. 9.1).

A very weak and not constant decreasing trend during growth is present in the carbon curve of two specimens (ACG252-1 and ACG261-1), whereas the other two show an increasing trend during growth (ACG200-8 and mainly ACG29bis-33).

9.6.2 Sclerochemical record in *Arctica islandica*

Five specimens belonging to *Arctica islandica* have been sampled for sclerochemical oxygen and carbon isotope analyses; one specimen has been found articulated in life position (ACG254-1), whereas the other four (ACG78-1, ACG78-7, ACG200-13 and ACG215-5) are disarticulated, probably undergoing a transport but not over long distances, as the taphonomic signature and the biofabric suggest. Shells from transported assemblages prevent the determination of an accurate habitat depth; thus palaeodepths were inferred in each bed according to the faunal association and to the sedimentary structures. Annual growth lines in section are well distinct, however supernumerary growth lines are also present in the shells, which may have induced small errors in the dating of annual increments. Notwithstanding the analyzed specimens record several annual growth increments (AGI), only about 8 to 13 were easily discernible and subject to sampling (Fig. 9.4). As growth rate decreases during the lifespan of bivalve mollusks (e.g. Goodwin et al., 2003), shells were sampled only in the first years of growth in order to avoid overlap between closely spaced annual records.

9.6.2.1 Oxygen isotopes

$\delta^{18}O$ values in *Arctica islandica* show quite a marked cyclicity from low to high values. The position of the growth lines here slightly precede the highest peaks of $\delta^{18}O$ in almost all the specimens.

Analyzing the shells, from the base to the top of the section, in four different stratigraphic intervals I have observed the following changes (Figs. 9.4, 9.5):

1) The shells in the stratigraphically lowest bed (103.70 m) have the highest excursion between $\delta^{18}O_{max}$ and $\delta^{18}O_{min}$ and, thus record a strong difference between the maximum and the minimum palaeotemperatures (16.0-16.1°C); the two specimens occurring in this bed show the same $\delta^{18}O_{max}$ - $\delta^{18}O_{min}$ variation and the same palaeotemperature excursions, suggesting that, although they are transported, they come from the same habitat.

2) a slightly increasing trend in $\delta^{18}O_{max}$ - $\delta^{18}O_{min}$ variation and thus in palaeotemperature excursion has been noted from 174 to 224.80 metres along the section, taking into account the different living depths of the three specimens (ACG200-13, ACG215-5, ACG254-1).

a

Species	Sample number	Position	Mean	$\delta^{18}O_{min}$	$\delta^{18}O_{max}$
Arctica islandica	ACG254-1	224.30 m	+1.21 ‰	+0.17 ‰	+2.21 ‰
Arctica islandica	ACG215-5	185.70 m	+2.95 ‰	+1.63 ‰	+4.46 ‰
Arctica islandica	ACG200-13	174 m	+2.98 ‰	+2.29 ‰	+3.65 ‰
Arctica islandica	ACG78-7	103.70 m	+2.50 ‰	+1.37 ‰	+5.08 ‰
Arctica islandica	ACG78-1	103.70 m	+2.87 ‰	+1.60 ‰	+5.30 ‰

b

$\delta^{18}O_{max}$ - $\delta^{18}O_{min}$	Temperature	T excursion	Living depth	V-SMOW	AGI sampled
+2,04 ‰	9.9-18.7 °C	8.8 °C	15m	+0.0 ‰	11
+2,83 ‰	4.4-16.7 °C	12.3 °C	10m	+1.0 ‰	8
+1,36 ‰	7.0-13.0 °C	6.0 °C	15-20m	+0.8 ‰	13
+3,71 ‰	1.7-17.8 °C	16.1 °C	20-25m	+1.0 ‰	12
+3,70 ‰	0.8-16.8 °C	16.0 °C	20-25m	+1.0 ‰	11

Species	Sample number	Position	Mean	$\delta^{13}C_{min}$	$\delta^{13}C_{max}$	$\delta^{13}C_{max-min}$	Living depth
Arctica islandica	ACG254-1	224.30 m	+1.18 ‰	+0.70 ‰	+1.60 ‰	+0.90 ‰	15m
Arctica islandica	ACG215-5	185.70 m	+1.90 ‰	+1.11 ‰	+2.88 ‰	+1.77 ‰	10m
Arctica islandica	ACG200-13	174 m	+1.77 ‰	+1.14 ‰	+2.33 ‰	+1.19 ‰	15-20m
Arctica islandica	ACG78-7	103.70 m	+2.24 ‰	+1.24 ‰	+3.62 ‰	+2.38 ‰	20-25m
Arctica islandica	ACG78-1	103.70 m	+2.80 ‰	+2.04 ‰	+4.52 ‰	+2.48 ‰	20-25m

Fig. 9.4. Oxygen (in blue; part b is a continuation of part a) and carbon (in orange) isotope data of the five specimens of *A.islandica*, analyzed for sclerochemistry. Aside from the max, min, max-min and mean values, the living depth and the number of annual growth increments sampled (AGI) is reported. For oxygen isotopes is also indicated the value of V-SMOW used in each stratigraphic level and the palaeotemperatures calculated with the modified equation of Grossman & Ku (1986).

As it is not possible to know the exact $\delta^{18}O_{sw}$ in each bed of the succession, its value has been assumed considering its position in the average oxygen curve correlated to the Atlantic MIS and Mediterranean stacks (Fig. 9.3):

1) a value of +0.8 ‰ for $\delta^{18}O_{sw}$ is used for *A. islandica* (174 m; C in Fig. 9.3); the use of this value is compatible with a cold time interval, as supported by: a) high bulk shell oxygen data from the same bed, thus indicating low palaeotemperatures; b) Atlantic MIS and Mediterranean stacks correlation with a cold stage.

2) a value of +1.0 ‰ for $\delta^{18}O_{sw}$ is used for three specimens of *A. islandica* (two at 103.70 m; B in Fig. 9.3; one at 185.70 m; D in Fig. 9.3); the use of this value is suggested by very cold events, colder than the previously described one (174 m), as supported by: a) high bulk shell oxygen data from the same

beds, thus indicating low palaeotemperatures; b) Atlantic MIS and Mediterranean stacks correlation with cold stages.

3) a value of +0.0 ‰ for $\delta^{18}O_{sw}$ is used for *A. islandica* (224.30 m; F in Fig. 9.3); the use of this value is compatible with a warmer time interval than the previous ones, as supported also by a correlation with a warmer stage in the Atlantic MIS and Mediterranean stacks.

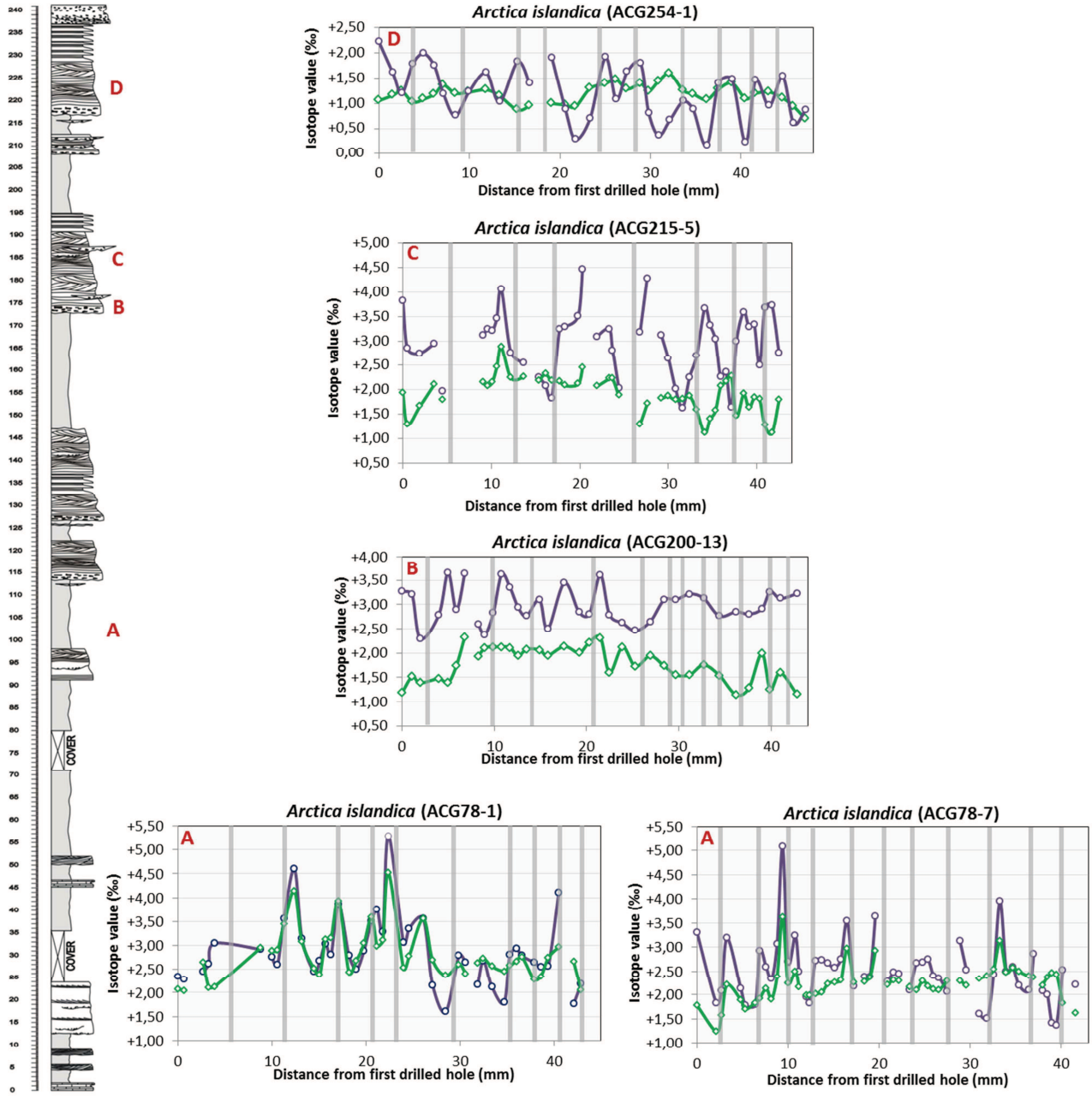

Fig. 9.5. Oxygen (in violet) and carbon (in green) stable isotope signals of *A. islandica* shells from the base to the top of the section. The position of the growth lines is represented by vertical grey bands.

9.6.2.2 Carbon isotopes

As for *Glycymeris* shells, I have not observed a characteristic cyclicity in *A. islandica* carbon curves as instead recorded by the oxygen ones (Fig. 9.5). In the majority of cases, I noted a positive correlation between the peaks of $\delta^{18}O$ and those of $\delta^{13}C$. Also, *A. islandica* shells occurring in the coldest intervals (at 103.70 m and at 185.70 m) record the highest mean carbon values (Fig. 9.4). A weak and not constant decreasing trend during growth is present in two specimens (ACG200-13 and ACG215-5).

9.7 Discussions

9.7.1 Growth lines formation

The formation of the growth lines is usually accompanied by an increase in the content of organic matrix. If we take into account that the latter forms at a relatively more constant rate than the mineral phase and it is energetically more expensive to produce (Palmer, 1983), the local enrichment in organic matrix may be better due to a non secretion of the mineral phase rather than to a secretion of additional organic matter. So that at time when little or no $CaCO_3$ is formed an organic rich band is created. Then calcification is renewed and the organic matrix residue is incorporated within the new shell material giving it a high organic content.

Based on what I have observed from the ultrastructural analysis, two situations can occur at the growth line from the point of view of the mineral phase:

1) Formation of small prisms (Pl. 6, fig. D; Pl. 7, figs. C, E; Pl. 14, fig. B; Pl. 15, figs. B-H in Appendix A). The prismatic phase which usually accompanies the growth line may be formed during the halt of the growth (and thus it represents a slow down, but not an effective stop) or it may be the first structure formed when the biomineralization process restarts. In the first case a mineral phase is secreted in agreement with the hypothesis 1 stated above (see growth lines formation paragraph); in the second case there is no secretion of calcium carbonate or secretion with dissolution, and prisms represents the first biomineral formed after the biomineralization restarts; this is in agreement with hypothesis 2, which invokes shell carbonate dissolution. But, why do growth lines have a prismatic structure? Prisms are considered comparatively ‘primitive’ among shell fabrics in mollusks (Suzuki & Uozumi, 1981) and thus they may represent the simpliest structure to form after a stress event.

2) Lack of mineral phase (Pl. 15, fig. A in Appendix A). This may be explained by a non secretion of $CaCO_3$ (hypothesis 1) or by a secretion followed by dissolution (hypothesis 2).

The mechanism of growth line formation still remains a poorly understood and complicated topic; much work is needed to completely understand the processes involved in their formation.

9.7.2 Sclerochemical analyses

9.7.2.1 What do *Glycymeris* shells tell?

9.7.2.1.1 Oxygen isotopes

The position of the growth lines in the shells of species of *Glycymeris* is in correspondence of the highest peaks of $\delta^{18}O$, indicating that growth lines formation occurs in the winter season, in agreement with previous findings in *Glycymeris* species (Peharda et al., 2012; Brocas et al., 2013). The $\delta^{18}O$ profiles of all the specimens evaluated in this study showed cyclic patterns over the sampled interval, which clearly indicate a seasonality signal. Each oxygen curves is affected by three factors (S, T and ISVV, see Chapter 8 for further information) which have a different role in each sampled bed, but they are all linked together and they can explain the climatic changes occurring along the Arda marine succession.

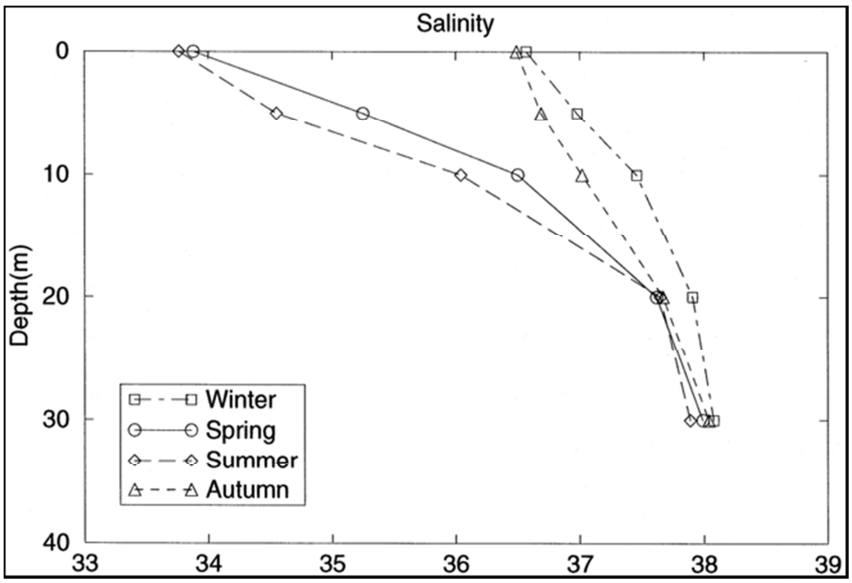

Fig. 9.6. Seasonal vertical profiles of salinity (psu) for the shallow northern Adriatic Sea (from Zavatarelli et al., 1998).

In the present analysis two species belonging to the genus *Glycymeris* have been analyzed: *Glycymeris inflata* and *Glycymeris insubrica*; the first species usually lives in deep water (10-70 m), whereas the latter is typical of shallow water depth (max 40 m, but often less) and lagoonal settings (see Chapter 3 for additional information about their palaeoecology). These different life habits have to be taken into account when analyzing the oxygen signals registered in these shells. Aside from T and ISVV, *G. insubrica* oxygen signals may be also affected by salinity variations; in fact it is known to tolerate salinity changes (Raineri, 2007). The Arda succession was deposited in an estuarine setting affected by fluvial floods; thus riverine freshwater influx largely influenced the system, mainly in the upper part of the section. According to Zavatarelli et al. (1998), in the North Adriatic sea salinity may vary of about 4 ‰ (from 33.50 to 37.50 ‰) in the uppermost 10 metres of depth, whereas salinity at depths below 20

metres is constant and higher, around 37-38 ‰ (Fig. 9.6). To be noted that the salinity decrease in surface water is more pronounced in spring and summer than in the other seasons (Fig. 9.6). For these reasons only the oxygen record of the species *G. insubrica* is influenced by salinity decrease; *G. inflata*, living below 20 m of depth, is not affected by salinity changes.

Salinity changes (mainly due to freshwater input) affect the oxygen signals of *Glycymeris insubrica* in two ways:

1) they produce a decrease in the mean oxygen values in the shallow water upper part of the section (from +0.21‰ at 174 m to -2.26‰ at 235.70 m); as fresh water is enriched in ^{16}O, the $\delta^{18}O$ values registered in the shells, will be lower. In fact, toward the top of the section riverine freshwater inputs increase, as suggested also by sedimentological evidence.

2) apparent increase in the calculated palaeotemperatures (up to 34.5°C at 235.70 m) and particularly in their excursion (14.1-19.0°C) in the upper part of the section (Fig. 9.1). According to Bušelić et al. (2015) $\delta^{18}O_{sw}$ likely fluctuates seasonally in association with evaporative fractionation processes and riverine freshwater inputs; these seasonal $\delta^{18}O_{sw}$ fluctuations would amplify the variability in the reconstructed temperatures accounting for the high palaeotemperature excursions observed in the shells from the upper part of the Arda section. The apparent high palaeotemperatures obtained, can be related to an increasing contribute of the salinity factor (dilution due to fresh water inputs) toward the top of the section, as also supported by sedimentological evidence. A salinity change of 2 ‰ would correspond to a shift in in the oxygen values of ~1 ‰ (Cohen & McCartney, 1996; Srivastava et al., 2007), which in turn is nearly 4-5°C in temperature. Taking into consideration that in the Northern Adriatic salinity may vary of about 4 ‰ in the first 10 metres of depth (Zavatarelli et al., 1998) (Fig. 9.6), calculated temperature could then result up to 8-10°C in excess then the effective ones.

Temperature and salinity, however, are not the only two factors which influence the oxygen signals in *Glycymeris* shells. The change in $\delta^{18}O$ of the seawater due to ice dynamics is the third important factor affecting oxygen curves. The use of +0.8 ‰ to calculate palaeotemperatures in a *G. insubrica* shell at 174 m is justified by the occurrence of a cold event at this time. This is supported by: 1) the correlation with a cold stage in the Atlantic MIS and Mediterranean stacks (C in Fig. 9.3); 2) evidence from the bulk shell oxygen data of the same bed, where co-occurring specimens of *G. insubrica, Aequipecten opercularis* and *A. islandica* registered high values of $\delta^{18}O_{shell}$ (+1.32‰ for *G. insubrica*; +2.38‰ for *A. opercularis* and +3.54‰ for *A. islandica*); 3) a co-occurring specimen of *A. islandica* which, analyzed for sclerochemistry, shows unrealistically low palaeotemperatures which cannot be explained without invoking a change in the seawater composition due to change in ice volume (see next

paragraph). The oxygen records in *Glycymeris* are thus controlled by temperature, by ice volume changes and by salinity (dilution due to freshwater input), which act in interplay.

The most prominent result of the sclerochemical analysis of these shells is the evidence of an increase in the amplitude of the cycles and in the excursion between $\delta^{18}O_{max}$ and $\delta^{18}O_{min}$ from the base to the top of the Arda section (Fig. 9.2). As a consequence, the Arda succession records an increase in the palaeotemperature excursions (from 5.7 °C to 19.0 °C) and thus an increase in seasonality (meant as winter-summer temperature excursion) at the top of the section toward the beginning of the continental Middle Pleistocene glaciations. This more than threefold increase in annual palaeotemperature excursion may be amplified by the facts that 1) *G. inflata* in the lower part of the section lives in deeper water than *G. insubrica* and 2) *G. insubrica* oxygen record in the upper part of the section is affected by riverine freshwater influx. However, even considering these factors, at least a twofold increase in seasonality is confidently recorded.

Although the mean oxygen curve obtained by bulk shell isotope data (see Chapter 8) does not record any cooling across the succession, a marked increase in seasonality is instead underscored by the sclerochemical analysis. Seasonality seems to be a very important component in abrupt climate switches, as it has been noted also during the last glaciation (Denton et al., 2005; Dr. J. Hennissen pers. comm.). Approaching the Middle Pleistocene Transition and the beginning of the continental glaciations in the Northern Hemisphere, the increase in seasonality represents thus a clear signal that a climatic deterioration is occurring in the Mediterranean region even if it is not accompanied by a cooling of the average seawater temperatures.

9.7.2.1.2 Carbon isotopes

The interpretation of the carbon isotopes recorded in bivalve shells is usually complicated, as ^{13}C-depleted metabolic CO_2 may be incorporated in the shell, altering the signal. Nevertheless, no significant decreasing trend during growth has been observed in species of *Glycymeris* of the Arda section, allowing to conclude that, if present, a vital effect affecting carbon isotopes is negligible.

The characteristic cyclicity, which is instead well distinct in the oxygen curves, is not recorded in the carbon curves (Fig. 9.2); therefore it is not always possible to identify a seasonal signal. However, some interesting observations can be obtained also from the carbon curves.

In the majority of cases the highest peaks of $\delta^{13}C$ slightly precede or are in correspondence of the highest peaks of $\delta^{18}O$, and respectively correspond to the autumn ($\delta^{13}C$ peaks slightly preceding peaks of $\delta^{18}O$) or winter seasons (positive correlation between $\delta^{13}C$ and $\delta^{18}O$) (Fig. 9.2). According to Zavatarelli et al. (1998), the nutrient levels in the northern Adriatic Sea nowadays are controlled by

river inputs, inducing intense phytoplankton development in winter and autumn. The higher peaks of $\delta^{13}C$ observed in *Glycymeris* shells may be thus explained with the autumn-winter phytoplankton bloom which remove the ^{12}C used by primary producers from the seawater leaving it enriched in ^{13}C.
Interesting information about salinity can be obtained also by carbon isotopes. Freshwater input is depleted in ^{13}C (due to the input of CO_2 derived from the decomposition of terrestrial plants) and therefore, a drop in salinity will cause a decrease in $\delta^{13}C$ (Gillikin, 2005). *G. insubrica* shells show a lower average value in the carbon isotopes relative to *G. inflata* (-0.13‰, -0.43‰, +0.24‰, -0.10‰ of *G. insubrica*, compared to +1.96‰ of *G. inflata*), indicating a drop in ^{13}C and thus and enrichment in ^{12}C. This is a further evidence that the record of *G. insubrica* is affected by salinity variation, in particular by dilution due to riverine freshwater influx. Also, lower carbon values often occur in correspondence of low oxygen values, suggesting freshwater input in the spring-summer seasons, as observed also nowadays in the Adriatic sea by Zavatarelli et al. (1998) and which then led in turn to the development of the phytoplankton bloom in autumn and winter ($\delta^{13}C$ peaks).
The higher carbon mean value of *G. inflata* (+1.96‰) may be explained by its different living depth; *G. inflata* was probably living below the thermocline, where it was not affected by salinity changes. Furthermore, according to Zavatarelli et al. (1998) during stratification periods (spring–summer), there is a strong nutrient increase in the bottom layers, as export organic matter sinks to the bottom; this situation is particularly evident on the western side of the Adriatic basin, the most affected by the river inputs, in agreement with the location of the Arda section. The high values of *G. inflata* can be thus explained with living depth below the thermocline, lack of salinity change and with spring-summer water stratification.

9.7.2.2 What do *Arctica* shells tell?

9.7.2.2.1 Oxygen isotopes

The position of the growth lines in *Arctica islandica* slightly precede the highest peaks of $\delta^{18}O$ in quite all the specimens. This is in agreement with the timing of the formation of the growth lines which usually form about one month after the seasonal maximum temperature and before the winter minimum temperatures are attained (Schöne et al., 2005c).
The $\delta^{18}O$ profiles of all the specimens evaluated in this study showed cyclic patterns over the sampled interval, which clearly indicate a seasonality signal. As described above and in Chapter 8 three are the main factors affecting the oxygen signals in carbonate shells: S, T and ISVV.
As all the analyzed *A. islandica* shells lived below the thermocline and below 10 m of depth (maximum depth for the freshwater influx effect in the Northern Adriatic sea; Zavatarelli et al., 1998),

they are not influenced by salinity variations; for this reason salinity changes are not considered an important factor in affecting the *A. islandica* isotope record.

Aside from temperature the main factor affecting the oxygen signal in *A. islandica* is represented by the change in the $\delta^{18}O$ seawater composition due to ice dynamics. In fact a different $\delta^{18}O$ for the seawater has been used in the equation to calculate palaeotemperatures in the four stratigraphic beds of the Arda succession: +0.0‰ at 224.30 m and +0.8 ‰ at 174 m, +1.0 ‰ at 103.70 m and 185.70 m; the use of these latter two values is justified by the correlation of these beds with cold stages in the Atlantic MIS and Mediterranean stacks (Fig. 9.3), and by high bulk shell oxygen data in co-occurring specimens from the same beds. In fact, assuming lower $\delta^{18}O_{sw}$ values, let's say around 0.0 ‰, in the temperature equation, the calculated palaeotemperatures would be unrealistically low and unlikely for these settings (Fig. 9.7; Zavatarelli et al., 1998).

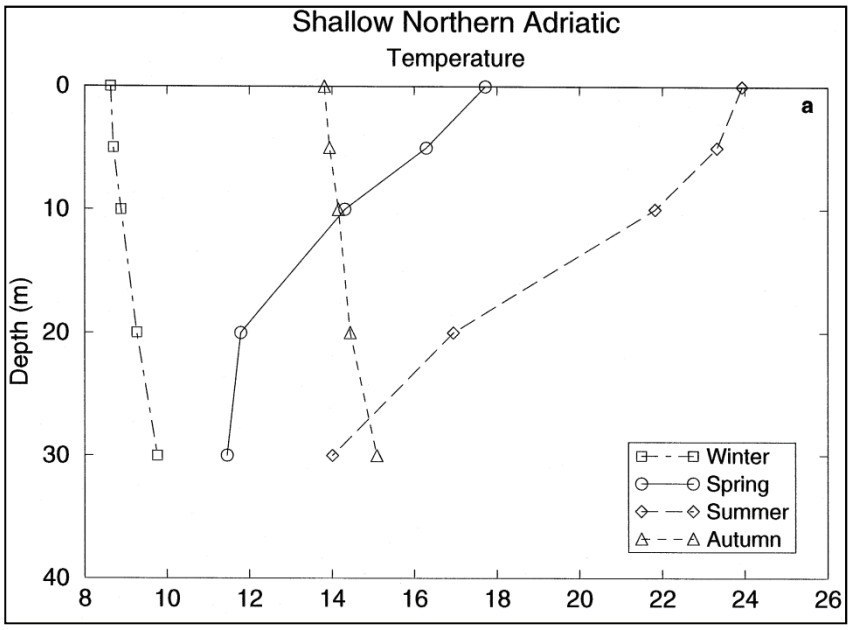

Fig. 9.7. Seasonal vertical profiles of temperature (°C) for the shallow northern Adriatic Sea (from Zavatarelli et al., 1998).

The stratigraphically lowest bed in which *A. islandica* first occurs in the Arda marine succession is at 103.70 m (B in Fig. 9.3). The two analyzed shells from this bed show the highest palaeotemperatures excursions (16.0°C and 16.1°C) and also the lowest palaeotemperatures compared to the other specimens. According to several authors (Kukla et al., 1979; Rio et al. in Van Couvering, 1997) the first appearance of *A. islandica* in the Arda section should be bracketed between 1.77-2.00 Ma. The time interval between 1.77 and 2.00 Ma corresponds in fact to the arrival of the boreal guests (i.e. taxa living nowadays at higher latitudes in the Northern Hemisphere as *A. islandica*) in the Mediterranean Sea indicating that a climatic deterioration occurred in the region.

Herbert et al. (2015) using the alkenone unsaturation method obtained sea surface temperature data for the Mediterranean Sea in the interval between 1.52 and 3.50 Ma. They observed a pronounced cooling at 2.09-2.05 Ma and then a large and apparently abrupt onset of multiple intensely cold glacial episodes beginning at ~1.84 Ma. This timing corresponds, as said above, to the arrival of boreal guests into the Mediterranean Sea (Zachariasse et al., 1990) and also to a pronounced drop in the abundance of the tropical planktonic foraminifer *Globigerinoides ruber* in the Mediterranean as well (Thunell et al., 1991). However, Herbert et al. (2015) observed, that this abrupt change at ~1.84 Ma in the Mediterranean Sea does not leave any identifiable signal in the oceanic marine oxygen isotope record, which does not display an increasing amplitude at this time (Lisiecki & Raymo, 2005; Lawrence et al., 2010).

The Northern Hemisphere Glaciation and the North Atlantic processes affect the continental and marine environment of the Mediterranean region as observed by previous studies (e.g. Becker et al., 2005, 2006). Herbert et al. (2015) thus suggested that particular continental feedbacks related to the Northern Hemisphere Glaciation produced an enhanced interglacial–glacial sensitivity over the Mediterranean region; they suggested that the abrupt change at ~1.84 Ma may signify that it crossed a threshold, with each succeeding glaciation including a significant expansion of ice in northern Europe, leading to large cooling over southern Europe and northern Africa. Recent findings by Martínez-Garcia et al. (2010) show that after 1.80 Ma the sub-Arctic region underwent a substantial cooling associated with sea-ice expansion; this major sub-Arctic cooling led to the formation and advection of cold deep waters from the Northern Hemisphere Seas into the North Atlantic basin, which was recorded further south in the North Atlantic (Sosdian & Rosenthal, 2009). The glacial amplification in the Mediterranean region must have been thus potent regionally, but did not involve significant additional ice volume build up on a global scale as any identifiable signal is registered in the oceanic marine oxygen isotope record.

The oxygen isotope data recorded in *A. islandica* shells from 103.70 m in the Arda section support the presence of a very cold event at ~1.84 Ma, as suggested by Herbert et al. (2015). In fact, preliminary data from pollen analysis of the Arda section suggest that from 91 to 110 m from the base of the section there is a peak of abundance of xerophytic plant pollen and microthermal plant pollen suggesting an increase in seasonality and colder winters (Dr. M. Pound, pers. comm.). The situation changes above, from 110 m, where mesothermal plant pollen and herbaceous plants increase, suggesting that afterwards there were milder winters, but an opening of the environment due to more seasonal rainfall. This is thus in agreement with the reconstruction of the climate in the Mediterranean region around 1.80 Ma.

A possible explanation of the high seasonality and the low palaeotemperatures registered in the shells at 103.70 m is to research in the inflowing of North Atlantic polar surface water in the Mediterranean Sea (up to 200 m of depth) and in the circulation pattern of the Adriatic Sea.

The Mediterranean climate is in fact directly influenced by cold currents from the Northern Hemisphere, whereas the atmospheric component affect the system only indirectly (e.g. Becker et al., 2005, 2006). The lack of an increasing amplitude in the oceanic marine oxygen isotope record at ~1.84 Ma may simply signify that any significant event occurs in the global dynamics of the Northern Hemisphere Glaciation in this interval; a substantial and local cooling associated with sea-ice expansion however has been noted in the sub-Arctic region after 1.80 Ma, which led to the formation and advection of cold water south in the North Atlantic (see above; Martínez-Garcia et al., 2010). Cold currents from the poles continued to arrive in the Mediterranean Sea as before (maybe colder due to the sub-Arctic cold waters) causing a progressively cooling of the seawater, until a cooling threshold was reached and crossed, acting as a trigger factor for the final arrival of the boreal guests.

The Northern Adriatic Sea is nowadays a site of dense and deep water formation (Cacho et al., 2000); cold currents from the North Atlantic inflowing in the Adriatic sea, could have enhanced the formation of denser and colder water than usual, resulting in the very low palaeotemperatures calculated in *A. islandica* shells. Dense, cold and thus more saline waters produced an increase in $\delta^{18}O_{sw}$; this may explain the very low palaeotemperatures apparently recorded.

Also, surface circulation patterns caused by the inflow of North Atlantic water in the Mediterranean Sea show a high annual-interannual variability (Cacho et al., 2000); as dense water formation in the Mediterranean Sea occurred during winter months, the high seasonality recorded in the shells is mostly due to enhanced winter cooling, without a correspondent summer cooling.

The cold event recorded in the *A. islandica* shells at 103.70 m in the Arda River succession thus represents an important and distinct cold episode, which indicates that an abrupt change occur in this moment in the Mediterranean Sea, which led to the arrival of the boreal guests.

The oxygen signals of the other three shells of *A. islandica* provide important information for the subsequent evolution. Taking into account the different living depths of the other three specimens (20 m for ACG200-13, 10 m for ACG215-5 and 15 m for ACG254-1), an increasing trend in $\delta^{18}O_{max}$ - $\delta^{18}O_{min}$ variation and thus in palaeotemperatures excursion is noted, thus indicating that seasonality increases toward the top of the section. This supports the increase in seasonality from 174 m up to the upper part of the section (224 m for the *A. islandica* record), inferred from the isotope record of *Glycymeris* shells. However, comparing the oxygen data from these *A. islandica* shells with those from the bed of its first occurrence (103.70 m), palaeotemperatures are higher, but their annual excursions is

lower. This suggests that the bed at 103.70 m (i.e. the arrival of boreal guests) represent a turning point in the evolution of the region.

From 110 m upward the Arda section records an increase in terrigenous input and sedimentation rates (up to 40 m/ka compared to 15 m/ka in the previous interval), and a shift in the pollen flora with taxa preferring milder winters becoming dominant (Dr. M. Pound preliminary data). All these data suggest that probably in this interval the Apennine chain was rapidly uplifting, causing a perturbation in the climate system.

The Apennine uplift may have acted as a shield from cold and dry continental air masses coming from the Northern Hemisphere, producing a strong orographic influence on the local climate. Cold marine currents continued to inflow into the Mediterranean Sea from the Atlantic and dense and cold water kept on forming in the Adriatic Sea; however the tectonic activity has to some degrees obscured the impact of the climatic variations linked to the Northern Hemisphere Glaciation.

The analysis of the oxygen isotope record recorded by *A. islandica* shells highlights the complex palaeoclimatic evolution which is registered by the biota of the Arda succession. Despite this, it is clear that the Northern Hemisphere Glaciation and its dynamics exerted a strong control on the palaeoclimatic evolution of the Mediterranean Sea.

9.7.2.2.2 Carbon isotopes

As for *Glycymeris* shells no significant decreasing trend has been observed in *A. islandica* shells during growth, allowing to conclude also in this case that, if present, vital effect affecting carbon isotopes is negligible. Analyzing the carbon isotope record in *A. islandica* is very difficult to detect a characteristic cyclicity, which is instead well distinct in the oxygen isotope curves; therefore it is not always possible to identify a seasonal signal.

In the majority of cases a positive correlation between the peaks of $\delta^{18}O$ and those of $\delta^{13}C$ is observed; this indicates higher values of $\delta^{13}C$ during the winter season. As discussed in the *Glycymeris* carbon isotopes paragraph, phytoplankton bloom in the Adriatic Sea occurs during winter and autumn (Zavatarelli et al., 1998). The positive correlation between $\delta^{18}O$ and $\delta^{13}C$ in *A. islandica* shells is thus explained with the winter phytoplankton bloom which removes ^{12}C by photosynthesis from the seawater, leaving it enriched in ^{13}C.

All the specimens of *A. islandica* show high carbon mean values, compared to *Glycymeris* shells (except for *G. inflata*). *A. islandica* shells lived below the thermocline, thus the high mean carbon isotope values may be due to the lack of salinity influence, depth and to spring-summer water stratification which enhanced export of organic matter (Zavatarelli et al., 1998).

It is worthy of note that the two coldest events recorded by *A. islandica* shells (the coldest at 103.70 m and the other one at 185.70 m), for which I used a V-SMOW of +1.0 ‰ to calculate palaeotemperatures, record also the highest mean carbon values (+2.80‰, +2.24‰ and +1.90‰).
During cold periods deep water masses are not only denser (thus high $\delta^{18}O$), but also better ventilated (thus high $\delta^{13}C$) (Cacho et al., 2000); this fact may account for the high carbon mean values in these beds.

9.8 Conclusions

The stable oxygen and carbon isotope analyses across growth lines of ten shells coming from seven stratigraphic beds from the lower part to the top of the Arda section allow to reconstruct the complex palaeoclimatic and palaeoenvironmental evolution of the region. The major difficulty in analyzing the oxygen and carbon shell profiles is due to the several factors affecting the isotope record; furthermore the Arda succession was deposited in an estuarine setting affected by river floods, thus hydrological variability enormously complicates the interpretation of stable isotope signals.
The palaeoclimatic and palaeoenvironmental evolution of the succession can be divided into three intervals, each of them controlled by the Northern Hemisphere Glaciation dynamics:

- Base of the section – 103.70 m. This interval records the palaeoclimatic conditions before the arrival of the boreal guests in the Mediterranean Sea and thus before the abrupt climatic changes at 1.84 Ma (e.g. Herbert et al., 2015). The isotope profiles of *Glycymeris inflata* records a low seasonality (5.7°C) and a high carbon values, which can be explained by both its living depth below the thermocline and by the minor control exerted by the Northern Hemisphere Glaciation on the Mediterranean climate in this interval.
- 103.70 – 110 m. This interval corresponds to the arrival of the boreal guests in the Mediterranean Sea. It represents a very cold episode, also supported by other proxies in the Mediterranean region (Herbert et al., 2015), during which shells record a high seasonality and very low palaeotemperatures. This is also supported by preliminary analysis of pollen data from the Arda section. The trigger factor promoting the arrival of boreal guests in the Mediterranean Sea is to research mainly in a change in the seawater. Cold currents from the North Atlantic entered the Mediterranean Sea with annual-interannual variability causing a progressively cooling of the seawater (Cacho et al., 2000). The abrupt change occurring in this interval may signify that a cooling threshold is reached and crossed, acting as a trigger factor for the final arrival of the boreal guests. Cold current inflows may have increase after 1.80 Ma when the sub-Arctic region underwent a substantial cooling associated with sea-ice expansion,

which led to the formation and advection of cold waters from the Northern Hemisphere Seas further south in the North Atlantic, and thus in Mediterranean Sea (Martínez-Garcia et al., 2010); this sub-Arctic ice expansion is indirectly linked to the Northern Hemisphere Glaciation dynamics, which in this moment exerted a strong control on the seawater temperatures.

- 110 m - top of the section. Shells occurring in this interval (both of species of *Glycymeris* and *Arctica*) record a clear increase in seasonality toward the top of the Arda section. However, they registered higher palaeotemperatures compared to the interval of the arrival of boreal guests described above, and in the case of *A. islandica* also a lower, but still increasing, seasonality. In this interval, the Apennine chain was rapidly uplifting, causing a perturbation in the Mediterranean climate system. The Apennine uplift may have acted as a shield for cold and dry continental air masses coming from the Northern Hemisphere, locally obscuring the impact of the climatic variations linked to the Northern Hemisphere Glaciation dynamics.

The complex palaeoclimatic and palaeoenvironmental evolution of the Arda River succession points out that the Mediterranean region was strongly affected by the Northern Hemisphere Glaciation dynamics, which exerted a strong control on the Mediterranean climate during most of the Early Pleistocene. The significantly cold event recorded at 103.70 m, indicates that the arrival of the boreal guests in the Mediterranean Sea was accompanied by a high seasonality and by particularly cold winters.

Seasonality increases approaching the Middle Pleistocene Transition and the beginning of the continental glaciations in the Northern Hemisphere, representing thus a clear signal of climatic deterioration in the Mediterranean Sea during the Early Pleistocene. However, any cooling trend in the average seawater temperatures has been observed both in sclerochemical and bulk shells oxygen isotope data in this interval.

The changes in seasonality may well have amplified and propagated the signal of climate change toward the Middle Pleistocene Transition, representing thus a very important component in abrupt climate switches.

Chapter 10
Conclusions

The Arda River marine section is 237.40 m-thick and consists of sandstones, siltstones and mudstones bounded at the top by continental conglomerates indicating a major sea level drop. The succession formed in an hyperpicnal system during phases of advance of fan deltas affected by high-density flows triggered by river floods and deposited when Apennine tectonic uplift renewed sediment dispersal and provided the basin with a steeper margin.

The rich macrofauna of the Arda section comprises 159 taxa: bivalves (the dominant group), gastropods, corals, serpulids, brachiopods, echinoids, barnacles, bryozoans and scaphopods. The fauna is characterized by both infaunal and epifaunal species, of shallow and deep infralittoral and circalittoral environments. The comparative sedimentological and palaeoecological analysis allows to conclude that the Arda marine succession was deposited in an infralittoral to a shallow circalittoral environment, where the maximum depth of the succession should not have exceeded 40-50 m. The palaeoecological analysis of the fauna also confirms the general regressive trend of the marine succession.

Based on mollusk and nannofossil biostratigraphy the Arda River section has a late Gelasian-Calabrian age (Early Pleistocene). Although U-Pb dating analysis gave no results, magnetostratigraphic analyses are in progress by Prof. G. Muttoni and his group, who may provide additional data to better constrain the age of the Arda section.

From a palaeoclimatic point of view the occurrence of boreal guests, such as *Arctica islandica, Pseudamussium septemradiatum* and possibly also *Mytilus edulis*, suggests that a climatic change

occurred in the Arda marine succession starting around 103 m from its base, with a shift to colder seawater temperatures or to a more seasonal climate with colder winters.
Preliminary data from pollen analysis suggest that a climatic change occurs also in the Arda flora; in particular pollen data suggest the presence between 91 and 110 m of an interval characterized by a high seasonality with taxa preferring colder winters, which is followed by an interval in which taxa preferring milder winters are dominant, thus possibly indicating a glacial/interglacial shift.

The isotope and sclerochemical analyses on bivalve shells, deemed to be pristine based on four different screening tests (SEM microstructural examination, Cathodoluminescence, X-ray Powder Diffraction and Feigl's solution), allowed to interpret in more details the palaeoclimatic evolution of the Arda section.
A mean oxygen curve has been constructed from the bulk data obtained from species of the three genera *Glycymeris, Aequipecten* and *Arctica*. Even if based on a discontinuous record, this curve can be correlated to the Atlantic and Mediterranean MIS stacks, and show a better correlation with the former, also based on benthic taxa. The observed cyclicity, even if irregular due to the discontinuous record of macrofossils, may be compatible with a control by obliquity.
The main outcome of the bulk isotope analysis is that seasurface palaeotemperatures do not show any significant cooling during Gelasian and Calabrian (Early Pleistocene). The lack of a cooling trend seems to be typical of the Mediterranean region (Lourens et al., 1996; Lourens, 2004) and may be due to factors such as local currents, uplift of the Apennines, and rates of continental weathering.
Sclerochemical analyses give further detail on the palaeoclimatic evolution of the section. Before the arrival of the boreal guests (base of the section to 103.70 m), bivalve shells record a low seasonality (5.7°C), suggesting that probably the Northern Hemisphere Glaciation exerted a minor control on the Mediterranean climate at this time. The stratigraphic interval corresponding to the arrival of the boreal guests in the Mediterranean Sea (103.70 – 110 m) is recorded in the shells as a very cold episode, as it is also supported by other proxies in the Mediterranean region (Herbert et al., 2015); besides low palaeotemperatures, *A. islandica* shells record a high seasonality. I interpret this as the result of cold currents from the North Atlantic entering the Mediterranean Sea with annual-interannual variability causing a progressively cooling of the seawater, particularly so during winter (SST of about 2°C); the abrupt change occurring in this interval may signify that a cooling threshold was reached and crossed, acting as a trigger factor for the arrival and successful recruitment of the boreal guests. As said above, an increase in seasonality is also confirmed by the pollen analysis, suggesting that both marine and continental environments underwent a significant change in this interval, with the Northern Hemisphere Glaciation dynamics exerting a strong control on the Mediterranean climate. This cold

episode is followed by a stratigraphic interval (110 m - top of the section) in which lower seasonality and higher palaeotemperatures are recorded compared to the previous beds. However, through this interval, a clear increasing trend in seasonality is observed in the shells, which culminates in the uppermost marine sediments at the top of the section. At this time the Apennine chain was rapidly uplifting, as suggested by a change in the pollen content, increase in the sedimentation rate and increase in terrigenous input, causing a perturbation in the Mediterranean climate system, which has to recover a new equilibrium. The Apennine uplift may have acted as a shield for cold and dry continental air masses coming from the Northern Hemisphere, locally obscuring the impact of the climatic variations linked to the Northern Hemisphere Glaciation dynamics. However, the signal of a progressive climate deterioration and of enhanced glacial/interglacial dynamics is still present in the bivalve shells in the form of an increasing seasonality.

To conclude, the complex palaeoclimatic and palaeoenvironmental evolution of the Arda River succession points out that the Mediterranean region was affected by the Northern Hemisphere Glaciation dynamics, which exerted a strong control on the Mediterranean climate during most of the Early Pleistocene. The distinctively cold event recorded at 103.70 m, indicates that the arrival of the boreal guests in the Mediterranean Sea was accompanied by a high seasonality and by particularly cold winters, as suggested by both bivalves and pollen analyses.

Then, after a return to background values, seasonality increases again approaching the Middle Pleistocene Transition and the beginning of the continental glaciations in the Northern Hemisphere; however, no cooling trend in the average seawater temperatures has been observed both in sclerochemical and bulk shells oxygen isotope data in this interval.

The changes in seasonality may well have amplified and propagated the signal of climate change toward the Middle Pleistocene Transition, representing thus a very important component in abrupt climate switches.

Appendix A

Systematic description and ultrastructure of species of the genera *Glycymeris, Aequipecten* and *Arctica*

A.1 Systematic descriptions

The systematic description of the species belonging to the genus *Glycymeris* Da Costa, 1778, *Aequipecten* Fischer, 1886 and *Arctica* Schumacher, 1817 are here presented. These species are very abundant and regularly present along all the Arda River marine succession; they have been selected for geochemical and isotopic analyses undertaken in this project and for this reason they are here in detail analyzed from the systematical point of view (Crippa & Raineri submitted).

The systematic descriptions below follow the classification of Cox et al. (1969) and Oliver & Holmes in Bieler & Mikkelsen (2006) for the Arcoidea, of Waller et al. in Bieler & Mikkelsen (2006) for the Pectinoidea and of Cox et al. (1969) and Bieler & Mikkelsen (2006) for the Arcticoidea.

Class BIVALVIA Linnaeus, 1758 (Buonanni, 1681)

Subclass PTERIOMORPHIA Beurlen, 1944

Order ARCOIDA Stoliczka, 1871

Superfamily ARCOIDEA Lamarck, 1809

Family GLYCYMERIDIDAE Dall, 1908

Genus *Glycymeris* Da Costa, 1778

Type-species. *Glycymeris glycymeris* (Linnaeus, 1758) from the Recent of the Mediterranean Sea.

Remarks. Cox et al. (1969) identified two subgenera for *Glycymeris* Da Costa, 1778: *Glycymeris* s.s. and *Glycymerita*. Here, I follow Squires (2010) in abandoning subgenera definition for *Glycymeris* and in considering *Glycymerita* as a distinct genus (Squires, 2010), as its shell surface has many prominently raised radial ribs with well defined narrow interspaces in contrast to the mainly smooth surface of *Glycymeris*.

Glycymeris, as other *Glycymeridídae*, has a deceptive valve orientation, which does not follow the classical rules: the larger adductor scar is the anterior one and not the posterior as usually happens in other bivalve groups (see Nicol & Jones, 1984).

Glycymeris glycymeris (Linnaeus, 1758)

Pl. 1, figs. 1,2; Pl. 2, figs. 1,3

1758 *Arca glycymeris* Linnaeus, p. 695

1966 *Glycymeris glycymeris* (Linnaeus) – Tebble, p. 33, pl. 2, figs. a-c

1970 *Glycymeris glycymeris* (Linnaeus) – Buccheri, p. 256

1974 *Glycymeris glycymeris* (Linnaeus) – Parenzan, p. 47, pl. 5, fig. 40

1980 *Glycymeris (Glycymeris) glycymeris* (Linnaeus) – Anfossi & Brambilla, p. 58, pl. 5 (1), figs. 7a-c

1986 *Glycymeris (Glycymeris)* aff. *G. (G.) glycymeris* (Linnaeus) – Domenech, p. 135, figs. 4I-J (cum syn.)

1986 *Glycymeris glycymeris* (Linnaeus) – Riedl, p. 359, pl. 122

1988 *Glycymeris glycymeris* (Linnaeus) – Gomez-Alba, p. 168, pl. 83, fig. 11

1993 *Glycymeris (Glycymeris) glycymeris* (Linnaeus) – Lozano Francisco et al., p. 172, pl. 5, figs. 1,2

Material. Six right valve: ACG14-12-22-24, ACG27bis-7, ACG243-1-2; twelve left valves:ACG14-1-2-3-4-5-11-13-23, ACG26-4, ACG27bis-8, ACG35-1, ACG241-1; one undetermined valve: ACG28-1.

Occurrence. AGC14, ACG26, ACG27bis, ACG28, ACG35, ACG241, ACG243, Arda River section, Castell'Arquato, Italy.

Description. Large to medium sized biconvex shell, equivalve, slightly inequilateral with circular outline; shell substance thick; valves slightly inflated with low and not very prominent orthogyrate to slightly opisthogyrate umbo; dorso-ventral diameter nearly equal to antero-posterior one. Ornamentation of both valves consisting of thin radial costellae, and irregular concentric growth lines; the latter pass to coarse growth lamellae in the postero-ventral part of the valve; ventral internal margin regularly fluted.

Interior of both valves with prionodont dentition with teeth relatively short, laterally V shaped, obsolescent in the central part and more evident laterally, determining a division in two part of the dentition; ligament area high, narrow, triangular and flat or slightly concave; external ligament amphidetic duplivincular well preserved.

Muscle scar dimyarian anisomyarian with integripalliate circular pallial line; anterior adductor muscle scar with triangular shape and larger than the posterior subcircular and suboval muscle scar; both adductor muscle scars are well impressed on a low myophoric platform; scars of radially directed fibers of muscle mantle along the pallial line.

Dimensions. Figs. A.1,A.2 and Table 1 in the appendix A.1.

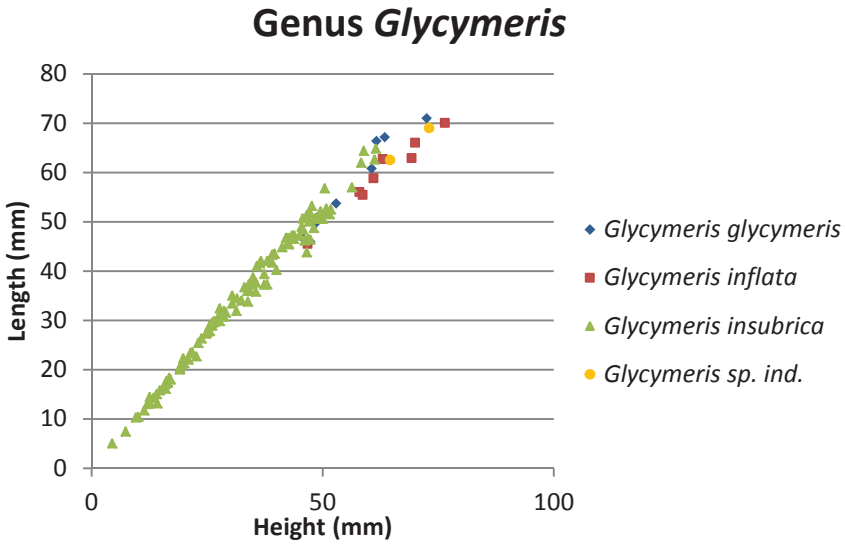

Fig. A.1. Height and length values of species of *Glycymeris*.

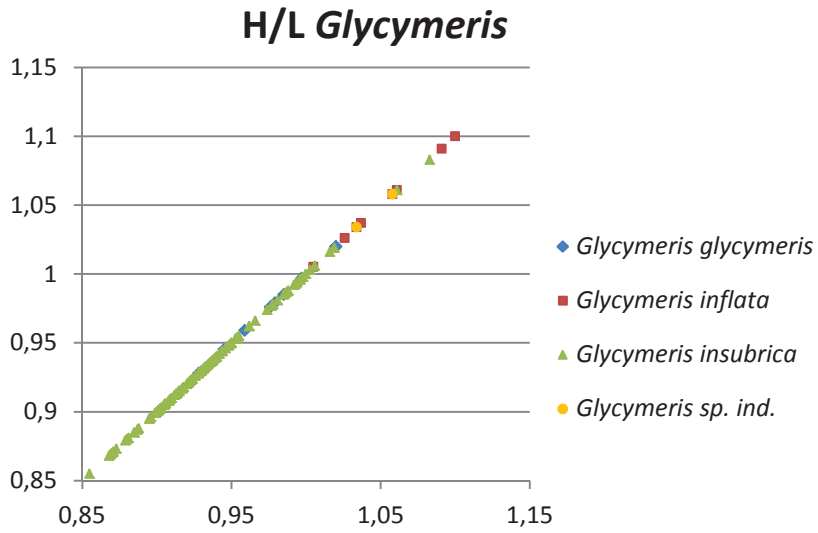

Fig. A.2. Height/length ratio of species of *Glycymeris*.

Discussion. *Glycymeris glycymeris* has a circular outline and poorly inflated valves; for these characters it differs from *Glycymeris bimaculata* (Poli, 1795), *Glycymeris inflata* (Brocchi, 1814) and *Glycymeris insubrica* (Brocchi, 1814). Furthermore the ligament area is slightly different from the other species of *Glycymeris*, because it is high but not laterally expanded.

Glycymeris glycymeris together with *Glycymeris inflata,* represent the larger species (Fig. A.1) with a H/L ratio nearly equal 1 (Fig. A.2), which allow to distinguish it from the other *Glycymeris* species.

Stratigraphic and geographic occurrence. *Glycymeris glycymeris* is known from the Miocene to the Recent from the Western Atlantic coast to the Mediterranean sea (Marasti & Raffi, 1980). See also Chapter 3)

Glycymeris inflata (Brocchi, 1814)

Pl. 1, fig. 3; Pl. 2, figs. 4,5; Pl. 3, fig. 1

1814 *Arca inflata* Brocchi, p. 494, pl. 11, fig. 7

1877 *Pectunculus inflatus* (Brocchi) – Seguenza, p. 282-283

1879-1882 *Pectunculus insubricus* var. (Brocchi) – Fontannes, p. 175, pl. 11, fig. 3

1898 *Pectunculus inflatus* (Brocchi) – Almera & Bofill, p. 126

1898 *Axinea inflata* (Brocchi) – Sacco in Bellardi & Sacco, p. 32, pl. VIII, figs. 1-10 (cum syn.)

1907 *Pectunculus inflatus* (Brocchi) – Cerulli Irelli, p. 119, pl. 9, fig. 7; pl. 10, figs. 1, 9

1914 ? *Pectunculus (Axinaea) insubricus* (Brocchi) – Bongo, p. 475

1933 *Pectunculus (Axinea) inflatus* (Brocchi) – Boni, p. 146

1935 *Pectunculus (Axinea) inflatus* (Brocchi) – Cowper Reed, p. 510

1937 *Pectunculus inflatus* (Brocchi) – Dubertret et al., p. 100

1938 *Pectunculus (Axinea) inflatus* (Brocchi) – Tavani, p. 147, pl. 5, fig. 2
1950 *Pectunculus (Axinea) inflatus* (Brocchi) – Festa, p. 96
1951 *Glycymeris inflata* (Brocchi) – Imbesi, p. 11
1951 *Glycymeris (Glycymeris) inflatus* (Brocchi) – Rossi Ronchetti, p. 20, figs. 5a-f
1952 *Pectunculus inflatus* (Brocchi) – Lecointre, p. 61
1955 *Pectunculus (Axinea) inflatus* (Brocchi) – Malatesta & Nicosia, p. 176
1957 *Glycymeris (Glycymeris) inflatus* (Brocchi) – Nicosia, p. 176
1957 *Glycymeris (Glycymeris) inflatus* (Brocchi) – Malatesta, p. 22
1958 *Glycymeris (Glycymeris) inflatus* (Brocchi) – Erunal Erentoz, p. 144, pl. 22, figs. 19,20
1962 *Glycymeris (Glycymeris) inflatus* (Brocchi) – Papani & Pelosio, pp. 306, 316, pl. 2, fig. 12
1963 *Glycymeris (Glycymeris) inflata* (Brocchi) – Malatesta, p. 233, pl. XIII, fig. 3
1968 *Glycymeris (Glycymeris) inflatus* (Brocchi) – Bonadonna, p. 286
1971 *Glycymeris (Glycymeris) inflata* (Brocchi) – Pesce & Rapetti, p. 124, pl. 1, fig. 3
1972 *Glycymeris (Glycymeris) inflata* (Brocchi) – Caprotti, p. 56, pl. 3, fig. 19
1973 *Glycymeris (Glycymeris) inflatus* (Brocchi) – Marasti, p. 100
1974 *Glycymeris (Glycymeris) inflata* (Brocchi) – Malatesta, p. 30, pl. 2, figs. 2a,b
1976 *Glycymeris inflata* (Brocchi) – Caprotti, p. 4, pl. 6, fig. 19
1980 *Glycymeris (Glycymeris) inflata* (Brocchi) – Anfossi & Brambilla, p. 58, pl. V(I), figs. 8a,b
1993 *Glycymeris (Glycymeris) inflata* (Brocchi) – Lozano Francisco et al., p. 174, pl. 5, figs. 5,6

Material. three articulated specimens: ACG10-4, ACG14-25, ACG24-33; twelve right valves: ACG9-3, ACG14-14, ACG29bis-1-5-7-9-28-29-30-33-34-36; nine left valves: ACG9-4, ACG14-6, ACG29bis-2-3-6-31-32-35-37.

Occurrence. ACG9, ACG10, ACG14, ACG24, ACG29bis, Arda river section, Castell'Arquato, Italy.

Description. Large sized, biconvex shell slightly inequivalve and inequilateral with subcircular, slightly elongated outline; shell substance thick; valves strongly inflated with prominent orthogyrate to slightly opisthogyrate umbo; dorso-ventral diameter larger than antero-posterior one. Both valves show a ridge in their posterior part, extending from the umbo to the ventral margin and forming an obtuse angle in the shell outline.

Ornamentation of both valves consisting of very fine, regular and dense radial costellae and in numerous concentric growth lines; the latter become growth lamellae irregularly spaced in the postero-ventral part of the valve; ventral interior margin regularly fluted.

Interior of both valves with prionodont dentition with teeth relatively short, laterally V shaped, becoming obsolescent or vertically directed in the middle part; ligament area high, laterally expanded, triangular and flat or slightly concave; external ligament amphidetic duplivincular well preserved.

Muscle scar dimyarian anisomyarian with integripalliate circular pallial line; anterior adductor muscle scar with triangular shape and slightly larger than the posterior subcircular to suboval muscle scar; both adductor muscle scars are well impressed on a myophoric platform (the posterior one is more elevated); scars of radially directed fibers of muscle mantle along the pallial line. Posterior pedal retractor scar with a small calcified platform.

Dimensions. Figs. A.1,A.2 and Table 2 in the appendix A.1.

Discussion. *Glycymeris inflata* mainly differs from *Glycymeris bimaculata* (Poli, 1795), *Glycymeris glycymeris* (Linnaeus, 1758) and *Glycymeris insubrica* (Brocchi, 1814) for its more elongated outline and for its peculiar ridge in the posterior part of the valve, which defines an obtuse angle in the shell outline. The height/length ratio is always higher than 1 (Fig. A.2). Furthermore it differs from *Glycymeris glycymeris* (Linnaeus, 1758) because it is strongly inflated and from *Glycymeris insubrica* (Brocchi, 1814) because it is larger and it has a weaker radial ornamentation.
Glycymeris inflata together with *Glycymeris glycymeris,* represent the larger species (Fig. A.1) with a H/L ratio higher than 1 (Fig. A.2), which allow to distinguish it from the other *Glycymeris* species.

Stratigraphic and geographic occurrence. *Glycymeris inflata* is a species known from the Miocene to the Pleistocene (Marasti & Raffi, 1980) of the Mediterranean sea. Its recent occurrence (Altaba et al., 2006) is still debated.

Glycymeris insubrica (Brocchi, 1814)
Pl. 1, fig. 4; Pl. 2, fig. 2; Pl. 3, figs. 2-7

1758 *Arca nummaria* Linnaeus, p. 695
1805 *Pectunculus cor* Lamarck, p. 217
1814 *Arca insubrica* Brocchi, p. 492, pl. XI, figs. 10a,b
1819 *Pectunculus violacescens* Lamarck, p. 52
1825 *Pectunculus insubricus* (Brocchi) – Borson, p. 124
1826 *Pectunculus insubricus* (Brocchi) – Risso, p. 318
1831 *Pectunculus insubricus* (Risso) – Bronn, p. 108
1837 *Pectunculus insubricus* (Brocchi) – Goldfuss, p. 161
1868 *Pectunculus insubricus* (Brocchi) – Mayer, p. 44-46
1873 *Pectunculus violacescens* (Lamarck) – Cocconi, p. 126
1878 *Pectunculus insubricus* (Brocchi) – Parona, p. 91
1879 *Pectunculus nummarius* (Linnaeus) – Jeffreys, p. 32

1886 *Pectunculus insubricus* (Brocchi) – Verri, p. 442

1895 *Pectunculus violacescens* (Lamarck) – Arduini, p. 50

1898 *Pectunculus insubricus* (Brocchi) – Almera & Bofill, p. 126

1898 *Axinea insubrica* and var. (Brocchi) – Sacco in Bellardi & Sacco, p. 33, pl. 8, figs. 11-21

1907 *Pectunculus (Axinea) insubricus* (Brocchi) – Cerulli Irelli, p. 121, pl. XI, fig. lb, 2.

1915 *Pectunculus insubricus* (Brocchi) – Dalloni, p. 453

1949a *Glycymeris insubricus* (Brocchi) – Ruggieri, p. 27

1949b *Glycymeris insubricus* (Brocchi) – Ruggieri, p. 69

1950 *Pectunculus (Axinea) insubricus* (Brocchi) – Festa, p. 96

1951 *Glycymeris (Glycymeris) insubricus* (Brocchi) – Rossi Ronchetti, p. 22, figs. 6a-f

1951 *Glycymeris violacescens* (Lamarck) – Imbesi, p. 129

1952 *Pectunculus violacescens* (Lamarck) – Lecointre, p. 62

1957a *Glycymeris insubricus* (Brocchi) – Ruggieri, p. 31

1957b *Pectunculus insubricus* (Brocchi) – Ruggieri, p. 6

1962 *Glycymeris insubricus* (Brocchi) – Papani & Pelosio, p. 16

1964 *Glycymeris (Glycymeris) cor* (Lamarck) – Erunal Erentoz & Oztemur, p. 262

1967 *Glycymeris (Glycymeris) cor* (Lamarck) – Conato et al., p. 261

1971 *Glycymeris (Glycymeris) cor* (Lamarck) – Pesce & Rapetti, p. 122, pl. 1, fig. 2

1974 *Glycymeris (Glycymeris) violacescens* (Lamarck) – Malatesta, p. 31, pl. 2, figs. 1a-c

1974 *Glycymeris violacescens* (Lamarck) – Parenzan, p. 50, pl. 6, fig. 43

1980 *Glycymeris (Glycymeris) insubrica* (Brocchi) – Marasti & Raffi, p. 8

1982 *Glycymeris (Glycymeris) insubrica* (Brocchi) – Benigni & Corselli, p. 675

1982 *Glycymeris (Glycymeris) insubricus* (Brocchi) – Andrés, p. 118, pl. 2, figs. 1-4

1982 *Glycymeris (s.s.)* aff. *violacescens* (Lamarck) – Martinell & Domenech, p. 382

1983 *Glycymeris (Glycymeris)* aff. *insubrica* (Brocchi) – Domenech, p. 93, pl. 3, figs. 1-3, 7, 8

1986 *Glycymeris (Glycymeris)* aff. *G. (G.) insubrica* (Brocchi) – Domenech, p. 137, figs. 4K-L

1988 *Glycymeris insubrica* (Brocchi) – Gomez-Alba, p. 170, pl. 84, fig. 4

1989 *Glycymeris (Glycymeris) insubrica* (Brocchi) – Andrés, p. 336, pl. 2, figs. 1-4 (cum syn.)

1992 *Glycymeris insubrica* (Brocchi) – Cossignani et al., p. 31, fig. 268

1993 *Glycymeris (Glycymeris) insubrica* (Brocchi) – Lozano Francisco et al., pl. 1, figs. 9-10

Material. Forty-one articulated specimen: ACG29-2, ACG46-1-2-3, ACG49-2-3, ACG91-3-10, ACG94-13; ACG97bis-1, ACG197-1-2, ACG198-5-6, ACG200-6-7, ACG202-1, ACG204-1-2, ACG210-1, ACG252-2, ACG256-1-2-3-4, ACG256bis-1-2, ACG258-1-2, ACG259-4, ACG261-1-2, ACG261bis-1-2-3, ACG262-1-2-3, ACG263-1-4, ACG265-4; sixty-four right valves: ACG29bis-4-8-10-13, ACG30-5, ACG31-1, ACG42-2, ACG42bis-2, ACG43-1, ACG45-2, ACG60-1, ACG66-1-2-5, ACG89-1-2-3, ACG90-3, ACG91-2-5, ACG92-1-2, ACG93-3-4-5-6-7, ACG94-1-4, ACG95-1-2, ACG96-3-4, ACG97-2-3-5-10, ACG98-1-2, ACG99-1, ACG197-4, ACG198-3, ACG200-15; ACG201-4, ACG204-7; ACG215-4, ACG252-1-6, ACG255-1, ACG257-1, ACG258-3-4, ACG259-2, ACG260-2, ACG262-4-5, ACG263-2, ACG264-1-2-4-5, ACG265-1, ACG267-1-2; sixty-five left valves: ACG9-2, ACG13-2, ACG29bis-12-14-17-19, ACG45-1, ACG49-1, ACG53-16, ACG59-1, ACG66-3-4-6, ACG68-1, ACG83-1, ACG90-1-2-4-12, ACG91-1-4, ACG92-3,

ACG93-1-2-13, ACG94-2-3-5-6, ACG96-1-2, ACG97-1-4-9-11-12, ACG98-3, ACG197-5-11, ACG199-1-2, ACG203-1-2-3, ACG204-3-4-5-6, ACG205-1-2-3, ACG206-1, ACG211-1, ACG252-3-4, ACG257-2, ACG259-1-3-5, ACG260-1, ACG263-5, ACG264-3, ACG265-2, ACG266-1, ACG267-3.

Occurrence. ACG9, ACG13, ACG29, ACG29bis, ACG30, ACG31, ACG42, ACG42bis, ACG43, ACG45, ACG46, ACG49, ACG53, ACG59, ACG60, ACG66, ACG68, ACG83, ACG89, ACG90, ACG91, ACG92, ACG93, ACG94, ACG95, ACG96, ACG97, ACG97bis, ACG98, ACG99, ACG197, ACG198, ACG199, ACG200, ACG201, ACG202, ACG203, ACG204, ACG205, ACG206, ACG210, ACG211, ACG215, ACG252, ACG255, ACG256, ACG256bis, ACG257, ACG258, ACG259, ACG260, ACG261, ACG261bis, ACG262, ACG263, ACG264, ACG265, ACG266, ACG267, Arda river section, Castell'Arquato, Italy.

Description. Medium sized, biconvex shell, nearly equivalve, slightly inequilateral with transverse, subquadrate to subrectangular outline; shell substance not so thick; some specimens have a rounded anterior margin and a straight posterior one; valves inflated with orthogyrate to slightly opisthogyrate umbo.

Ornamentation of both valves consisting of fine, regular and dense radial costellae, numbering 1-3 in 5 mm at the ventral margin in adult specimens; radial ornamentation more marked than concentric one; concentric and very thin growth lines, which in some specimens become more pronounced in the ventral part where they form coarse lamellae; ventral interior margin regularly fluted. In some juvenile specimens and in the juvenile region of the adult specimens the violet color ornamentation is preserved with concentric variations of tone and reddish mottles.

Interior of both valves with prionodont dentition with teeth relatively short, laterally V shaped, becoming obsolescent or vertically directed medially; ligament area laterally expanded but low, triangular, flat or slightly concave; external ligament amphidetic duplivincular.

Muscle scar dimyarian anisomyarian with integripalliate circular pallial line; anterior adductor muscle scar with triangular shape, slightly larger than the posterior subcircular to suboval muscle scar; both adductor muscle scars are well impressed on a myophoric platform; scars of radially directed fibers of muscle mantle along the pallial line. Subrhomboidal posterior pedal retractor scar.

Dimensions. Figs. A.1,A.2 and Table 3 in the appendix A.1.

Discussion. *Glycymeris insubrica* has a great intraspecific variability; according to Andrés (1989) two forms can be distinguish: the first, called "*insubrica*", corresponds to that described by Brocchi (1814), whereas the second, called "*violacescens*", corresponds to that described by Lamarck (1819); these two forms differs mainly for the outline, more quadrangular, regular and equilateral in the

"*violacescens*" form. *Glycymeris violacescens* and *Glycymeris insubrica* are now considered synonym; *G. violacescens* is usually used to identify the Recent specimens, whereas *G. insubrica* is for fossil ones.

According to several authors (from Sacco in Bellardi & Sacco, 1898 to Sirna, 1978), in addition to *Glycymeris violacescens* (Lamarck, 1819), other synonyms of *G. insubrica* are *Glycymeris cor* (Lamarck, 1805) and *Glycymeris nummaria* (Linnaeus, 1758). *Glycymeris nummaria* is considered a *nomen oblitum* by Sirna (1978), although WoRMS considers this specific name as the valid one. *Glycymeris cor* has been invalidated because of the inadequate description given for it by Lamarck (1805). For these reasons I have determined the specimens under exam as *Glycymeris insubrica* (Brocchi, 1814).

In general, *Glycymeris insubrica* has a medium sized shell, a subquadrate to subrectangular outline, a pronounced radial ornamentation and a low ligament area; for these characters it differs from *Glycymeris inflata* (Brocchi, 1814), from *Glycymeris bimaculata* (Poli, 1795) and from *Glycymeris glycymeris* (Linnaeus, 1758).

Looking at the graph in fig. A.1 *Glycymeris insubrica* is the species with the smallest size but it also represents the species with the higher number of specimens; among these specimens juvenile forms may occur, which thus may lower the measurements; despite that, the majority of the specimens remain smaller than other *Glycymeris* species. *G. insubrica* has a H/L ratio smaller than 1, which allow to distinguish it from other *Glycymeris* species (Fig. A.2).

Stratigraphic and geographic occurrence. *Glycymeris insubrica* is known from the Early Miocene to the Recent from the Atlantic ocean to the Mediterranean Sea (Marasti & Raffi, 1980). See also Chapter 3.

Glycymeris sp. ind.

Material. Two right valves: ACG14-7, ACG24-4; one left valve: ACG76-25.

Occurrence. ACG14, ACG24, ACG76, Arda river section, Castell'Arquato, Italy.

Description. Large sized, biconvex shell, equivalve, equilateral with subcircular to subquadrate outline; shell substance very thick; valves inflated with orthogyrate to slightly opisthogyrate umbo.

Ornamentation consisting of very fine and regularly arranged radial costellae and concentric growth lines; the latter in the ventral part of the valve become dense and coarse growth lamellae; this produces

a clear division of the valve in two parts: 1) the juvenile-adult dorso-median part characterized by thin growth lines and 2) the oldest ventral part with coarse growth lamellae; ventral interior margin regularly fluted.
Interior of valve with prionodont dentition with coarse teeth, curved, lacking medially; ligament area high, laterally expanded, triangular and flat; external ligament amphidetic duplivincular.
Muscle scars dimyarian anisomyarian with integripalliate circular pallial line; anterior adductor muscle scar with triangular shape and larger than the posterior subcircular one; both adductor muscle scars are well impressed on a myophoric platform; scars of radially directed fibers of muscle mantle along the pallial line.

Dimensions. Figs. A.1, A.2 and Table 4 in the appendix A.1.

Discussion. These specimens have intermediate characters among the above described species: they have a H/L ratio higher than 1 as *Glycymeris inflata* (Fig. A.2), a subcircular outline as *Glycymeris glycymeris* and a thick shell with strong teeth as *Glycymeris bimaculata* (Poli, 1795). At the same time they differs from specimens of *Glycymeris inflata* because they lack the characteristic angle in the anterior valve outline and from *Glycymeris glycymeris* because they are more inflated and have a more prominent umbo. *Glycymeris bimaculata* is the most similar species even if the Arda specimens do not attain the large size typical of the representatives of this species; furthermore they are not well preserved so a specific assignment is difficult.
Glycymeris sp. ind. is similar in size to *G. inflata* and *G. glycymeris* (see Fig. A.1), presuming the affinity with one of these two species; however, as observed in the systematic description, the external and internal characters of *Glycymeris* sp. ind. are different from *G. inflata* and *G. glycymeris*, promoting the fact that it is a distinct species, although the preservation conditions do not allow a more accurate assignment.

Order PECTINOIDA Adams & Adams, 1857
Superfamily PECTINOIDEA Rafinesque, 1815
Family PECTINIDAE Rafinesque, 1815
Subfamily AEQUIPECTININAE Nordsieck, 1969
Genus *Aequipecten* Fischer, 1886

Type-species. *Ostrea opercularis* Linnaeus, 1758 from the Recent of France.

Remarks. Similar to *Chlamys* Roding, 1798, but it differs by its more rounded outline, nearly equal auricles, shallower byssal notch, and fewer, usually not bifurcating radial ribs.

Aequipecten opercularis (Linnaeus, 1758)

Pl. 4, figs. 1-3, 5-7; Pl. 5, fig. 1

1758 *Ostrea opercularis* Linnaeus, p. 698
1873 *Pecten opercularis* (Linnaeus) – Cocconi, p. 385
1884 *Pecten opercularis* (Linnaeus) – Meli, p.12
1898 *Pecten opercularis* (Linnaeus) – Almera & Bofill, p. 112
1902 *Pecten opercularis* (Linnaeus) – De Stefani, p. 5
1906 *Chlamys (Aequipecten) opercularis* (Linnaeus) – Ugolini, p. 163
1907 *Chlamys (Aequipecten) scabrella* (Lamarck) – Cerulli Irelli, p. 92, pl. 5, figs. 17, 18
1910 *Aequipecten opercularis* (Linnaeus) – Schaffer, p. 36, pl. 16, figs. 11-15
1962 *Chlamys opercularis* (Linnaeus) – Boni & Sacchi Vialli, p. 109, pl. 12, figs. 4, 6; pl. 13, fig. 17; pl. 14, fig. 10
1962 *Chlamys (Aequipecten) opercularis* (Linnaeus) – Papani & Pelosio, p. 15
1965 *Lyropecten (Aequipecten) opercularis* (Linnaeus) – Glibert & Van de Poel, p. 26
1966 *Chlamys (Aequipecten) opercularis* (Linnaeus) – Tebble, p. 60, pl. 5, fig. b,d
1968 *Aequipecten (Aequipecten) opercularis* (Linnaeus) – Bonadonna, p. 282
1969 *Aequipecten opercularis* (Linnaeus) – Waller, pl. 1, figs. 5, 7-10
1969 *Aequipecten opercularis* (Linnaeus) – Nordsieck, p. 49, pl. VII, fig. 32.00
1970 *Lyropecten (Aequipecten) opercularis* (Linnaeus) – Buccheri, p. 256
1970 *Chlamys (Aequipecten) opercularis* (Linnaeus) – Raffi, p. 110
1971 *Aequipecten (Aequipecten) opercularis* (Linnaeus) – Pesce & Rapetti, p. 126, pl. 2, fig. 2 (cum syn.)
1972 *Chlamys (Aequipecten) opercularis* (Linnaeus) – Caprotti, p. 58, pl. 1, fig. 5
1974 *Chlamys (Aequipecten) opercularis* (Linnaeus) – Malatesta, p. 45, pl. 3, figs. 3a,b
1976 *Chlamys opercularis* (Linnaeus) – Caprotti, pl. 4, fig. 5
1986 *Chlamys (Aequipecten) opercularis* (Linnaeus) – Faraone, p. 42, figs. 7-14
2009 *Aequipecten opercularis* (Linnaeus) – Jimenez et al., p. 7, figs. 3c-e

Material. Two articulated specimens: ACG132-4, ACG133-1; 261 right valves: ACG2-2-3-4, ACG4-10-13, ACG6-5, ACG9-6, ACG11-1, ACG12-5, ACG13-3-8, ACG14-15, ACG24-7-14, ACG25-2-3-7-8-14-18, ACG26-1-2-3-6-8, ACG27-6, ACG27bis-3-5-6, ACG30-1-7-8, ACG32-1-2, ACG34-3, ACG37-8, ACG41-1-3-4-5-6-7-9-10-12-13-15-16-24-25-26-27-29, ACG41bis-2-3-4-5-6, ACG42-1-3-4-5-6-7-8-9-10-13-14-18-19-20-21-22-23, ACG42bis-1-5-6-7-8-10-11-14-16-17-20-23, ACG43-3, ACG44-1-2, ACG51bis-1-2-3-4-6-7-8-10, ACG52-1B, ACG53-1-3-6-7-8-9-10-11-12-14, ACG54-1-4-5, ACG55-1, ACG56-5, ACG57-2-3-4, ACG59-2-3-5-6-8, ACG60-2-3-5, ACG66-12-13, ACG68-2, ACG70-1-3, ACG76-4-5-6-7-8-9-10-11-12-13-18-20-21, ACG77-1, ACG80-1-2-3, ACG81-1-2-3, ACG82-2, ACG83-2-3, ACG84-1-2-3-4-5-6-7, ACG85-1, ACG89-6-8, ACG90-6-10, ACG91-8, ACG91bis-1-2-3, ACG92-4-8, ACG93-8-10-11, ACG94-10, ACG97-7-8; ACG100-1-2-4, ACG101-1-2, ACG102-3, ACG103-1-2-3, ACG104-1-2-3, ACG105-1, ACG116-1,

ACG132-1-3, ACG194-2-4-6-7, ACG195-1-3-5-7, ACG197-6-7-9-10, ACG198-2-3-4, ACG199-3, ACG200-1-3-4-5, ACG200bis-1-2, ACG201-1-2-3, ACG207-1-3-4, ACG208-2-3-4, ACG215-1-2-3, ACG217-1-2-6, ACG220-4-5, ACG222-1-2-3-6, ACG223-2-3-4-5, ACG235-2-3-5, ACG236-1-3-4-6, ACG237-1-4, ACG238-1-2, ACG239-1-3-4, ACG240-1-2-3, ACG243-4, ACG252-5, ACG253-1, ACG255-2; 150 left valves: ACG6-6, ACG12-1, ACG13-4-10, ACG25-4-5-6-13-20, ACG26-5-7, ACG27-7, ACG27bis-1-2-4, ACG29bis-16-18, ACG30-2, ACG31-2, ACG33-1-2, ACG34-1-2, ACG37-8, ACG41-2-8-11-14-22-23-31, ACG41bis-1, ACG42-11-15-16-17, ACG42bis-3-4-9-12-13-15, ACG44-3, ACG50-1, ACG51-1-2-3-4, ACG51bis-5-9-11-12, ACG52-1A, ACG53-5-13-15, ACG55-2-3, ACG56-1-2-4-10, ACG57-1, ACG59-4-7, ACG60-4-6, ACG61-1, ACG66-7-8-9-10, ACG70-2, ACG76-14-15-16-17-18, ACG82-1-5, ACG89-4-5-7-9-10, ACG90-7-8-11-14-20, ACG91-6-7-9, ACG92-5-6-7, ACG93-9, ACG94-7-8-9, ACG97-6, ACG101-3-4, ACG102-1-2, ACG103-4-5-6, ACG104-4-5, ACG132-2, ACG133-2-3-4, ACG194-1-3-5, ACG195-2-4-6, ACG196-1, ACG197-8-11, ACG198-1-7, ACG199-4-5, ACG200-2, ACG202-2, ACG207-2, ACG208-1, ACG209-1-2, ACG212-1, ACG213-1, ACG213bis-1, ACG217-3, ACG222-4, ACG223-1, ACG235-1-4, ACG236-2-5-6, ACG237-2-3, ACG238-3-4-5, ACG239-2, ACG243-3; One undetermined valves: ACG196-2.

Occurrence. ACG2, ACG4, ACG6, ACG9, ACG11, ACG12, ACG13, ACG14, ACG24, ACG25, ACG26, ACG27, ACG27bis, ACG29bis, ACG30, ACG31, ACG32, ACG33, ACG34, ACG37, ACG41, ACG41bis, ACG42, ACG42bis, ACG43, ACG44, ACG50, ACG51, ACG51bis, ACG52, ACG53, ACG54, ACG55, ACG56, ACG57, ACG59, ACG60, ACG61, ACG66, ACG68, ACG70, ACG76, ACG77, ACG80, ACG81, ACG82, ACG83, ACG84, ACG85, ACG89, ACG90, ACG91, ACG91bis, ACG92, ACG93, ACG94, ACG97; ACG100, ACG101, ACG102, ACG103, ACG104, ACG105, ACG116, ACG132, ACG133, ACG194, ACG195, ACG196, ACG197, ACG198, ACG199, ACG200, ACG200bis, ACG201, ACG202, ACG207, ACG208, ACG209, ACG212, ACG213, ACG213bis, ACG215, ACG217, ACG220, ACG222, ACG223, ACG235, ACG236, ACG237, ACG238, ACG239, ACG240, ACG243, ACG252, ACG253, ACG255, Arda river section, Castell'Arquato, Italy.

Description. Medium sized biconvex shell, inequivalve with orthogyrate, convex umbo; circular outline with height/length ratio nearly equal to 1. Right valve equilateral with slightly curved cardinal margin; anterior and posterior auricles very different in size and shape: the anterior one is large, subrectangular with a deep byssal notch; the posterior one is smaller and with a triangular outline. Left valve slightly inequilateral, more convex than the right valve, with the dorsal region representing the great convexity; posterior part more developed than the anterior one; cardinal margin straight; anterior and posterior auricles nearly similar in size, the anterior is slightly larger than the posterior one and has a shallow byssal notch.

Ornamentation of both valves consisting of 16-21 radial costae, coarser in some specimens, flatter in others; costae subquadrangular to subrounded in section, nearly of the same width of the interspaces; some specimens show a secondary ornamentation on the costae, consisting in 1-2 thinner costae; growth lines thin and dense, more evident in the costal interspaces; in some specimens growth lines are coarser and impart a lamellose pattern. Auricles ornamented by thin costae and growth lines; anterior

auricle of the right valve ornamented by coarser costae and by very dense growth lines in a triangular zone in correspondence of the byssal notch; ctenolium present. Valve interior reflects the external ornamentation.

Interior of both valves with isodont dentition with a triangular resilium pit. Monomyarian, well marked muscle scar; the rounded and larger muscle scar represents the attachment of the striated muscle, and the beanlike muscle scar represents the attachment of the smooth muscle.

Dimensions. Fig. A.3 and Table 5 in the appendix A.1.

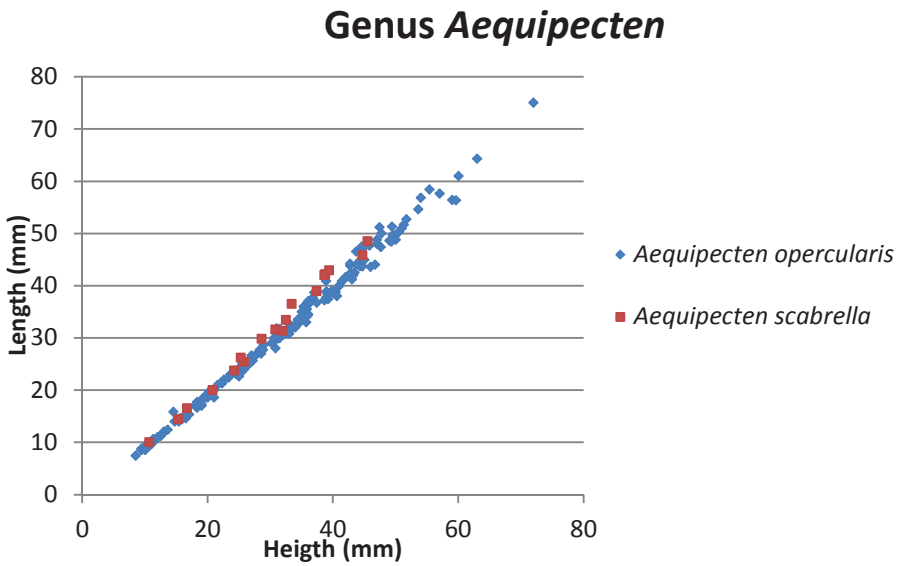

Fig. A.3 Height and length values of species of *Aequipecten*

Discussion. *Aequipecten opercularis* is a very common species in the Arda River succession. According to Jimenez et al. (2009) this species is similar to *A. scabrella* (Lamarck, 1819); they differ as *A. opercularis* has a less curved umbo and a circular and more regular outline than *A. scabrella*, which is very asymmetric (the antero-posterior diameter is larger than the dorso-ventral one); furthermore *A. scabrella* has coarser and fewer costae and more convex valves. Probably these two species had a common origin in the Miocene as in this time interval they are difficult to distinguish one from the other (Malatesta, 1974).

Aequipecten angelonii (De Stefani & Pantanelli, 1878) is also similar to *A. opercularis*, mainly in the juvenile stages. In adulthood, representatives of the two species differ since the shell of *A. angelonii* is thicker, the auricles are less developed, the radial ribs have a very characteristic triangular section, and it has spines.

Among the two species of *Aequipecten* (Fig. A.3) I do not observe particular trend as in *Glycymeris* species (Fig. A.1). In fact *A. scabrella* and *A. opercularis* show similar size and in both cases height and length are nearly equal (H/L ratio equal 1) indicating a subcircular outline.

Stratigraphic and geographic occurrence. *Aequipecten opercularis* is known from the Miocene to the Recent of the Atlantic Ocean and the Mediterranean Sea (Marasti & Raffi, 1980). See also Chapter 3.

Aequipecten scabrella (Lamarck, 1819)

Pl. 5 figs. 2-4

1819 *Pecten seniensis* Lamarck, p.182

1819 *Pecten scabrellus* Lamarck, p. 183

1879 *Pecten scabrellus* (Lamarck) – Meli, p. 5, 6

1879-1882 *Pecten scabrellus* (Lamarck) – Fontannes, p. 187, pl. 12, figs. 2, 3

1898 *Pecten scabrellus* (Lamarck) – Almera & Bofill, p. 111

1902 *Pecten scabrellus* (Lamarck) – De Stefani, p. 5

1906 *Aequipecten scabrellus* (Lamarck) – Ugolini, p. 167

1913 *Chlamys scabrellus* (Lamarck) – Gignoux, p. 369

1914 *Chlamys (Aequipecten) scabrellus* (Lamarck) – Bongo, p. 472

1933 *Chlamys (Aequipecten) seniensis* (Lamarck) – Venzo, p. 81, pl. 7, figs. 18, 21; p. 82

1936 *Pecten (Aequipecten) seniensis* (Lamarck) – Friedberg, pl. II, figs. 37-3

1940 *Chlamys scabrella* (Lamarck) – Roger, p. 332, 342

1950 *Chlamys (Aequipecten) scabrella* (Lamarck) – Festa, p. 94

1952 *Chlamys scabrella* (Lamarck) – Lecointre, p. 55

1955 *Chlamys (Aequipecten) scabrella* (Lamarck) – Moroni, p. 130

1958 *Chlamys scabrella* (Lamarck) – Erunal Erentoz, p. 149, pl. 24, figs. 3, 4

1959 *Chlamys (Aequipecten) seniensis* (Lamarck) – Anderson, p. 98, pl. XIV, figs. 8a, b

1963 *Chlamys scabrella* (Lamarck) – Venzo & Pelosio, p. 148, pl. 47, fig. 2

1966 *Aequipecten (Aequipecten) seniensis* (Lamarck) – Compagnoni, p. 168, pl. 1, figs. 2a,b

1970 *Chlamys (Aequipecten) scabrella* (Lamarck) – Raffi, p. 114, pl. 27, figs. 1,2; pl. 29, figs. 2a,b (cum syn.)

1972 *Chlamys (Argopecten) seniensis* (Lamarck) – Caprotti, p. 59, pl. 1, fig. 3

1974 *Chlamys (Aequipecten) seniensis* (Lamarck) – Malatesta, p. 47, pl. 3, figs. 6a,b

1976 *Chlamys (Aequipecten) seniensis* (Lamarck) – Caprotti, pl. 4, fig. 3

1986 *Chlamys (Aequipecten) scabrella* (Lamarck) – Faraone, p. 14, fig. 15

2009 *Aequipecten scabrella* (Lamarck) – Jimenez et al., p. 7, figs. 3f-i, 4a,b

Material. twenty-two right valves: ACG1-1, ACG2-5, ACG3-4-5-6-7, ACG4-3-5-6-7-8-9-11-15, ACG5-3-4, ACG6-2, ACG8-2, ACG12-4, ACG13-11, ACG33-4, ? ACG66-11; thirteen left valves: ACG1-2, ACG2-6, ACG3-3, ACG4-2-4-12, ACG5-2, ACG6-4-8, ACG12-2-3-6, ACG13-5.

Occurrence. ACG1, ACG2, ACG3, ACG4, ACG5, ACG6, ACG8, ACG12, ACG13, ACG33, ? ACG66, Arda river section, Castell'Arquato, Italy.

Description. Medium sized biconvex shell, inequivalve and inequilateral; slightly transverse suboval outline and orthogyrate, convex umbo; cardinal margin straight; dorso-ventral diameter smaller than antero-posterior one; posterior region more developed than the anterior one. Right and left valves auricles similar in shape (triangular) and size, with the anterior one larger than the posterior one; the anterior auricle has a small byssal notch in both valves.

Ornamentation of both valves consisting of 13-17 coarse radial costae, thinner than the costal interspaces, and of thin and dense concentric growth lines; costae are quadrangular in section near the umbo, becoming rounded in the ventral region; the change in the outline of the section usually occurs in correspondence of a growth halt where the shell forms a sharp step; after this transition radial costae and interspaces near the ventral margin become ornamented by thinner ribs: 3-6 on the costae, 2-3 in the costal interspaces; in some specimens, mainly adult ones, there are 1-3 growth halts forming 1-3 sharp steps, but only in correspondence of the first halt the change in section and in ornamentation of the costae takes place. Auricles ornamented by thin costae, more numerous in the posterior one. Valve interior reflects the external ornamentation.

Interior of both valves with isodont dentition with a triangular resilium pit. Monomyarian, not well impressed, rounded muscle scar.

Dimensions. Fig. A.3 and Table 6 in the appendix A.1.

Discussion. According to several authors (e.g. Raffi, 1970; Faraone, 1986; Jimenez et al., 2009) *Aequipecten scabrella* shows a wide morphological intraspecific variability and, therefore, some species should be considered synonyms. In particular, based on comparison and revision of the available literature (e.g. Raffi, 1970; Malatesta, 1974), *Aequipecten radians* (Nyst & Westendrop, 1839), *Aequipecten seniensis* (Lamarck, 1819) and *Aequipecten bollenensis* (Mayer, 1876), here considered junior synonyms of *Aequipecten scabrella*.

Aequipecten opercularis (Linnaeus, 1758) differs from *A. scabrella* by its more symmetrical valves, its more regular outline, its lower convexity and by its thinner and more numerous costae.

As observed in the *A. opercularis* discussion, *A. scabrella* and *A. opercularis,* show similar size (Fig. A.3) and in both cases height and length are nearly equal (H/L ratio equal 1) indicating a subcircular outline.

Stratigraphic and geographic occurrence. *Aequipecten scabrella* is known from the Miocene to the Gelasian(Lower Pleistocene) of the Mediterranean Sea (Marasti & Raffi, 1980).

Subclass HETERODONTA Neumayr, 1884
Order VENEROIDA Adams & Adams, 1856
Superfamily ARCTICOIDEA Newton, 1891
Family ARCTICIDAE Newton, 1891
Genus *Arctica* Schumacher, 1817

Type-species. *Arctica vulgaris* (Linnaeus, 1767) from the Pliocene of England.

Remarks. *Arctica* differs from *Pelecyora* Dall, 1902 from the Eocene of the USA, because the former has a thicker shell and lacks the pallial sinus; it differs from *Callista* Poli, 1791 from the Recent of the Mediterranean area as the latter is glossy, usually without sculpture and with the pallial sinus.

Arctica islandica (Linnaeus, 1767)
Pl. 4 fig. 4; Pl. 5, figs. 5-6

1767 *Venus islandica* Linnaeus, p. 1131
1778 *Venus buccardium* Born, p. 63, pl. 4, fig. 11
1778 *Pectunculus crassus* Da Costa, p. 183, pl. 14, fig. 5
1817 *Arctica vulgaris* Schumacher, p. 145, pl. 13, fig. 3
1864 *Cyprina islandica* var. *crassior* Jeffreys, p. 305
1898 *Cyprina islandica* - Sacco in Bellardi & Sacco, V. 28, p. 10, pl. II, figs. 1-2 (cum syn.)
2001 *Arctica islandica* Gofas et al. in Costello et al., p. 2010

Material. Four articulated specimens: ACG253-2, ACG254-1-4-6; thirty-one ventral valves: ACG86-4-5, ACG200-9-10-12-13, ACG202-3, ACG213bis-3, ACG214-1-2, ACG215-5-6-8-10, ACG216-1-2-3, ACG217-5, 6ACG220-1-2-3, ACG224-1, ACG226-3, ACG228-1-2, ACG242-1-2, ACG243-5, ACG253-3-4, ACG254-3; sixteen dorsal valves: ACG78-1-2-6, ACG200-11-14, ACG213bis-2, ACG215-7-9, ACG216-4, ACG217-4, ACG222-5, ACG225-1, ACG226-1-2, ACG229-1, ACG254-2; fragments: ACG78-3, ACG241-4.

Occurrence. ACG78, ACG86, ACG200, ACG202, ACG213bis, ACG214, ACG215, ACG216, ACG217, ACG220, ACG222, ACG224, ACG225, ACG226, ACG228, ACG229, ACG241, ACG242, ACG243, ACG253, ACG254, Arda river section, Castell'Arquato, Italy.

Description. Large sized, biconvex and strong shell, equivalve and inequilateral; suboval outline with rounded anterior margin and straight posterior one; shell substance very thick; both valves show a low ridge in the posterior part, extending from the umbo to the ventral margin; umbo convex, prosogyrate and prominent; cardinal margin strongly curved; narrow nymphs occupied by thick, arched and black external ligament; dorso-ventral diameter is nearly equal to antero-posterior one.

Ornamentation of both valves consisting of: 1) irregular and numerous concentric growth lines in the anterior and middle part of the valve and 2) growth lamellae in the posterior part; these two different ornamentation pattern are bounded by a low ridge.

Interior of both valves with heterodont dentition; right valve with three prominent cardinal teeth and a single posterior lateral tooth; left valve with three cardinals teeth and one posterior lateral tooth, with the anterior cardinal continuous with a series of small ridges and denticulations.

Suboval muscle scar dimyarian anisomyarian with integripalliate circular pallial line; anterior adductor muscle scar slightly larger than the posterior one; scars of radially directed fibers of muscle mantle along the pallial line.

Dimensions. Fig. A.4 and Table 7 in the appendix A.1.

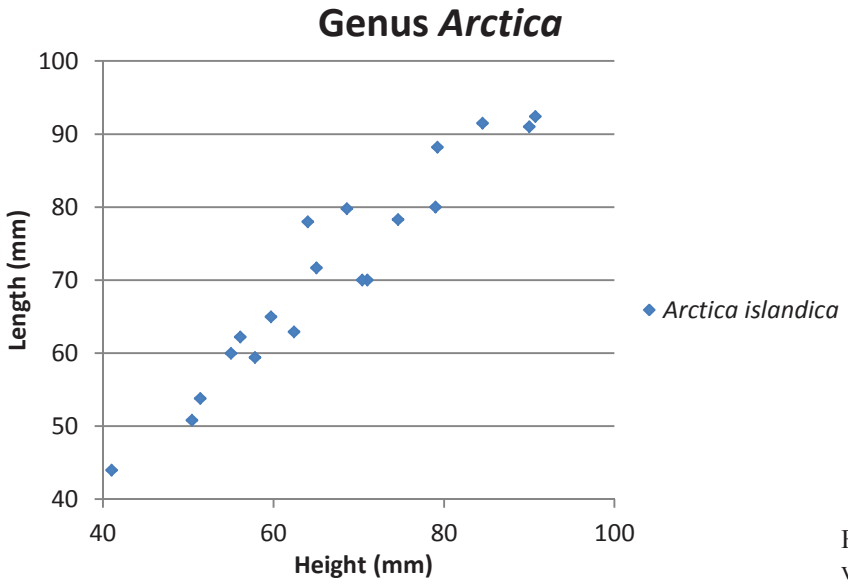

Fig. A.4 Height and length values of *Arctica islandica*.

Discussion. *Arctica islandica* is the only living species of its family. The taxonomy and nomenclature is well defined although the old name *Cyprina islandica* is sometimes still used in recent literature. It has a very thick shell and it first occurrence in the Arda section is at 103.70 m from the base of the section. This species probably represents the most popular boreal guest which migrates into the Mediterranean Sea during the climatic deterioration of the Early Pleistocene. The Mediterranean populations became extinct about 9.8 Ka ago as a consequence of the climate shift to warm water conditions (Dahlgren et al., 2000).
Arctica islandica is the species with the bigger minimum and maximum dimension (min. 41 mm, max 92.4 mm) and usually have a H/L minor than 1, pointing out a slightly transverse outline (Fig. A.4).

Stratigraphic and geographic occurrence. *Arctica islandica* is known from the Oligocene of Hungary to the Recent (Malatesta & Zarlenga, 1986). From 1.77Ma to 9.8 Ka (Calabrian-Late Pleistocene) it was present in the Mediterranean Sea. Nowadays is found at high latitudes in the Western Atlantic Ocean along the American coast and in Europe along the coasts of Iceland, Great Britain and the Scandinavian peninsula (Dahlgren et al., 2000). See also Chapter 3.

A.2 Ultrastructural analysis

The analysis of the shell ultrastructure at the SEM has important implications: besides being a useful method to check the preservation of the shells before undertaking isotopic and geochemical analyses, it gives information about the shell fabric which can be helpful, among others, to understand systematic relationships between bivalve groups and shell biomineralization processes.

In the ultrastructural descriptions of species of *Glycymeris, Aequipecten* and *Arctica* I followed the terminology used by Carter (1990). Paragraph A.2.1 has been published (Crippa, 2013).

A.2.1. *Glycymeris* shell ultrastructure

A.2.1.1 Fossil and recent specimens

Four fossil species of *Glycymeris* from the Arda section were analyzed: *Glycymeris inflata, Glycymeris glycymeris, Glycymeris insubrica* and *Glycymeris* sp. ind. In addition two Recent specimens from Brittany, France belonging to *Glycymeris glycymeris* were studied for comparison. All fossil and recent specimens show the same ultrastructures; they have an aragonitic shell with an outer crossed lamellar layer, an inner irregular and cone complex crossed lamellar layer and an irregular simple prismatic pallial myostracum; all the mineralized shell layers are penetrated by cylindrical tubules (Fig. A.5).

Outer layer. The outer layer is composed by simple crossed lamellae (CL) and occupies the whole outer part of the shell, under the organic periostracum, from the marginal band to the hinge plate, defining a sort of "zebra pattern" (Pl. 6, figs. B, C, G). In particular, the hinge plate and the marginal band, which is the growth surface between the pallial line and the outer shell margin (Waller, 1980), are composed entirely by simple crossed lamellae. The thickness of the outer layer shows an identical trend among different specimens: the maximum thickness is in the marginal band, then it begins to decrease starting from the pallial line, reaches its minimum dorsally at the umbonal curvature and returns to be thicker in the hinge plate (Fig. A.5). The hierarchical organization of the lamellae is here easily discernible. First order lamellae are extremely variable in thickness (5-30 μm) and appear as a series of linear to branching oriented lenses, which could also curved (Pl. 6, figs. C, G); they are clearly observable at SEM thanks to the alternated brightness - linked to differences in electron scattering (Tschudin, 2001) - of the adjacent first order lamellae, which are inclined in two opposite directions (Pl. 6, figs. C-H). The first order lamellae show a double pattern in the outer layer (Pl. 6, figs. B, C, G): 1) in the internal part they are linear and parallel to each other, 2) in the external part they are irregular, almost parallel to the outer surface and with a better contrast compared to the adjacent lamellae in the inner part and, linear and parallel to each other in the outer part.

The third order lamellae are usually 0.3-1 μm thick and sometimes the fourth order granules that form the third order elements are observable in well preserved fossil specimens and in the recent ones (Pl. 6, fig. H). They are very similar to the fourth order elements figured by Dauphin & Denis (2000, fig. 2J); in contrast the second order lamellae are not always well defined.

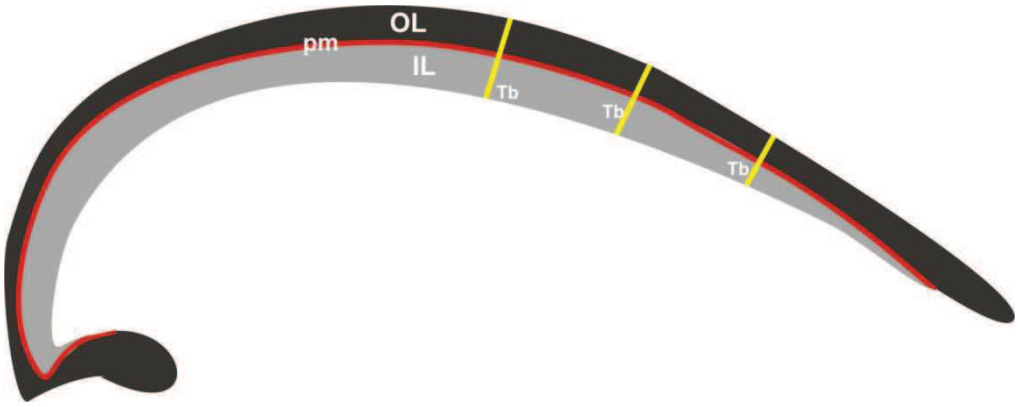

Fig. A.5. Longitudinal section of the shell of species of *Glycymeris* showing the mineralized layers. OL: outer layer; IL: inner layer; pm: pallial myostracum; Tb: tubules.

Inner layer. The inner layer is present only internally with respect to the pallial line. It is delimited by the pallial myostracum and it does not extend inside the hinge plate (Fig. A.5). As for the outer layer, also for the inner shell layer a typical thickness trend can be recognized among different specimens: it starts dorsally to the pallial line and increases its thickness towards the umbonal region, where it disappears abruptly (Fig. A.5). The inner layer is composed by complex crossed lamellae (CCL), both irregular and cone ones (Pl. 7, figs. A-F). The cone complex crossed lamellae consist of an aggregation of elongate rectangular rods of aragonite which radiate from the central part of the cone (Kobayashi & Samata, 2006) (Pl. 7, figs. B, D, F), as it has been observed also by Tschudin (2001, fig. 3) at the SEM. The distinct lamellar hierarchy of the outer layer is not so clear. The inner layer is less organized and more irregular in relation to the outer layer. Only the third order elements are evident, showing a similar thickness to those of the outer layer (Pl. 7, figs. A-C, E, F).

Pallial myostracum. The outer and inner layers are separated by a pallial myostracum which is formed by a stockade of parallel and elongated irregular simple prisms (ISP). It starts at the pallial line and finishes abruptly at the internal margin of the hinge plate (Fig. A.5; Pl. 6, figs. A, B; Pl. 7, figs. G, H; Pl. 8, figs. A, B). The thickness of the pallial myostracum varies among the specimens. It is clearly distinguishable and it cannot been confused with the inner layer growth lines, which are usually thinner. Furthermore, the pallial myostracum identifies the boundary between the inner and outer layers, which are easily recognizable at the SEM because usually the inner layer shows a darker coloration than the outer layer (Pl. 6, figs. A, B; Pl. 8, fig. A).

Growth lines. They cross both the inner and outer layers with a different orientation and they stand out in a different way in the two layers. In fact, in the inner layer, they are more distinct than in the outer layer and they are parallel to the inner and outer shell surfaces (Pl. 6, fig. A), following the curvature of the shell; they consist of parallel and elongated irregular simple prisms (Pl. 7, figs C, E). In the outer shell layer the growth lines are evident mainly in the marginal band and in the hinge plate, whereas in other parts of the shell they are not so easy to distinguish. In the marginal band they are slightly inclined to the outer surface, then they curve to become nearly parallel to the outer surface (Pl. 6, fig. G; Pl. 8, fig. F). In the hinge plate they are concentric and parallel to the direction of growth of the hinge plate itself (Pl. 8, fig. E). They seem to be composed by an elongation of the third order lamellae (Pl. 6, fig. D). Growth lines on the outer surface of the shell appear as concentric striations, which correspond internally to the outer layer growth lines (Pl. 6, figs. D, G; Pl. 8, fig. F).

Other layers. An irregular prismatic layer is present in the inner part of the hinge plate of the best preserved specimens. It is composed by elongated and parallel simple prisms perpendicular to the inner surface of the shell with prism widths of 0.5-3 μm; it appears as a prolongation of the irregular prismatic pallial myostracum in the hinge plate. It represents the attachment site for the pedal retractor muscles (Pl. 8, figs. C-E).

Tubules. Both fossil and recent species of *Glycymeris* here analyzed show a densely perforated structure (Pl. 6, figs. A, B; Pl. 7, fig. B; Pl. 8, figs. A, F-H; Pl. 9, figs. A-D). Tubules penetrate all the shell layers: no data is available on their relationship to the periostracum as the latter is not preserved in the studied specimens. In the examined material, tubules do not appear as empty perforations but they are filled seemingly by the resin used for the specimens preparation (Pl. 7, fig. B; Pl. 8, figs. F, G; Pl. 9, figs. A-D).

The distribution of tubules is restricted to the part of the shell characterized by the occurrence of the inner layer, that is from the pallial line to the umbonal region up to the point where the inner layer suddenly disappears. No tubule has been found in the marginal band or in the hinge plate. In both the inner and outer layers they cut the crossed lamellar fabric pointing out that they are formed by dissolution after the secretion of the layers (Pl. 7, fig. B; Pl. 8, figs. A, F-H; Pl. 9, figs. A-D). Tubules diameter varies among the different specimens of the analyzed species but within the same specimen they have more or less the same diameter, which ranges between 2 and 10 μm in agreement with the ranges reported by Waller (1980).

Tubules are mostly parallel to each other and perpendicular to the outer and inner shell surfaces with no intersection between them and no bifurcation (Pl. 6, figs. A, B; Pl. 8, figs. A, F). They perforate all the mineralized layers in a straight line without changing their direction at the passage between the inner and outer layers (Pl. 8, fig. A). The end of the tubule, penetrating the outermost shell layer, flares

at its distal opening (Pl. 9, fig. B). In a few instances there is a change of their direction, but only in correspondence with the pallial line or in the umbonal region where the inner layer disappears. Here, tubules are inclined and protrude in the marginal band and in the hinge plate with an angle of 60-65 degrees; in these regions (end of the inner layer in the pallial line and in the hinge plate) both inclined and straight tubules gradually decrease their length disappearing without reaching the outer surface (Pl. 6, fig. B; Pl. 8, fig. F).

A.2.1.2 Discussions

Fossil and recent specimens at the SEM share the same ultrastructure, with an outer crossed lamellar layer, an inner irregular and cone complex crossed lamellar layer and an irregular simple prismatic pallial myostracum (Fig. A.5; Pl. 6, figs. A, B), as described by Carter (1990) in species of the genus *Glycymeris*.

In contrast Popov (1992) and Rogalla & Amler (2007) subdivided the outer layer of Carter (1990) into a middle and an outer layer, thus describing three layers in addition to the pallial myostracum. However, their subdivision mainly results from a change in the pattern of the first order elements in the simple crossed lamellae rather than from the occurrence of two real distinct layers. In fact the middle and outer layers of Popov (1992) and Rogalla & Amler (2007) correspond respectively to pattern 1 and pattern 2 of the outer layer (see previous paragraph; Pl. 6, figs. B, C, G). For these reasons, the subdivision of Carter (1990) in two layers in addition to the pallial myostracum is here preferred and followed.

The analysis at SEM highlights that fossil and recent specimens of different species of *Glycymeris* show the same ultrastructure; an important consequence of this similarity is that the ultrastructure of the shells of the species of the genus *Glycymeris* has not changed for over 2 million years. These species are particularly conservative in their morphological diversity and this conservative character is seen not only in their morphology, but also in their shell ultrastructure. This is an interesting and not obvious conclusion: for example in the bivalve *Arctica islandica,* North American specimens show a slightly different fabric with respect to the conspecific ones from Kattegat, Öresund and Kiel Bay; in fact shell fabric in this case seems to be less organized in instable settings (Kattegat, Öresund and Kiel Bay) rather than in fully marine conditions (North America), thus indicating that environmental perturbations can affect the shell ultrastructure (see *A. islandica* paragraph).

The analysis of *Glycymeris* shell ultrastructure has interesting implications also on the debated position of the family Glycymerididae Dall, 1908, either considered as being part of the superfamily Arcoidea Lamarck, 1809 or of the superfamily Limopsoidea Dall, 1895. Newell (1969) includes the

Glycymerididae in the Limopsoidea near the family Limopsidae Dall, 1895, based on the rounded shell form and on the weak ornamentation. However, the two families differ by several morphological characters: the Glycymerididae have a massive form with a duplivincular ligament, lack a functional byssus and have a slightly larger anterior adductor muscle, whereas the Limopsidae are generally small with an alivincular–multivincular ligament, a functional byssus and a larger posterior adductor muscle (Oliver & Holmes, 2006). Subsequently, Carter (1990) and Oliver & Holmes (2006) placed the family Glycymerididae in the superfamily Arcoidea near the family Cucullaeidae Stewart, 1930 because of their similar hinge dentition, ligament structure and shell ultrastructure. Both the families are characterized by the lack (or rarity) of crossed-matted/lineated fabric and of an outer prismatic layer in their shell ultrastructure. In the specimens here examined no crossed matted/lineated fabric and no outer prismatic layer have been observed confirming the affinity of the genus *Glycymeris* with the family Cucullaeidae and hence its closer relationship with the superfamily Arcoidea, rather than with the superfamily Limopsoidea.

Tubular structures are known from unmineralized and mineralized shells of bivalves, polyplacophorans, fissurellid gastropods, brachiopods, bryozoans, ostracods and cirripedian crustaceans (e.g. Owen & Williams, 1969; Klepal & Barnes, 1975; Keyser, 1980) and they have also been discovered in Early Cambrian mollusk-like organisms (Kouchinsky, 2000). They are a fundamental character in the Arcoida shells (Shibata, 1979) and thus of *Glycymeris* ultrastructure. They are present in both fossil and recent specimens, but their function is far from being clarified. They do not result from bioerosion: tubules are usually straight and regular, whereas burrows of bioerosion are usually larger in diameter (even if bacteria can produce smaller erosions) and form complex and irregular networks (Shibata, 1979); furthermore, according to Reindl & Haszprunar (1996), no boring algae, fungi or bacteria have been found to penetrate the shell.

Tubules are occupied in alive specimen by caeca which are extensions of the outer mantle epithelium composed each by a single, specialized epithelial cell (Reindl & Haszprunar, 1996), which is chemically active at its tip, apparently capable of dissolving calcium carbonate in order to perforate the shell (Waller, 1980). It thus seems that, although the mantle projections that form tubules are able to dissolve calcium carbonate, they cannot completely penetrate the organic material forming the periostracum (Waller 1980). When the shell-dissolving tip of a cellular projection reaches the undersurface of the periostracum, its etching effect spreads out, as shown by the flared distal extremity of the tubule (Pl. 9, fig. B).

Waller (1980) noticed that the complex fabric of the inner shell layer is secreted around the mantle projection forming the tubule and is not crossed, indicating that in this area the tubules are primary

rather than secondary. In the examined specimens tubules cut the fabric also in the inner shell layer suggesting that also in this case they are formed secondarily, after the secretion of the inner layer (Pl. 7, fig. B; Pl. 8, fig. A; Pl. 9, fig. A).

The function of the tubules and caeca is still debated, and several are the hypotheses proposed (Lutz & Rhoads, 1977; Waller, 1980; Reindl & Haszprunar, 1996).

The most supported one is that they represent a deterrence for boring organisms and this functional interpretation is strengthened by the taxonomic distribution of tubules. They are common in epifaunal bivalves in many unrelated groups (Oberling 1964), but are uncommon in infaunal taxa (Waller, 1980). La Perna (2006) found tubules in the epibyssate juveniles of *Ambrogia mytiloides* (Brocchi, 1814) but they are absent in the endobyssate adults of the same species and this may represent another evidence that shell tubules are actually involved in deterring microborers, as the caeca could remain chemically active during the bivalve life. In the examined specimens some of the tubules seem to extend to the marginal band or to the hinge plate in order to protect through chemical secretion also these regions that cannot otherwise be reached by tubules as the mantle does not occur here. In fact the mantle edge at the ventral margin is highly mobile and constantly shifting relative to the shell surface, so that it would be impossible for fine epithelial extensions into the shell to form or to be maintained (Waller, 1980). The marginal band and the hinge plate are important zones to protect from boring organisms and if tubules have actually a deterrence function one would expect to find more tubules here than in other regions of the shell and especially to find them perforating also the periostracum. However, in these regions tubules, if present, do not reach the outer surface (Pl. 6, fig. B; Pl. 8, fig. F) and they do not perforate the periostracum. Furthermore the hard crossed lamellar ultrastructure and the thick shell already represent an adequate defense mechanism from boring organisms. These new observations together with those deriving from the literature allow to conclude that a deterrence function for the tubules is unlikely.

Tubules are not limited to aragonitic shells (e.g. tubules perforating the calcitic layers of Mytilidae as observed by Carter, 1990), but most of them are found in the aragonitic crossed lamellar fabric. The latter has a lower organic content with respect to the other bivalve fabrics and it is also the hardest structure and in consequence the less elastic. Organic material is very expensive to produce and the shell has to be produced quickly and, metabolically speaking, cheaply (Palmer, 1983). Tubules may thus have the function to increase the volume of the organic content in the shell at lower metabolic cost without increasing the shell surface.

A.2.1.3 Conclusions

The analysis of the shells of several species of *Glycymeris* indicates a strong similarity between fossil and recent fabrics; the outer simple crossed lamellar layer, the inner irregular and cone complex crossed lamellar layer and the irregular simple prismatic pallial myostracum are clearly distinct and nearly identical in both the fossil and recent specimens.

Fossil and recent shell ultrastructures show the same fabric suggesting that:

- fossil specimens from the Castell'Arquato Formation of the Arda River (Western Emilia, Italy) are pristine and suitable for geochemical and isotopic analyses;
- *Glycymeris* ultrastructure has not changed for the last 2 million years;
- the lack of crossed matted/lineated fabric and of a prismatic outer shell layer confirms the affinity of the genus *Glycymeris* with the family Cucullaeidae and hence their closer relationship to the superfamily Arcoidea;
- the tubules deterrence function for boring organisms is unlikely. They may instead function to increase the volume of the shell organic content at lower metabolic cost without increasing shell surfaces.

A.2.2 *Aequipecten* shell ultrastructure

A.2.2.1 Fossil specimens

Two fossil species from the Arda section and belonging to the genus *Aequipecten* were here analyzed: *Aequipecten scabrella* and *Aequipecten opercularis*; they have a very complex ultrastructure, sometimes difficult to interpret due to the numerous layers that are present; these shells tend to flake in correspondence to the contacts between the different layers with epoxy resin often penetrating inside these sharp contacts. The shell is formed both by low magnesium calcite and aragonite, with the right and left valves having the same ultrastructure and mineralogy. They have three main layers in addition to the pallial myostracum: a calcitic foliated inner and outer layers and an aragonitic prismatic and crossed lamellar middle layer (Fig. A.6; Pl. 9, figs. E-H, Pl. 10, fig. A).

Outer and inner layers. They are composed of a foliated fabric, build-up of blade-like elongate parallel crystals (laths) of calcite with arrow-point endings which coalesce laterally forming laminae (folia). Following the hierarchical organization of Carter (1990) laths represent the third order elements, folia the second order ones and lenses formed by several folia are the first order elements.

The foliated ultrastructure shows the following distribution within the shell: 1) the outer layer extends throughout the whole shell becoming thinner in its dorsal margin and thickening toward the ventral one; 2) the inner layer extends from the beak to the proximity of the adductor muscle scar, attaining its

maximum thickness near the beak. Inside the shell they are separated by the middle layer, but in the umbonal area inner and outer layers are in contact.

Three ultrastructural types have been recognized among the foliated fabric:

1) Regular foliated (RF) ultrastructure, formed by parallel and regular calcitic laths arranged in folia dipping at the same angle. The arrow-point endings of the laths are overall directed in the same direction (Fig. A.6; Pl. 9, figs. E-H; Pl. 10, figs. A-E; Pl. 11, figs. A, B, E, G; Pl. 12, figs. A, C, D).

2) Crossed foliated ultrastructure (CF), consisting of parallel to branching first order lenses, is clearly identifiable at the SEM because of alternation of bright band due to differences in electron scattering. It is also easily recognizable as the arrow-point ending of the laths dips in two opposite directions. As in the regular foliated ultrastructure, they are neatly arranged (Fig. A.6; Pl. 9, fig. H; Pl. 10, figs. F-H; Pl. 11, fig. H; Pl. 12, fig. H). Crossed foliated fabric is the analogous, in terms of organization, to the aragonitic crossed lamellar one.

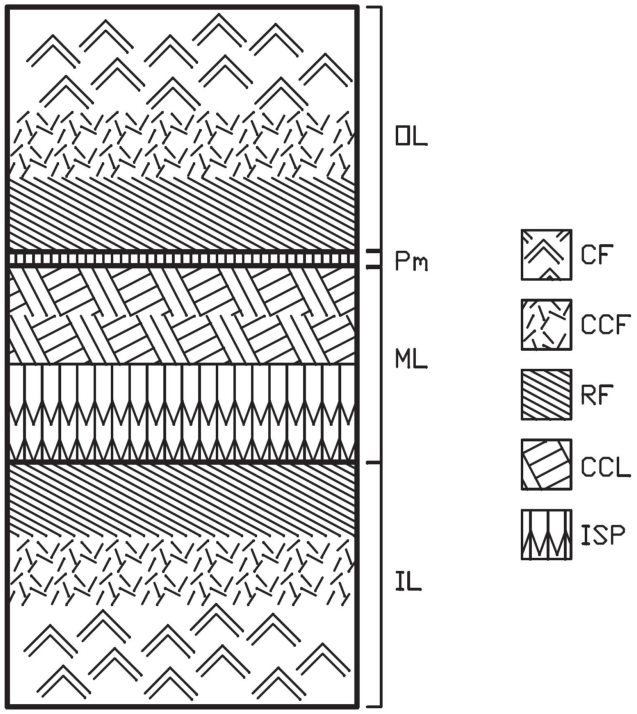

Fig. A.6. Simplified section showing the complex fabric of the shell of species of *Aequipecten*. OL: outer layer; ML: middle layer; IL: inner layer; Pm: pallial myostracum.

3) Complex crossed foliated ultrastructure (CCF). In several areas within the shell highly irregular orientated folia occur displaying a dendritic and chaotic arrangement (Fig. A.6; Pl. 9, figs. E, F, H; Pl. 10, figs. A, H; Pl. 11, figs. A-D; Pl. 12, figs. F, H). The complex crossed foliated fabric can be correlated to the aragonitic complex crossed lamellar layer as they share the same poorly organized and irregular structure. Furthermore, the aragonitic complex crossed lamellar fabric is characterized by two subtypes, the irregular type and the cone complex one, which have been observed also in the complex crossed foliated fabric; in particular the cone complex crossed foliated subtype is here very clear (Pl. 11, fig. B; Pl. 12, fig. H).

These three fabrics are all present in the outer and inner layers, giving origin to a very complex and confused organization; the transition among these types is gradual and the shell structure seems to pass from crossed foliated to complex crossed foliated to regular foliated fabrics, although this order is not always clear (Fig. A.6; Pl. 10, fig. H; Pl. 11, figs. A, B; Pl. 12, fig. H).

Middle layer. Strictly confined to the inner part delimited by the pallial line there is an aragonitic prismatic and crossed lamellar layer (Grade 4c of Pectinoidea ultrastructural trends of Carter, 1990). These two fabrics constitute the middle shell layer which thins both in radial and antero-posterior directions and disappears inside the shell near the umbonal region. The middle layer can be very thick, having both the crossed lamellar and prismatic ultrastructure well developed (Fig. A.6; Pl. 9, figs. E-H; Pl. 11, figs. D-H; Pl. 12, figs. A-D).

The middle layer is composed by:

1) Simple crossed lamellar and complex crossed lamellar ultrastructure. It consists of elongate, lenticular to branching first order lamellae built up of parallel aragonite crystal aggregations, which may alternate in two opposite directions showing a characteristic cross pattern (crossed lamellar) or may exhibit three or more orientations (complex crossed lamellar), as it has been observed also in *Glycymeris* shells (Pl. 9, figs. E-H; Pl. 11, figs. D-H; Pl. 12, figs. A-D). This layer can be very thick and develops into two sublayers often separated by an aragonitic irregular simple prismatic layer (Pl. 9, figs. G, H; Pl. 11, fig. G). The latter can be distinguish from the pallial myostracum as it is thicker and more irregular. The upper sublayer is composed of simple crossed lamellae with first order elements, regularly shaped and branching, and it is usually thin relative to the lower one. The lower sublayer beneath the prismatic structure is composed of complex crossed lamellar ultrastructure, showing more irregularly shaped first-order lamellae in comparison to the upper sublayer (Pl. 9, figs. G-H; Pl. 11, fig. G; Pl. 12, fig. B).

2) Irregular simple prismatic ultrastructure. This structure is composed of a stockade of parallel aragonitic irregular simple prisms showing a high length/width ratio (Fig. A.6; Pl. 9, figs. F-H; Pl. 10, fig. A; Pl. 11, fig. F; Pl. 12, fig. C). The prisms are simple, have straight or irregular boundaries and are elongated in the radial direction with their length axes perpendicular to the shell surface. The irregular simple prismatic structure attains its maximum thickness in the adductor muscle scar area; in fact this fabric is usually associated with muscle attachment. In all directions outside the muscle scar area the prismatic ultrastructure thins out, interfingering with the crossed lamellar structure and showing one or more digitations.

The middle layer is complex and has a different organization in the different shells. In fact as observed above, the prismatic layer can show one or several interdigitations with the crossed lamellar layer, forming a complex stratified structure. To summarize and simplify starting below the pallial

myostracum, the general organization of the middle layer is the following: a thin simple crossed lamellar sublayer followed by a thin irregular simple prismatic layer, followed by a complex crossed lamellar sublayer and finally by a thick irregular prismatic one.

Few specimens have the original aragonitic middle layer not preserved, but replaced by prisms of diagenetic calcite. In specimens displaying diagenesis the middle layer is in fact leached and infilled with sparry calcite (Pl. 12, figs. F-H).

Pallial myostracum. The outer and middle layers are separated by a pallial myostracum which is formed by a stockade of aragonitic parallel simple prisms, with organized regular pattern (Fig. A.6; Pl. 9, figs. F-H; Pl. 11, figs. E-H; Pl. 12, figs. A-C). It starts at the pallial line and gradually vanished inside the shell following the disappearance of the middle layer. It is very thin (2-3μm) and sometimes it is not easily distinguishable as it happens in other genera.

Growth lines. Specimens of species of *Aequipecten* have numerous and distinct growth lines across the outer shell surface, which form the spinose micrornamentation observed at the SEM (Pl. 12, fig. E). However, only from mid-valve length to the ventral margin they are spinose, whereas dorsally they are represented by low ondulation. Notwithstanding growth lines are easily detectable on the outer shell surface they are very difficult to follow inside the shell. In the marginal band they are clearer than in other part of the shell and appear as lines with different brightness due to electron scattering; aside this, they are not associated to a particular fabric as it happens in the genera *Arctica* or *Glycymeris*, where growth lines inside the shell are composed by irregular simple prisms. As growth lines are not discernible inside the shell, the species of the genus *Aequipecten* have not been used for sclerochemical purposes.

A.2.2.2 Discussions

The shell ultrastructures observed in *Aequipecten scabrella* and *Aequipecten opercularis* here analyzed, is in agreement with previous findings on other pectinid species (Zamarreño et al., 1996; Checa et al., 2007).

The shell of specimens belonging to species of *Aequipecten* is generally very well preserved showing no evidence of diagenetic alteration; however, few specimens coming from two cemented, yellowish-reddish sandstones occurring in the basal part of the section (Units A and D, see Chapter 3), have the original aragonitic middle layer not preserved, but replaced by prisms of diagenetic calcite. In specimens displaying diagenesis the middle layer is leached and infilled with sparry calcite (Pl. 12, figs. F-H); sparry calcite is often made by polygonal, anhedral crystals, but it may also be prismatic. In carbonate shells it forms during diagenesis by neomorphism of aragonite; in fact aragonite is an unstable form of calcium carbonate and when the shell undergoes diagenetic alteration it is the first

part of the shell to be replaced by calcite. The alteration mainly affects specimens belonging to *Aequipecten scabrella* and a few shells of *Aequipecten opercularis*.

The *Aequipecten* ultrastructure is articulate, but every layer has a specific function inside the shell. Foliated fabric is particularly frequent in bivalves, where it forms the bulk of the shells of several epibenthic groups (Checa et al., 2007). Although it has been shown that the foliated structure is more susceptible than others to attack by both the chemicals released by drilling gastropods and corrosive seawaters and it is weak in most mechanical tests (Harper, 2000), there are a number of possible advantages of the foliated ultrastructure; it has a low organic content and density compared to others calcitic fabric allowing reduced shell density for swimming and soft-bottom species, and fracture localization. Furthermore, as it has a low organic content, foliated fabric might be relatively cheap to secrete and this could mean that many of the perceived weaknesses might be overcome by the ability to create a thicker shell (Esteban Delgado, 2008). As the foliated ultrastructure is weak, the presence of a very resistant aragonitic middle layer is an obvious adaptation for adding strength to the shell. The aragonitic layer represents also a relict of the past; in fact, originally, all of these shells were aragonitic, but the evolution trend led to the replacement of aragonite by the less energetic costly low magnesium calcite.

A.2.2.3 Conclusions

The *Aequipecten* shell ultrastructure is very complex and sometimes it is difficult to interpret due to the numerous layers that are present; the shell is formed both by low magnesium calcite and aragonite, with the right and left valves having the same ultrastructure and mineralogy. They have three main layers in addition to the pallial myostracum: a calcitic foliated inner and outer layers and an aragonitic prismatic and crossed lamellar middle layer; further subdivisions are present inside each layer, resulting in a very articulate shell ultrastructure.

The shell of specimens belonging to species of *Aequipecten* is generally very well preserved showing no evidence of diagenetic alteration; however, few specimens, show in their middle layers sparry calcite, indicating that the shells underwent diagenetic alteration processes.

A.2.3 *Arctica* shell ultrastructure

A.2.3.1 Fossil and recent specimens

Arctica islandica represents the only extant species belonging to the genus *Arctica*, and also the only one living in the recent geological past (Pliocene-Pleistocene); for this reason in the following shell

ultrastructural description I refer to the species *A. islandica,* and not to the genus, as no other species belonging to *Arctica* is present in the Arda succession. A recent specimen of *A. islandica* from Iceland was also analyzed for comparison with fossil specimens.

A. islandica has an aragonitic shell with an outer homogenous-crossed lamellar/crossed acicular layer, an inner fine complex crossed lamellar layer and an irregular simple prismatic pallial myostracum (Fig. A.7; Pl. 13, figs. A, B).

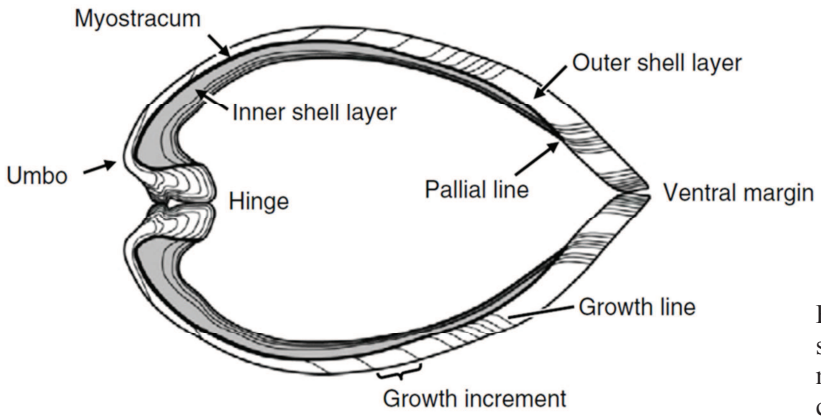

Fig. A.7. Longitudinal section of the shell of *Arctica islandica* in which the mineralized layers and the main characters of the shell are shown (from Schöne, 2013).

Outer layer. The outer layer is composed by a complex fabric with crystals gradually changing in size and shape (Pl. 13, figs. C-H; Pl. 14, figs. A-E; Pl. 15, figs. A-C). The thickness of the outer layer shows an identical trend among different specimens: the maximum thickness is in the marginal band, then it begins to decrease starting from the pallial line, reaches its minimum dorsally at the umbonal curvature and returns to be thicker at the hinge plate (Fig. A.7). There is a transitional band in which the outer homogeneous (HOM) fabric passes to crossed lamellar/crossed acicular one (CL/CA) toward the inner part. These two different fabrics can be considered as two sublayers, although they are not sharply delimited but show a gradual change:

1) Outer sublayer (oOSL). This sublayer is present in the outer part of the outer shell layer (Pl. 13, figs. A-H; Pl. 14, figs. A-E; Pl. 15, figs. A, C). It is composed of a homogenous fabric, which is made by the aggregation of aragonitic granules; it does not provide any discernible substructure except for an obscurely granular pattern of round and angular particles of less than a few microns in diameter (1-4 μm). It seems that within this sublayer, the crystals continued to increase in size toward the external shell surface, as observed also by Schöne et al. (2013) (Pl. 13, figs. G, H).

Small tubular channels, which are empty, are present in the homogeneous fabric, surrounded by larger and radially arranged crystals (Pl. 13, fig. D).

2) Inner sublayer (iOSL). The homogeneous structure of the outer shell sublayer grades into an aragonitic crossed lamellar/crossed acicular fabric in the inner outer shell layer (Pl. 13, figs. G, H; Pl. 14, figs. A, B). Unlike the outer sublayer, here the fabric is regular and well organized.

As observed above, these sublayers are not sharply delimited, but they show a gradual transition; from the outermost part to the pallial myostracum disorganized homogeneous crystals decrease in size and pass gradually to crossed lamellar/crossed acicular fabric (Pl. 13, figs. F-H; Pl. 14, figs. A, B). In both recent and fossil specimens the homogeneous and the crossed lamellar/crossed acicular sublayers are well developed.

Inner layer. The inner layer is delimited by the pallial myostracum and it is present only internally with respect to the pallial line, not extending inside the hinge plate (Fig. A.7; Pl. 13, figs. A, B; Pl. 14, figs. C-H; Pl. 15, figs. D-H). As for the outer layer, also for the inner shell layer a typical thickness trend is recognized: it starts dorsally to the pallial line and increases its thickness towards the umbonal region, where it disappears (Fig. A.7). The inner aragonitic layer has a fine complex crossed lamellar fabric (FCCL), crossed by several growth lines subparallel to the pallial myostracum.

Pallial myostracum. The inner and outer layers are separated by the pallial myostracum, which is composed of irregular simple prisms (Pl. 14, figs. C-E). Unlike *Glycymeris* and *Aequipecten*, where it is quite evident, in *Arctica* shells the pallial myostracum is not very easy to observe mainly because: a) the fabrics of iOSL and inner layer are very similar, and they do not produce a real contrast between the two layers which could be helpful in enhancing the contact; b) the typical irregular simple prismatic structure which characterized the pallial myostracum is not always observable and when it is present it is very thin or it may be confused with inner layer growth lines.

Growth lines. A lot of attention has been given in the last decades to growth lines in the species *Arctica islandica*, as they are widely used in sclerochronological analysis for palaeoenvironmental, palaeoclimatic and aging purposes (see Chapter 9).

Growth lines are present both in the outer and in the inner shell layers (Pl. 13, figs. A, B; Pl. 14, figs. A, B; Pl. 15, figs. A-H). In the outer shell layer they are curved and slightly inclined, becoming nearly parallel to the outer surface in the innermost part of the shell (Pl. 13, figs. A, B). The fabric of the growth lines changes in the two sublayers of the outer shell layer, becoming more distinct in the innermost part; in the homogenous fabric of oOSL growth lines show two different structures: 1) broad, originally organic-rich valleys containing stacks of smaller, frayed irregular simple prisms, sometimes very difficult to observe, or lacking prisms (Pl. 15, fig. A); 2) quite evident irregular simple prismatic fabric (Pl. 15, fig. C). In the crossed lamellar/crossed acicular iOSL growth lines are more clear than in oOSL; they are distinctly developed and consist of ca. 3.5-6 μm long, irregular simple prisms (Pl. 15, fig. B).

Growth lines on the outer surface of the shell appear as concentric striations, which correspond internally to the outer layer growth lines. In the hinge plate they are concentric and parallel to the direction of growth of the hinge plate itself and are composed of irregular simple prisms.

In the inner layer they are more distinct than in the outer layer; they are parallel to the inner and outer shell surfaces, following the curvature of the shell and consist of parallel and elongated irregular simple prisms (Pl. 15, figs. D-H). In some cases they are so crowded that the fine complex crossed lamellar fabric of the inner layer is entirely masked by the irregular prismatic fabric of the growth lines (Pl. 15, fig. G). In certain inner growth lines, an aligned porosity can be detected along the earlier-deposited side of the prisms composing the growth line, as observed also by Karney et al. (2011); it represents a local enrichment of matrix within this aligned porosity (Pl. 15, fig. H).

Other layers. An irregular prismatic layer is present in the inner part of the hinge plate in both recent and fossil specimens (Pl. 16, fig. A). It consists of elongated and irregular simple prisms perpendicular to the inner surface of the shell. It probably represents the attachment site for the pedal retractor muscles.

Only in the umbonal zone a spherulitic fabric appears in patches; it consists of radially distributed elongated crystals which nucleate at a specific region (Pl. 16, figs. B-D). Very small holes are observed inside these structures probably representing the center of nucleation of the spherulite.

A.2.3.2 Discussions

In agreement with previous findings (Ropes et al., 1984; Dunca et al., 2009; Schöne et al., 2013), the crystal fabric of *A. islandica* shows significant variability across the outer and inner shell layers. Some authors (Ropes et al., 1984; Karney et al., 2011) in describing *A. islandica* fabric divided the outer and inner layers into two sublayers called GI I and GI II, representing respectively the growth line and the growth increment. Notwithstanding the different fabric, GI I and GI II are here not considered as two different sublayers; in fact growth lines are not real shell layers but they are structures which interrupt the inner and outer layers. For these reasons growth increments GI II are here described as outer and inner layers, whereas growth lines GI I are illustrated in the corresponding paragraph, thus adopting the same organization in describing the shell ultrastructure used for previous genera *Glycymeris* and *Aequipecten*.

Two characters are worthy to be here discussed relative to *A. islandica* ultrastructure: the presence of small tubular channels in the oOSL and of the spherulitic fabric in the umbonal region.

Small and empty tubular channels are present in the homogeneous fabric, surrounded by larger and radially arranged crystals; they are different from tubules present in *Glycymeris* shells, as in *A.*

islandica they do not cut the fabric, suggesting that they are primary formed. These channels have been observed also by Dunca et al. (2009, figs. 3 e, f) but their origin is unknown.
Spherulites, according to Marin et al. (2012), represent the starting point of the growth of prisms; these authors observed in the marine gastropod *Haliotis tuberculata*, that spherulites are often produced in 'emergency situations', for filling a hole, in the case of shell repair. However, this fabric in *A. islandica* occurs inside the hinge plate and it does not extend to the outer shell surface, excluding a muscle attachment or a shell repair function because it has no contact with the external; for the moment its function remains unknown.

Recent and fossil specimens show the same well preserved ultrastructure; they both have an homogeneous and crossed lamellar/crossed acicular outer layer, a simple prismatic pallial myostracum and a fine complex crossed lamellar inner layer.
According to Ropes et al. (1984) *Arctica islandica* shells from the east coast of North America have an outer layer mainly composed by crossed lamellar/crossed acicular ultrastructure, showing also an outermost, thin, sublayer of homogenous granular structure. Dunca et al. (2009) observed that *Arctica islandica* shells from Skagerrak, Norway and Iceland have a structure comparable to that of North American specimens. In contrast, shells from the Baltic Sea (Kattegat, Öresund and Kiel Bay) have a poorly organized ultrastructure, with the outer layer mostly consisting of a homogeneous fabric, with thin, not well expressed growth lines lacking the prismatic structure.
Compared to *A. islandica* from fully marine settings (North Sea and Iceland), the life span of the Baltic Sea specimens is distinctly shorter, the shells are generally thinner and smaller and show a less organized ultrastructure; in fact poorly organized homogenous structures have been reported in specimens from more restricted and less stable environments (Dunca et al., 2009). Bivalves, which live under strong environmental fluctuations (as the Baltic Sea) have an outer layer mostly composed by homogeneous fabric, whereas specimens which live in more stable setting (as North America) develop a better organized ultrastructure (crossed lamellar/crossed acicular fabric). The Arda fossil specimens seems to have an intermediate structure between Baltic Sea and North American specimens, as they show an outer layer composed by both homogeneous and crossed lamellar/crossed acicular fabrics; also the recent specimen from Iceland has the same ultrastructure. This suggests that probably the Arda river specimens were subjected to some environmental perturbations; however, these were not so strong as a crossed lamellar/crossed acicular sublayer develops in the shell and growth lines often show the prismatic structure; furthermore shells are usually thick and large, in contrast to the thin and small specimens of the Baltic Sea.

Shell growth and shell crystal fabric represent thus an integrated response of the physiological and biochemical activities of the organism to the surrounding environmental conditions (Stemmer et al., 2013). This is thus an interesting point which should be analyzed in detail with further ultrastructural analysis in order to understand if actually environmental conditions can affect the fabric and its organization.

A.2.3.3 Conclusions

The analysis of the shells of *A. islandica* indicates a strong similarity between fossil and recent fabrics; they both have an homogeneous and crossed lamellar/crossed acicular outer layer, a simple prismatic pallial myostracum and a fine complex crossed lamellar inner layer. This indicates that fossil specimens from the Castell'Arquato Formation of the Arda River (Western Emilia, Italy) are pristine and suitable for geochemical and isotopic analyses.

A. islandica specimens of the Arda river show a similar ultrastructure to the ones occurring in North America, Iceland and in the North Sea, although with small differences; this suggests that the shells from the Arda section were probably subjected to some environmental perturbations, which however were not so strong to prevent the development of an organized ultrastructure and of thick and large shells.

PLATES

PLATE 1

All specimens are x1. (a) external view, (b) internal view, except when indicated.

(1a-b) *Glycymeris glycymeris*, left valve (ACG14-3);

(2a-b) *Glycymeris glycymeris*, right valve (ACG14-22);

(3a-b) *Glycymeris inflata*, right (a) and left (b) valves of an articulated specimen (ACG24-33);

(4a-b) *Glycymeris insubrica*, right valve (ACG97-10).

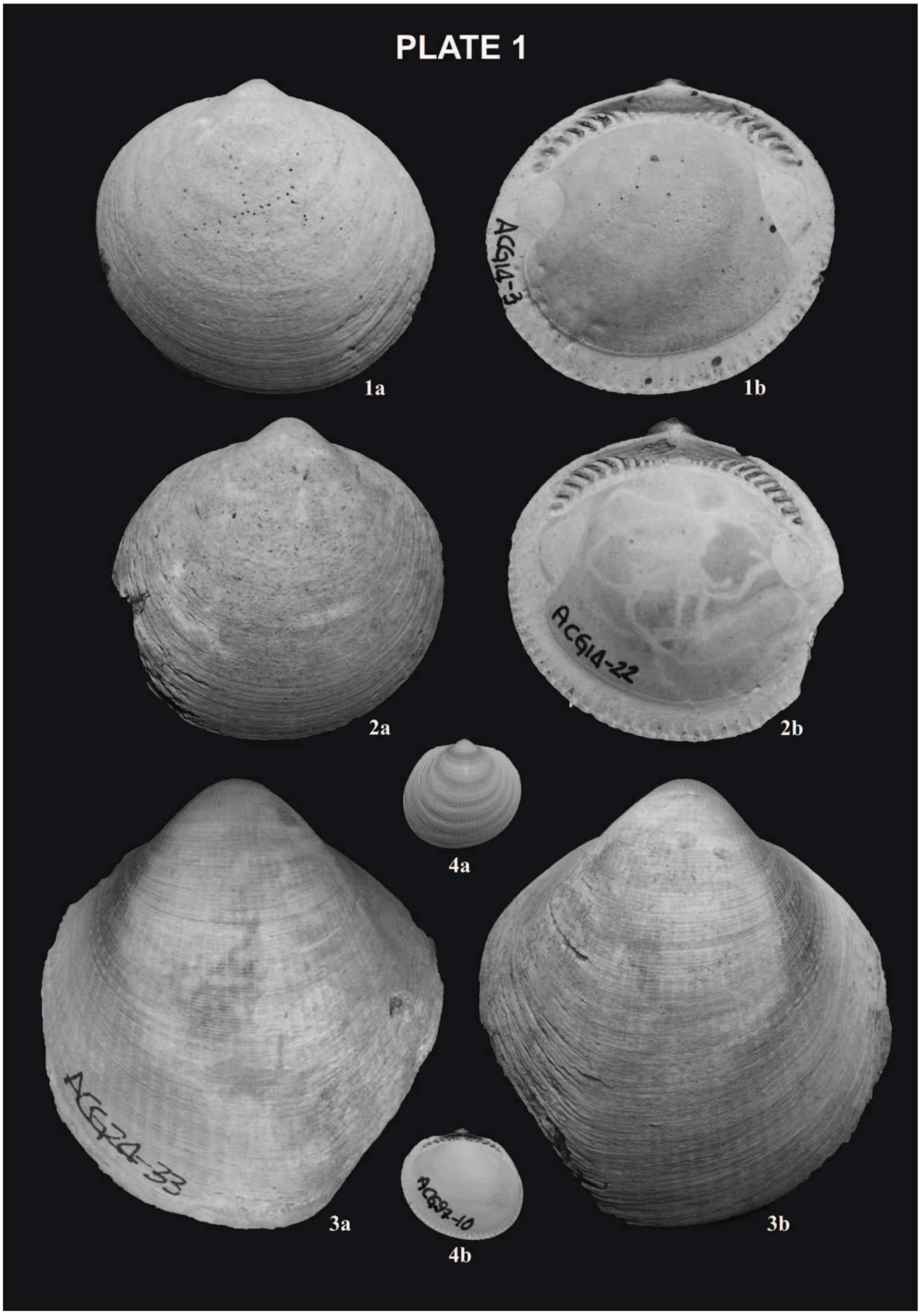
PLATE 1
1a
1b
2a
2b
4a
3a
3b
4b

PLATE 2

All specimens are x1; (a) external view, (b) internal view.

(1a-b) *Glycymeris glycymeris*, right valve (ACG27bis-7);

(2a-b) *Glycymeris insubrica*, left valve. Note the well preserved color pattern (ACG197-5);

(3a-b) *Glycymeris glycymeris,* right valve (ACG243-1);

(4a-b) *Glycymeris inflata*, right valve (ACG29bis-7);

(5a-b) *Glycymeris inflata*, right valve (ACG29bis-28).

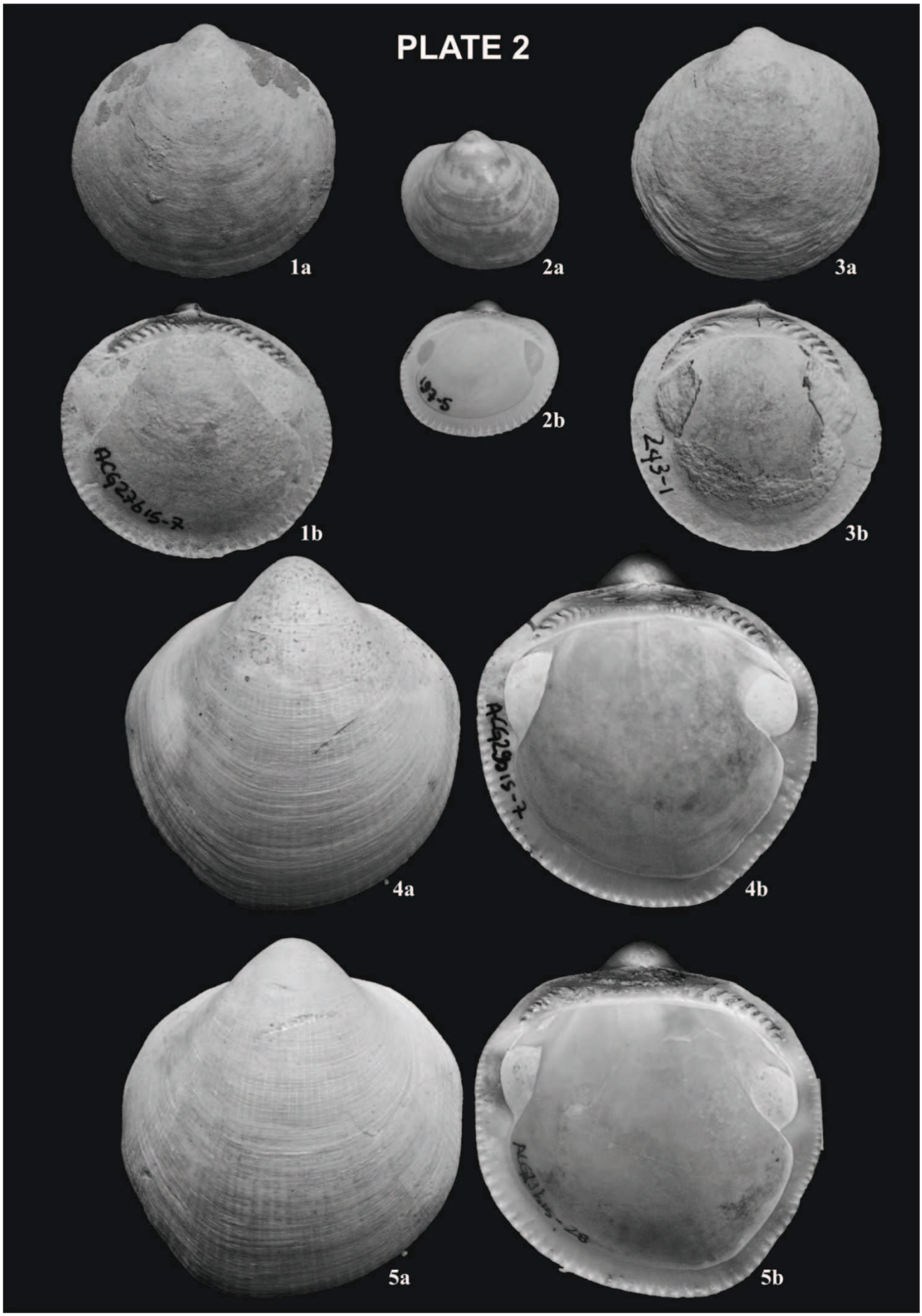
PLATE 2
1a
2a
3a
1b
2b
3b
4a
4b
5a
5b

PLATE 3

All specimens are x1; (a) external view, (b) internal view.

(1a-b) *Glycymeris inflata*, left valve (ACG29bis-32);

(2a-b) *Glycymeris insubrica*, left valve (ACG204-3);

(3a-b) *Glycymeris insubrica*, right valve (ACG264-4);

(4a-b) *Glycymeris insubrica*, left valve. Note the well preserved external ligament (ACG259-1);

(5a-b) *Glycymeris insubrica*, left valve (ACG94-6);

(6a-b) *Glycymeris insubrica*, left valve (ACG204-4);

(7a-b) *Glycymeris insubrica*, right valve (ACG197-4).

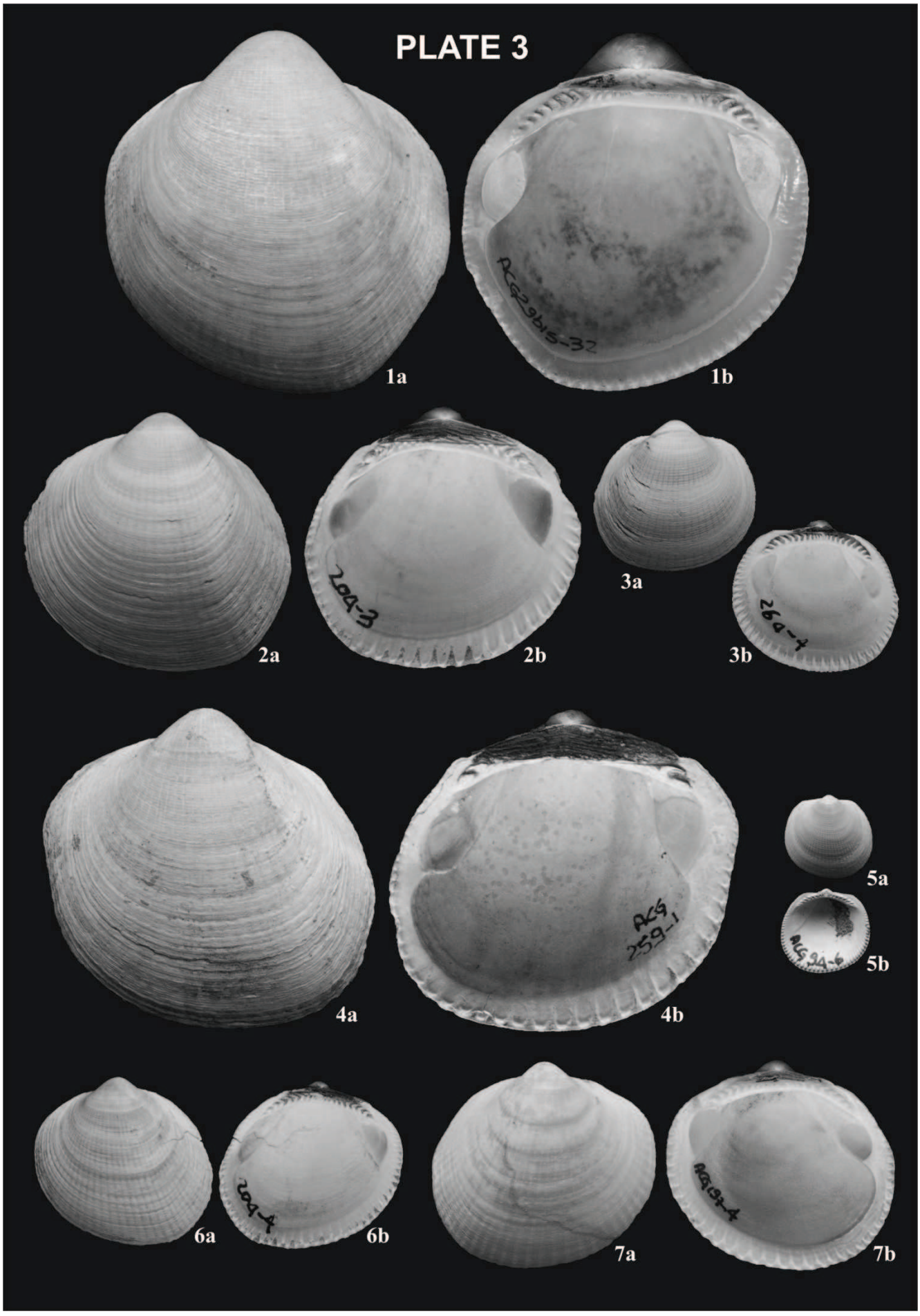
PLATE 3
1a
1b
2a
2b
3a
3b
4a
4b
5a
5b
6a
6b
7a
7b

PLATE 4

All specimens are x1; (a) external view, (b) internal view.

(1a-b) *Aequipecten opercularis,* right valve (ACG197-6);

(2a-b) *Aequipecten opercularis*, right valve (ACG222-1);

(3a-b) *Aequipecten opercularis*, right valve (ACG97-8);

(4a-b) *Arctica islandica*, right valve (ACG215-8);

(5a-b) *Aequipecten opercularis*, right valve (ACG198-2);

(6a-b) *Aequipecten opercularis*, left valve (ACG239-2);

(7a-b) *Aequipecten opercularis*, right valve (ACG104-2).

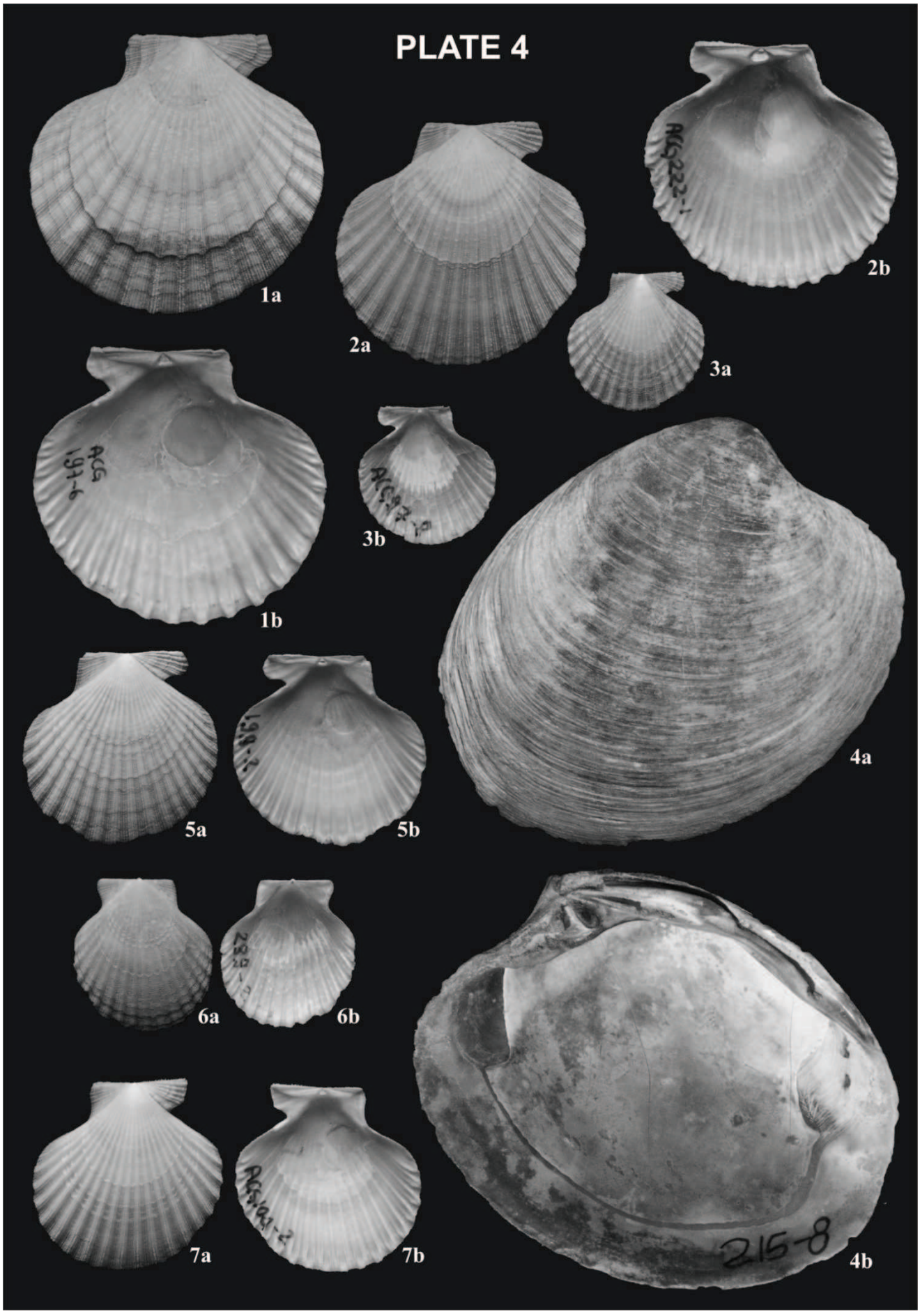
PLATE 4
1a
2a
2b
3a
1b
3b
4a
5a
5b
6a
6b
7a
7b
4b
215-8

PLATE 5

All specimens are x1; (a) external view, (b) internal view.

(1a-b) *Aequipecten opercularis*, left valve (ACG194-5);

(2a-b) *Aequipecten scabrella*, left valve (ACG4-2);

(3a-b) *Aequipecten scabrella*, right valve (ACG4-9);

(4a-b) *Aequipecten scabrella*, right valve (ACG4-5);

(5a-b) *Arctica islandica*, left valve (ACG254-6);

(6a-b) *Arctica islandica*, left valve (ACG253-2).

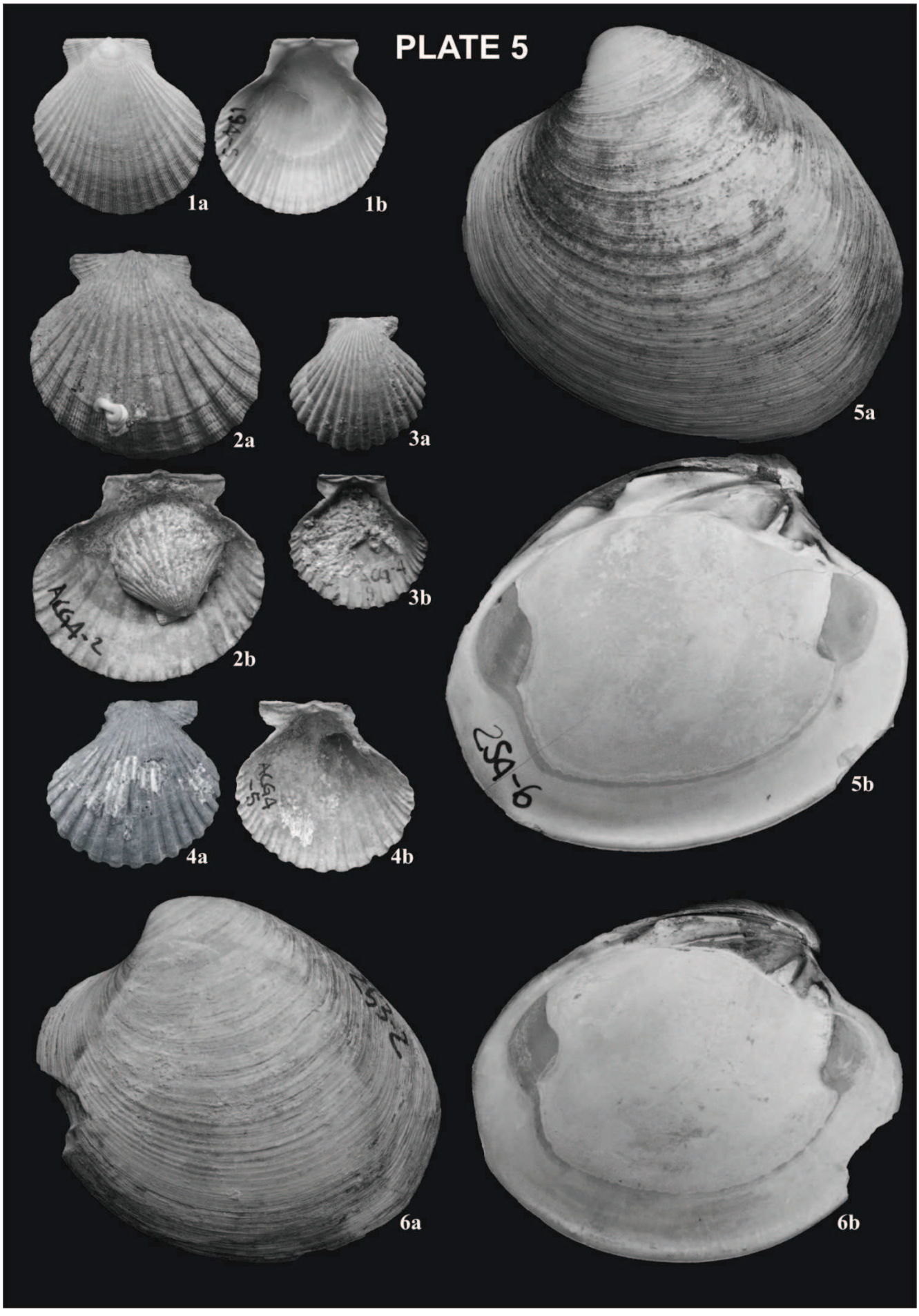
PLATE 5
1a
1b
2a
3a
5a
2b
3b
4a
4b
5b
6a
6b

PLATE 6

Scanning electron microscope images showing the ultrastructure of shells of species of *Glycymeris*; IL: inner layer; GL: growth line; OL: outer layer; OS: outer shell surface; Pm: pallial myostracum; Tb: tubules.

A – Longitudinal section of the shell showing the outer layer, the pallial myostracum and the inner layer with its growth lines; note the darker coloration of the inner layer with respect to the outer layer. Fossil specimen of *Glycymeris glycymeris* (ACG27bis-8).

B - Longitudinal section of the ventral part of the valve showing the outer layer with the external "zebra pattern", the pallial myostracum and the inner layer, which is gradually disappearing near the pallial line; also note that here some tubules are not perpendicular to the outer surface but they are inclined and protrude in the marginal band gradually decreasing their length and disappearing without reaching the outer surface. Fossil specimen of *Glycymeris inflata* (ACG29bis-1).

C - Double pattern of the first order lamellae of the outer layer: irregular, branching and better contrasted in the external part and linear and parallel to each other in the internal part. Fossil specimen of *Glycymeris glycymeris* (ACG27bis-8).

D - First order lamellae of the outer layer crossed by growth lines. Recent specimen of *Glycymeris glycymeris* (AG1).

E - Well preserved first order lamellae of the outer layer; note the empty spaces between the lamellae, probably occupied in alive specimen by organic matrix. Fossil specimen of *Glycymeris insubrica* (ACG9-2).

F - Well preserved crossed lamellae of the outer layer: first, second and third order elements are clearly observable. Fossil specimen of *Glycymeris glycymeris* (ACG14-4).

G - Double pattern of the outer layer with branching to subparallel first order lamellae, crossed by growth lines. Recent specimen of *Glycymeris glycymeris* (AG1).

H - Detail of a first order lamella showing the fourth order granules that compose the third order rods. Recent specimen of *Glycymeris glycymeris* (AG1).

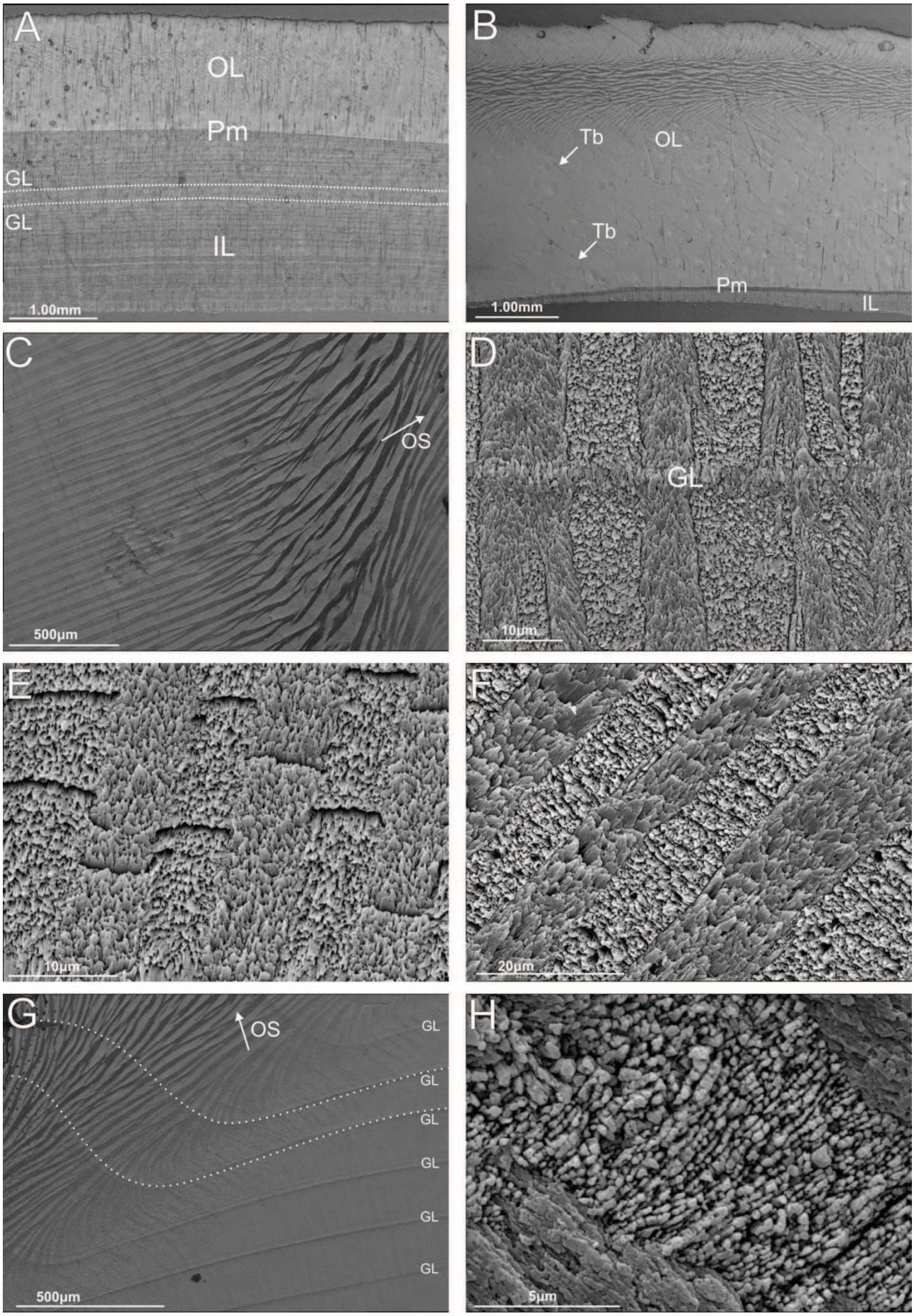
A
OL
Pm
GL
GL
IL
1.00mm
B
Tb
OL
Tb
Pm
IL
1.00mm
C
OS
500µm
D
GL
10µm
E
10µm
F
20µm
G
OS
GL
GL
GL
GL
GL
GL
500µm
H
5µm

PLATE 7

Scanning electron microscope images showing the ultrastructure of shells of species of *Glycymeris;* IL: inner layer; IS: inner shell surface; GL: growth line; OL: outer layer; Pm: pallial myostracum; Tb: tubules.

A - Irregular complex crossed lamellar inner layer with third order rods inclined in different directions. Fossil specimen of *Glycymeris inflata* (ACG29bis-1).

B - Cone complex crossed lamellar inner layer cut by a tubule. Fossil specimen of *Glycymeris insubrica* (ACG49-1).

C - Irregular complex crossed lamellar inner layer crossed by growth lines made of irregular simple prisms. Recent specimen of *Glycymeris glycymeris* (AG2).

D - Cone complex crossed lamellar inner layer; third order elements radiate from the cone apices. Fossil specimen of *Glycymeris glycymeris* (ACG14-11).

E - Irregular complex crossed lamellar inner layer crossed by irregular prismatic growth lines; prisms of growth lines are made by third rods prolongation. Recent specimen of *Glycymeris glycymeris* (AG2).

F - Cone complex crossed lamellar inner layer. Fossil specimen of *Glycymeris insubrica* (ACG98-3).

G - Prismatic pallial myostracum disappearing in the inner part of the hinge plate. Fossil specimen of *Glycymeris glycymeris* (ACG27bis-8).

H - Prismatic pallial myostracum; note that the pallial myostracum is usually thicker than the inner layer growth lines and can be easily distinguish. Fossil specimen of *Glycymeris insubrica* (ACG59-1).

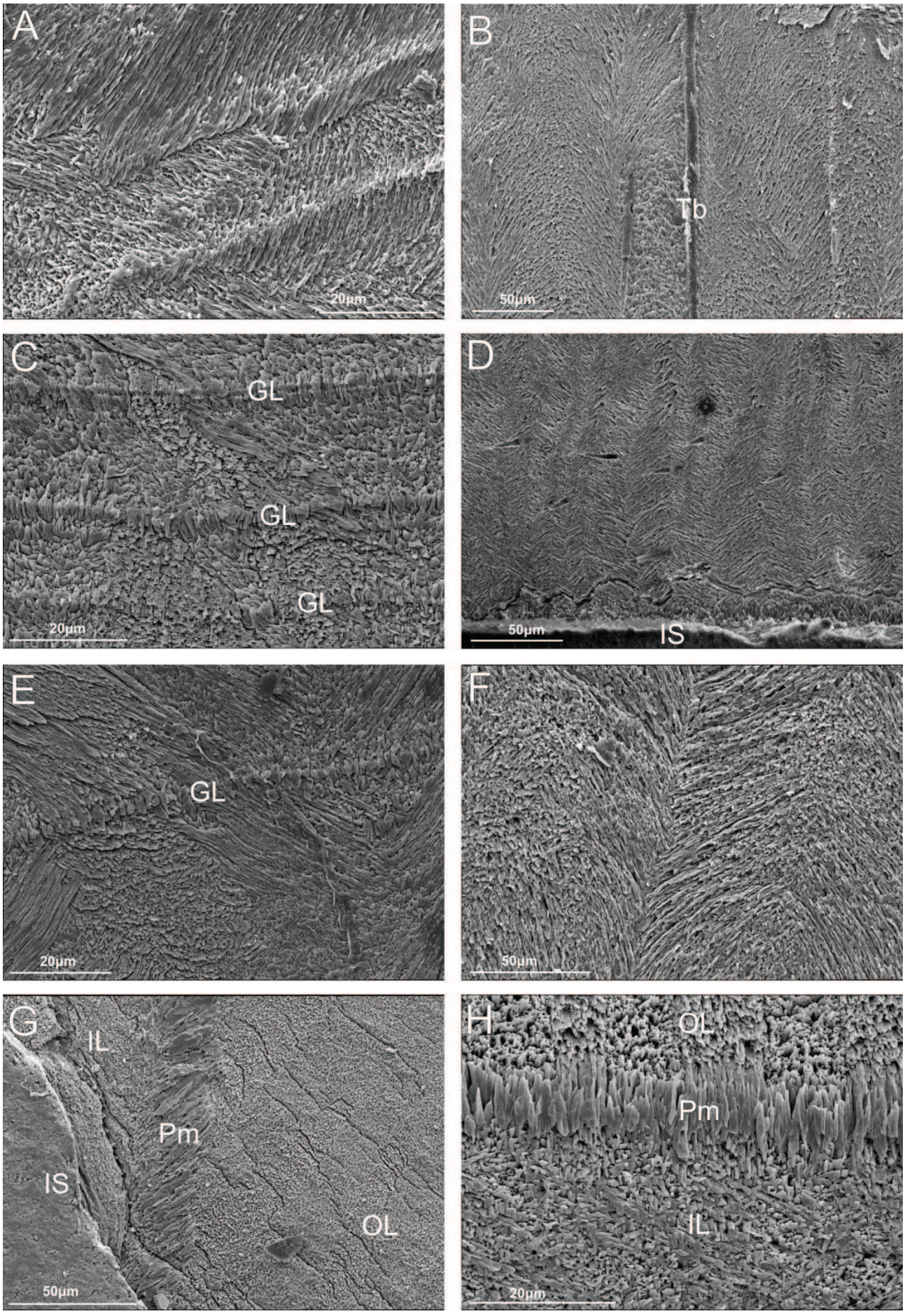
A
20µm
B
Tb
50µm
C
GL
GL
GL
20µm
D
50µm
IS
E
GL
20µm
F
50µm
G
IL
Pm
IS
OL
50µm
H
OL
Pm
IL
20µm

PLATE 8

Scanning electron microscope images showing the ultrastructure of shells of species of *Glycymeris*; ISP: irregular simple prisms; IL: inner layer; IS: inner shell surface; GL: growth line; Mb: marginal band; OL: outer layer; OS: outer shell surface; Pm: pallial myostracum; Tb: tubules.

A – Sharp contact between outer and inner layers represented by the prismatic pallial myostracum; note that tubules cross all the mineralized layers cutting the fabric. Fossil specimen of *Glycymeris glycymeris* (ACG27bis-8).

B – Sharp contact between outer and inner layers underlined by a very regular prismatic pallial myostracum. Fossil specimen of *Glycymeris insubrica* (ACG83-1).

C – Irregular simple prismatic layer in the inner part of the hinge plate representing the attachment site for pedal retractor muscles. Fossil specimen of *Glycymeris insubrica* (ACG31-1).

D – Irregular simple prismatic layer in the inner part of the hinge plate representing the attachment site for pedal retractor muscles. Fossil specimen of *Glycymeris insubrica* (ACG204-1).

E – Irregular simple prismatic layer in the inner part of the hinge plate; note also concentric growth lines. Fossil specimen of *Glycymeris* sp. (ACG76-25).

F – Detail of the marginal band on the left, showing that tubules gradually decrease their length and do not reach the outer surface; note the curve growth lines that are traceable also on the outer surface of the shell. Fossil specimen of *Glycymeris insubrica* (ACG53-16).

G – Tubule in the outer layer; note that the fabric is cut by the tubule, suggesting that it should be secondarily formed. Fossil specimen of *Glycymeris* sp. (ACG24-4).

H – Tubule cutting the fabric in the outer layer. Fossil specimen of *Glycymeris insubrica* (ACG197-2).

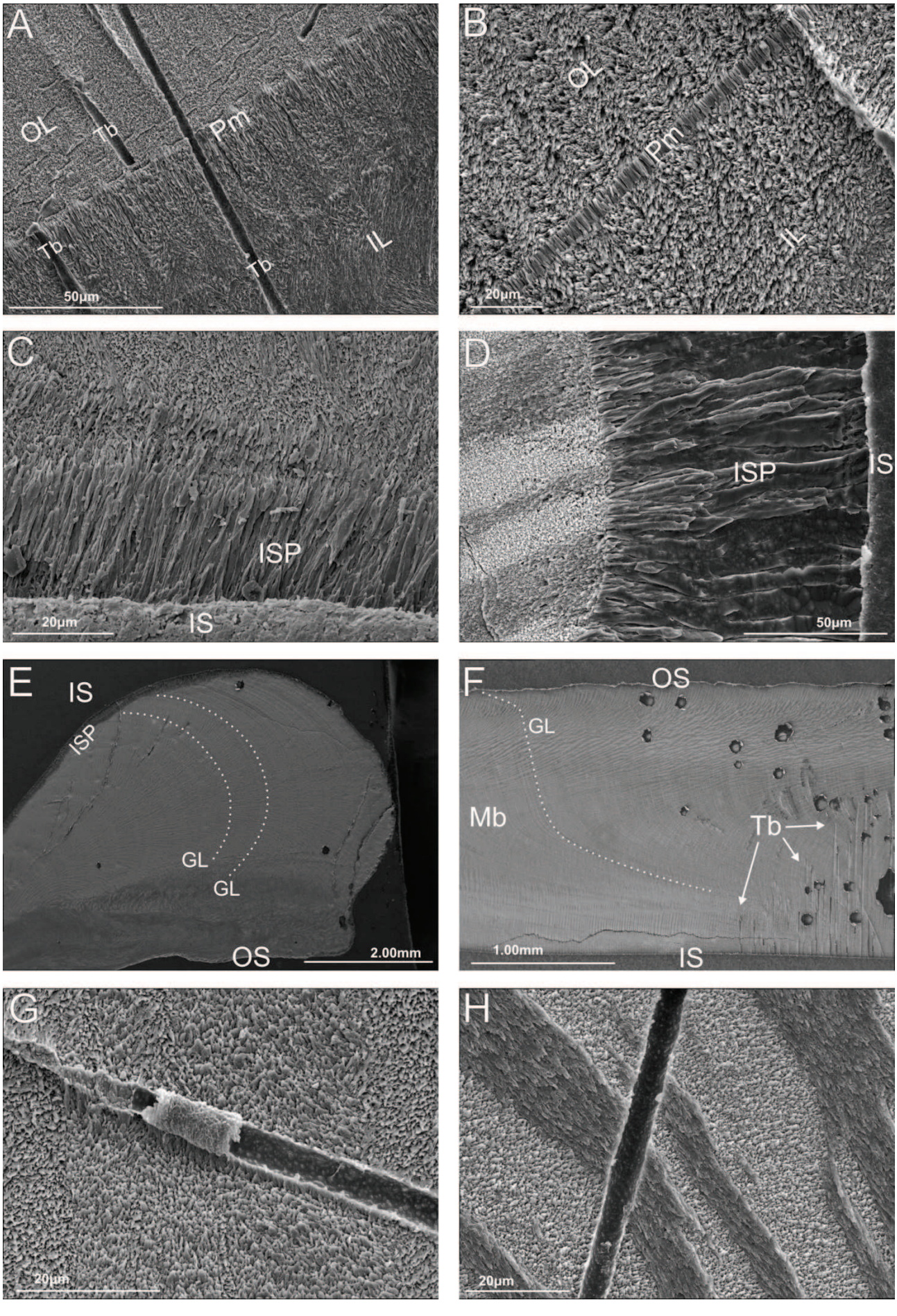
A
OL
Tb
Pm
Tb
Tb
IL
50µm
B
OL
Pm
IL
20µm
C
ISP
20µm
IS
D
ISP
IS
50µm
E
IS
ISP
GL
GL
OS
2.00mm
F
OS
GL
Mb
Tb
1.00mm
IS
G
20µm
H
20µm

PLATE 9

Scanning electron microscope images showing the ultrastructure of shells of species of *Glycymeris* and *Aequipecten*; CL: crossed lamellar; CCL: complex crossed lamellar; GL: growth line; ISP: irregular simple prisms; IL: inner layer; ML: middle layer; OL: outer layer; OS: outer surface; Pm: pallial myostracum.

A - Parallel cylindrical tubules cutting the irregular complex crossed lamellae and the growth lines of the inner layer; the tubule is formed after the secretion of the shell layer because it cuts the fabric. Fossil specimen of *Glycymeris insubrica* (ACG59-1).

B - Flared distal end of tubule near the outer surface; note that the tubule flares only in its distal end confirming that the chemical secretion occurs only in the tip of the unicellular mantle extension. Recent specimen of *Glycymeris glycymeris* (AG1).

C - Tubule cutting the well preserved first and second order lamellae of the outer layer. Fossil specimen of *Glycymeris glycymeris* (ACG14-11).

D - Cylindrical tubules filled by the epoxidic resin cut the simple crossed lamellar fabric of the outer layer. Recent specimen of *Glycymeris glycymeris* (AG2).

E – Longitudinal section of the shell showing the outer, middle and inner layers. The inner layer is composed of a complex crossed foliated fabric; the middle layer has a prismatic and crossed lamellar ultrastructure; the outer layer shows a regular foliated fabric near the middle layer passing to a complex crossed foliated fabric towards the outer surface. Right valve of *Aequipecten opercularis* (ACG24-14).

F - Longitudinal section of the shell showing the outer, middle and inner layers. The inner layer is composed of a complex crossed foliated fabric. The middle layer has a prismatic and a crossed lamellar ultrastructure (note the thickness of the irregular simple prismatic fabric). The outer layer shows a regular foliated fabric. Left valve of *Aequipecten opercularis* (ACG213-1).

G – Section showing the complex organization of the shell. The outer and inner layers are composed of a regular foliated fabric. The middle layer shows a double pattern of crossed lamellae (simple and complex) separated by a thin layer of irregular simple prisms; below, there is a thick layer of irregular simple prisms. Right valve of *Aequipecten opercularis* (ACG100-2).

H – Longitudinal section of the shell showing a middle layer as in fig. G and an outer layer composed of a regular foliated fabric close to the middle layer, then passing to a complex crossed foliated to crossed foliated fabric. Right valve of *Aequipecten opercularis* (ACG11-1).

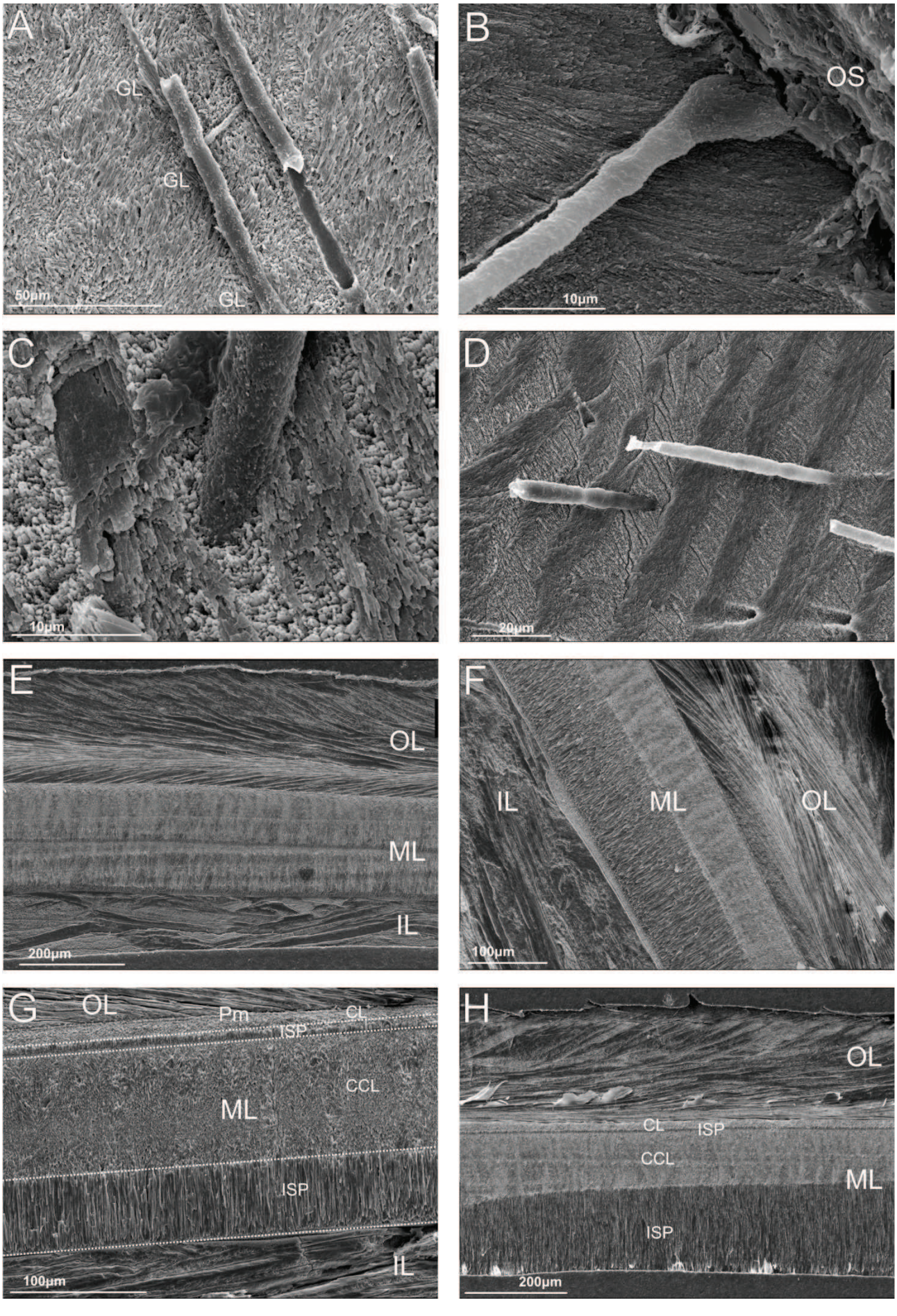
A
GL
GL
GL
50μm
B
OS
10μm
C
10μm
D
20μm
E
OL
ML
IL
200μm
F
IL
ML
OL
100μm
G
OL
Pm
CL
ISP
CCL
ML
ISP
IL
100μm
H
OL
CL
ISP
CCL
ML
ISP
200μm

PLATE 10

Scanning electron microscope images showing the ultrastructure of shells of species of *Aequipecten*; CF: crossed foliated; CCF: complex crossed lamellar; IL: inner layer; ML: middle layer; OL: outer layer.

A – Longitudinal section of the shell showing a regular foliated outer layer, a prismatic middle layer and a complex crossed foliated inner layer. Left valve of *Aequipecten opercularis* (ACG235-4).

B – Regular foliated fabric in the umbonal region. Right valve of *Aequipecten opercularis* (ACG70-3).

C – Regular foliated fabric in the marginal band. Right valve of *Aequipecten opercularis* (ACG93-8).

D – Regular foliated fabric of the inner layer; note the arrow-pointed ending of the laths all pointing in the same direction. Right valve of *Aequipecten opercularis* (ACG70-3).

E – Regular foliated fabric in the umbonal region. Right valve of *Aequipecten opercularis* (ACG37-8).

F – Crossed lamellar middle layer and crossed foliated inner layer. Right valve of *Aequipecten opercularis* (ACG43-3).

G – Crossed foliated fabric of the inner layer; note that the lath endings point in two opposite directions (white arrows). Left valve of *Aequipecten opercularis* (ACG90-7).

H – Gradual transition from a complex crossed foliated fabric to a crossed foliated one in the outer layer. Left valve of *Aequipecten opercularis* (ACG66-7).

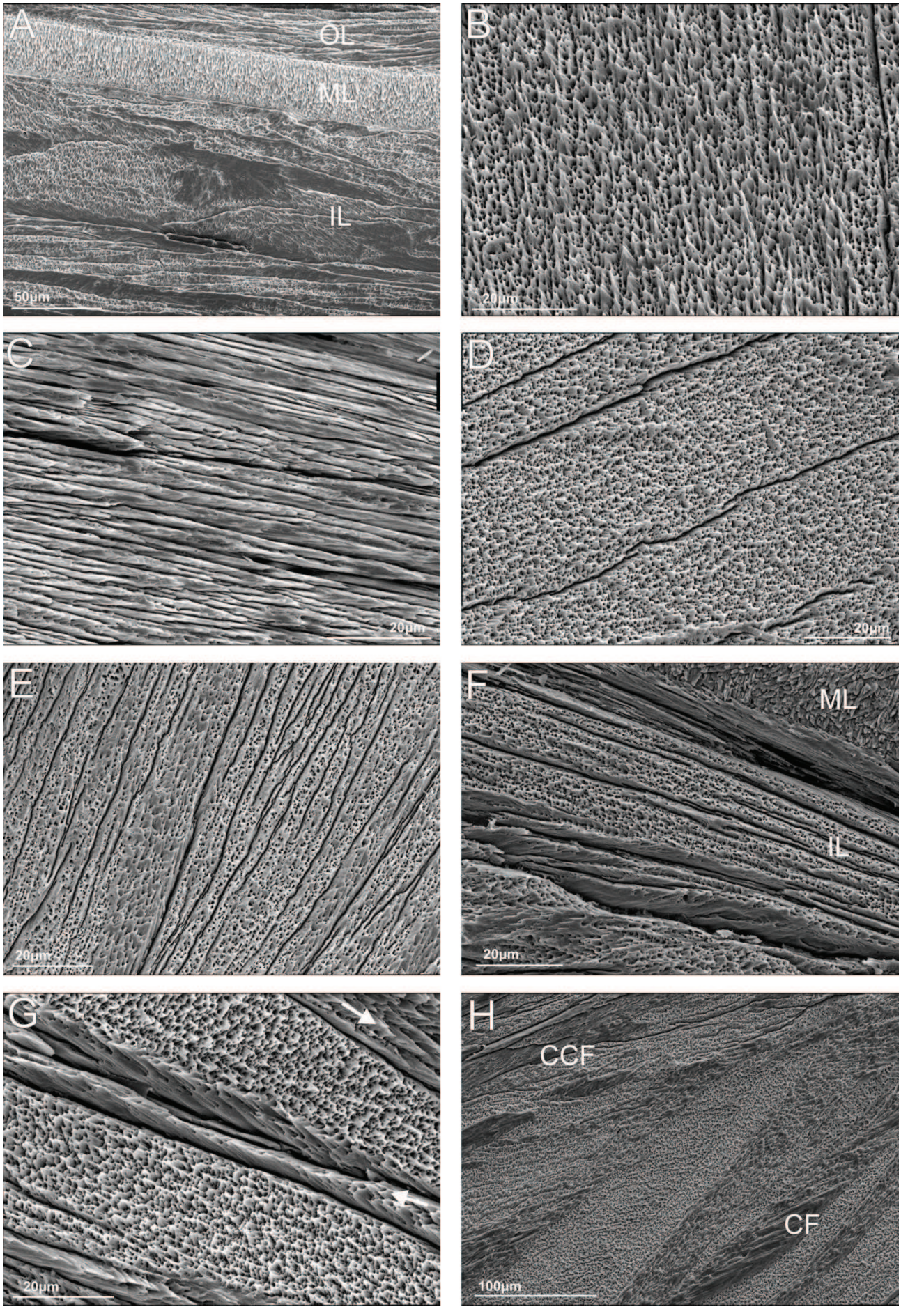
A
OL
ML
IL
50µm
B
20µm
C
20µm
D
20µm
E
20µm
F
ML
IL
20µm
G
20µm
H
CCF
CF
100µm

PLATE 11

Scanning electron microscope images showing the ultrastructure of shells of species of *Aequipecten*; CF: crossed foliated; CCF: complex crossed foliated; CL: crossed lamellar; CCL: complex crossed lamellar; ISP: irregular simple prisms; IL: inner layer; IS: inner shell surface; ML: middle layer; OL: outer layer; OS: outer shell surface; Pm: pallial myostracum; RF: regular foliated.

A – Complex crossed foliated fabric of the outer layer passing to regular foliated toward the interior of the valve. Right valve of *Aequipecten opercularis* (ACG81-1).

B – Cone complex crossed foliated fabric of the inner layer passing to regular foliated towards the central part of the shell. Left valve of *Aequipecten opercularis* (ACG97-6).

C – Complex crossed foliated outer layer. Right valve of *Aequipecten opercularis* (ACG252-5).

D – Contact between the crossed lamellar middle layer and the complex crossed foliated inner layer. Right valve of *Aequipecten opercularis* (ACG24-14).

E – Regular foliated outer layer separated from the middle layer by an irregular simple prismatic pallial myostracum. The middle layer has a crossed lamellar fabric. Right valve of *Aequipecten opercularis* (ACG41-3).

F – Middle layer showing the crossed lamellar fabric passing to irregular simple prisms. Left valve of *Aequipecten opercularis* (ACG133-2).

G – Regular foliated outer layer separated from the middle layer by an irregular simple prismatic pallial myostracum. In the middle layer CL and CCL are separated by a thin layer of irregular simple prisms. Right valve of *Aequipecten opercularis* (ACG24-14).

H – Crossed lamellar middle layer and crossed foliated outer layer. Right valve of *Aequipecten opercularis* (ACG30-7).

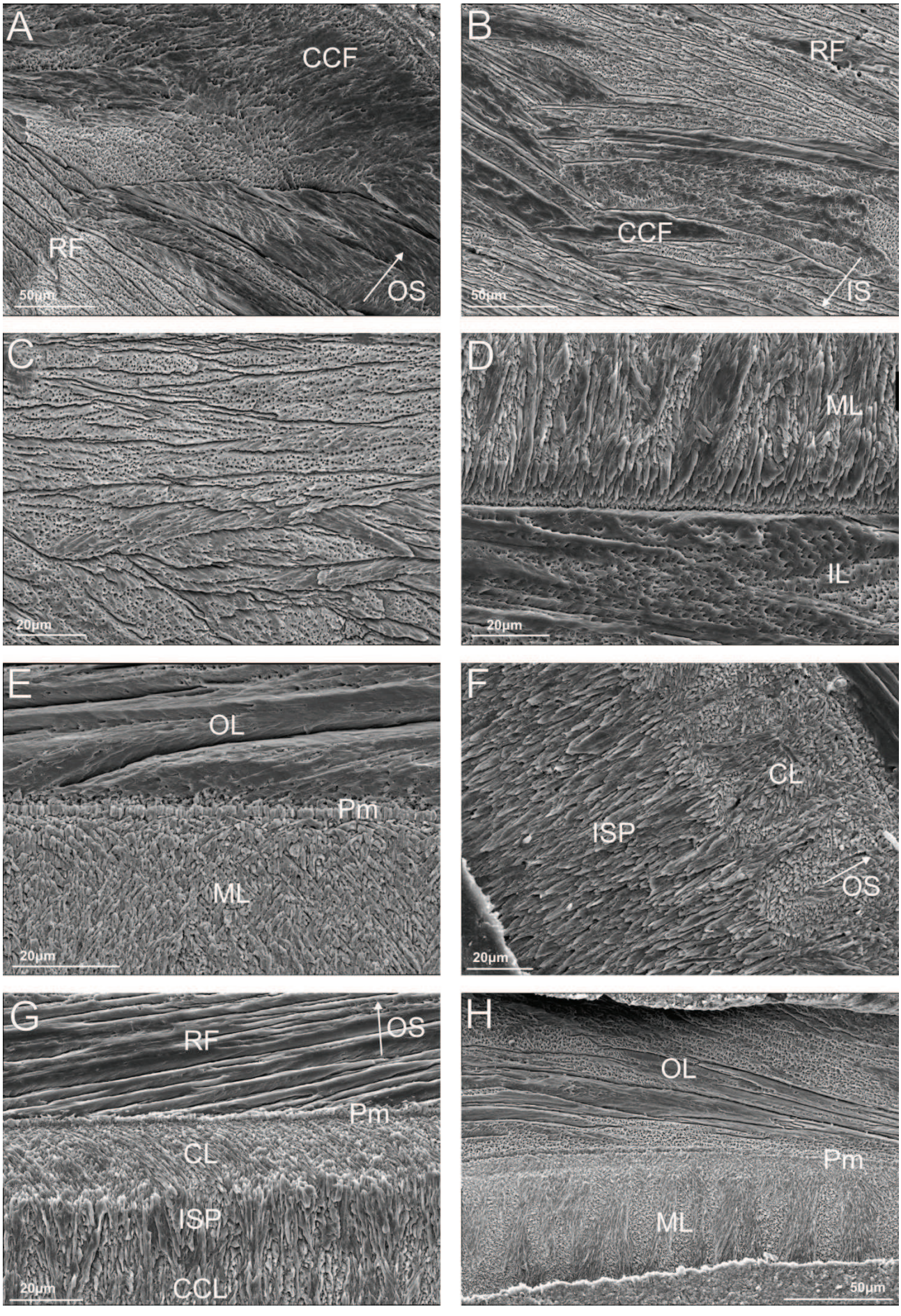
A
CCF
RF
OS
50μm
B
RF
CCF
IS
50μm
C
20μm
D
ML
IL
20μm
E
OL
Pm
ML
20μm
F
CL
ISP
OS
20μm
G
RF
OS
Pm
CL
ISP
CCL
20μm
H
OL
Pm
ML
50μm

PLATE 12

Scanning electron microscope images showing the ultrastructure of shells of species of *Aequipecten*; CF: crossed foliated; CCF: complex crossed foliated; CL: crossed lamellar; CCL: complex crossed lamellar; IL: inner layer; IS: inner shell surface; ISP: irregular simple prisms; ML: middle layer; OL: outer layer; OS: outer shell surface; Pm: pallial myostracum; SC: sparry calcite.

A – Regular foliated outer layer separated from a crossed lamellar middle layer by a simple prismatic pallial myostracum. Left valve of *Aequipecten opercularis* (ACG52-1a).

B – Middle layer showing the double pattern of crossed lamellae above and cone complex crossed lamellae below. Left valve of *Aequipecten opercularis* (ACG56-1).

C – Regular foliated outer layer, irregular simple prismatic pallial myostracum and, crossed lamellar and irregular simple prismatic middle layer. Left valve of *Aequipecten opercularis* (ACG235-4).

D – Contact between the crossed lamellar middle layer and the regular foliated outer layer. Left valve of *Aequipecten opercularis* (ACG91-6).

E – Longitudinal section of the shell showing pointed growth lamellae, which produce the ornamentation on the outer shell surface. Right valve of *Aequipecten opercularis* (ACG44-2).

F – Section of an altered shell, showing a complex crossed foliated outer and inner layer and a middle layer filled by sparry calcite. Right valve of *Aequipecten scabrella* (ACG2-5).

G – Sparry calcite replacing the aragonitic middle layer in an altered shell. Left valve of *Aequipecten scabrella* (ACG6-8).

H – Middle and outer layer of an altered shell. Note the sparry calcite replacing the aragonitic crossed lamellae. The outer layer show a gradual transition from a cone complex crossed foliated (with evident cones made by calcitic laths) to a crossed foliated fabric. Left valve of *Aequipecten scabrella* (ACG6-8).

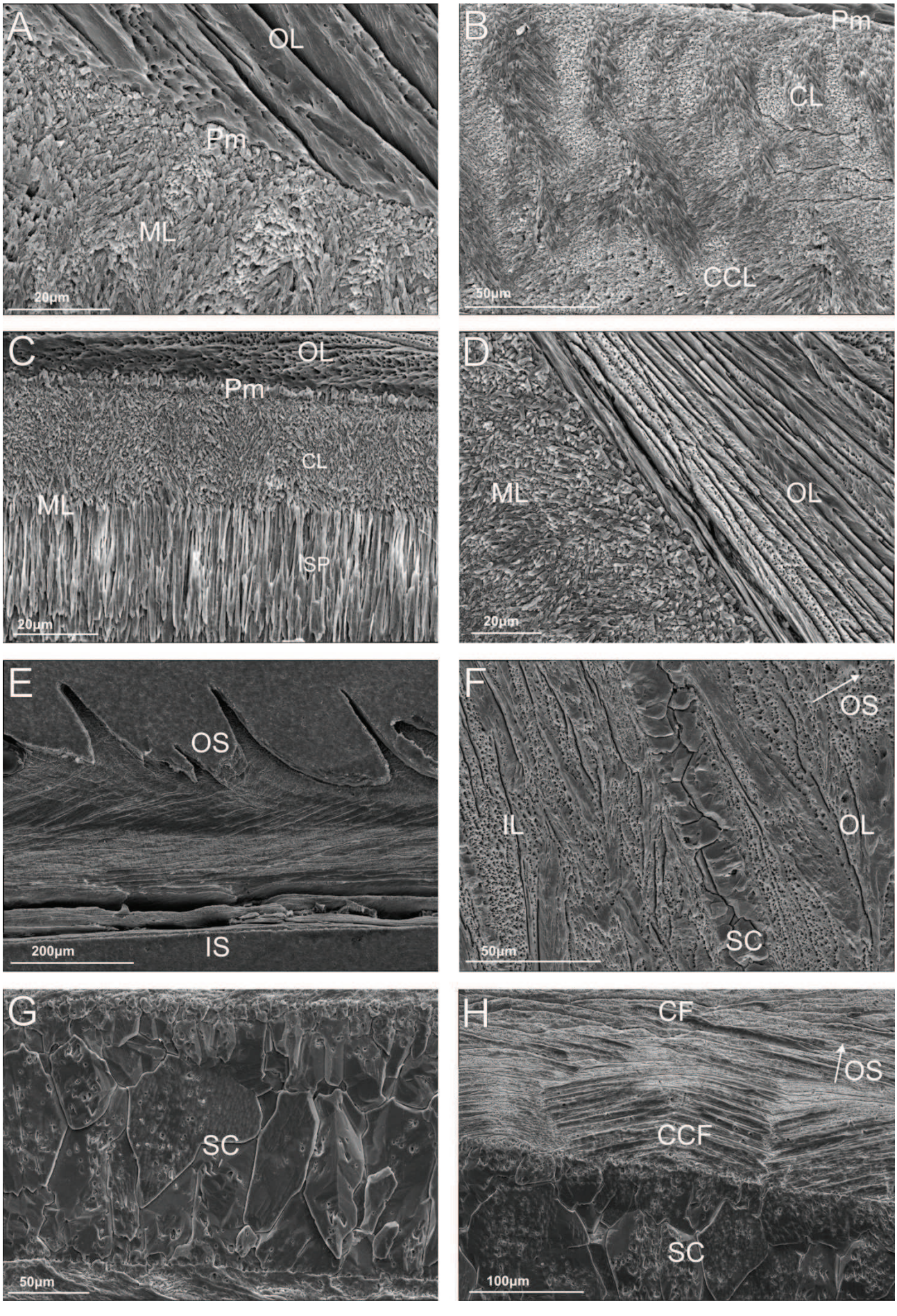
A
OL
Pm
ML
20μm
B
Pm
CL
CCL
50μm
C
OL
Pm
CL
ML
ISP
20μm
D
ML
OL
20μm
E
OS
200μm
IS
F
OS
IL
OL
SC
50μm
G
SC
50μm
H
CF
OS
CCF
SC
100μm

PLATE 13

Scanning electron microscope images showing the ultrastructure of shells of *Arctica islandica;* CL/CA: crossed lamellar/crossed acicular; dog: direction of growth; GL: growth line; HOM: homogeneous; IL: inner layer; OL: outer layer.

A – Longitudinal section of the shell showing the inner and outer layers; the outer layer is crossed by curved growth lines. Fossil specimen of *Arctica islandica* (ACG78-1).

B – Longitudinal section of the shell showing the inner and outer layers; outer layer is crossed by curved growth lines. Fossil specimen of *Arctica islandica* (ACG253-2).

C – Homogeneous fabric of the outer layer. Recent specimen of *Arctica islandica* (AG3).

D – Homogeneous fabric of the outer layer; note the small tubular channels (white arrows), empty inside, surrounded by radially directed larger crystals. Fossil specimen of *Arctica islandica* (ACG225-1).

E – Homogeneous fabric of the outer layer. Fossil specimen of *Arctica islandica* (ACG78-2).

F – Outer layer with granules of the homogeneous fabric gradually passing to a crossed lamellar/crossed acicular crystals. Recent specimen of *Arctica islandica* (AG3).

G – Gradual transition of the homogeneous fabric to a crossed lamellar/crossed acicular one. Fossil specimen of *Arctica islandica* (ACG228-1).

H – Gradual transition of the homogeneous fabric to a crossed lamellar/crossed acicular one. Fossil specimen of *Arctica islandica* (ACG254-1).

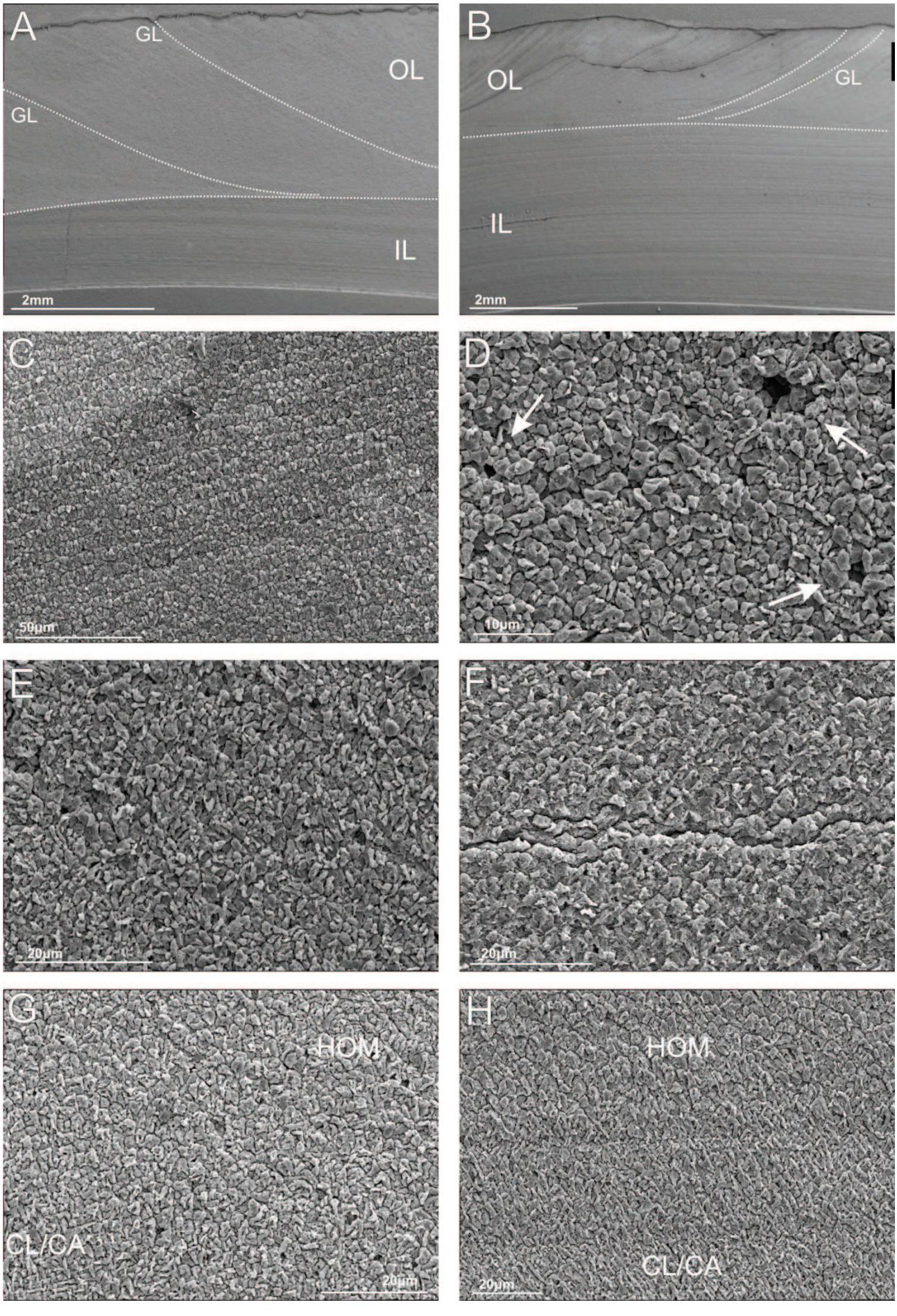
A
GL
OL
GL
IL
2mm
B
OL
GL
IL
2mm
C
50µm
D
10µm
E
20µm
F
20µm
G
HOM
CL/CA
20µm
H
HOM
CL/CA
20µm

PLATE 14

Scanning electron microscope images showing the ultrastructure of shells of *Arctica islandica;* CL/CA: crossed lamellar/crossed acicular; GL: growth line; HOM: homogeneous; IL: inner layer; OL: outer layer; Pm: pallial myostracum.

A – Outer layer showing a gradual transition from a homogeneous fabric to a crossed lamellar/crossed acicular one. Note the poor distinct growth line. Fossil specimen of *Arctica islandica* (ACG200-10).

B – Outer layer showing the transition from homogeneous fabric to crossed lamellar/crossed acicular one. In this case the simple prismatic fabric of the growth line represent the contact between the HOM and CL/CA structures. Fossil specimen of *Arctica islandica* (ACG226-1).

C – Homogeneous outer layer and fine complex crossed lamellar inner layer separated by a simple irregular prismatic pallial myostracum. Fossil specimen of *Arctica islandica* (ACG228-1).

D – Homogeneous outer layer and fine complex crossed lamellar inner layer separated by a simple irregular prismatic pallial myostracum. Fossil specimen of *Arctica islandica* (ACG226-3).

E – Homogeneous outer layer and fine complex crossed lamellar inner layer. The pallial myostracum here is not clear; a thin layer of simple irregular prisms seems to be present, but it is difficult to observe. Fossil specimen of *Arctica islandica* (ACG202-3).

F – Fine complex crossed lamellar inner layer. Fossil specimen of *Arctica islandica* (ACG228-1).

G – Fine complex crossed lamellar inner layer. Fossil specimen of *Arctica islandica* (ACG229-1).

H – Fine complex crossed lamellar inner layer. Fossil specimen of *Arctica islandica* (ACG86-4).

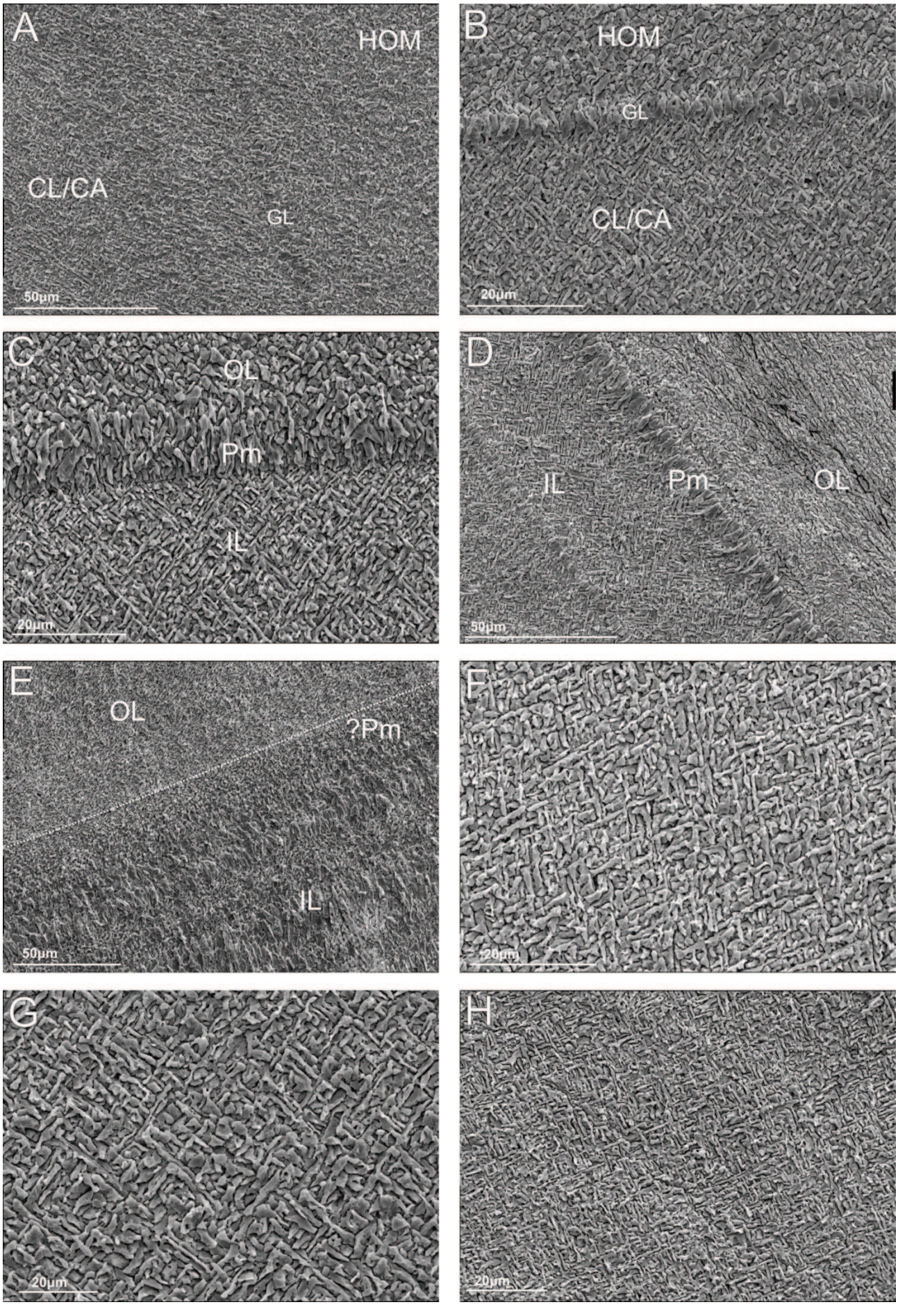
A
HOM
CL/CA
GL
50µm
B
HOM
GL
CL/CA
20µm
C
OL
Pm
IL
20µm
D
IL
Pm
OL
50µm
E
OL
?Pm
IL
50µm
F
20µm
G
20µm
H
20µm

PLATE 15

Scanning electron microscope images showing the ultrastructure of shells of *Arctica islandica;* GL: growth line.

A – Broad, originally organic-rich valley representing a growth line in the homogeneous outer layer and lacking the irregular prismatic structure. Fossil specimen of *Arctica islandica* (ACG200-13).

B – Irregular simple prisms forming a growth line in the crossed lamellar/crossed acicular sublayer. Fossil specimen of *Arctica islandica* (ACG254-4).

C – Irregular simple prisms forming a growth line in the homogeneous outer layer. Fossil specimen of *Arctica islandica* (ACG213bis-3).

D – Growth line in the fine complex crossed lamellar inner layer. Fossil specimen of *Arctica islandica* (ACG86-4).

E – Growth line in the fine complex crossed lamellar inner layer. Fossil specimen of *Arctica islandica* (ACG78-2).

F – Growth lines in the fine complex crossed lamellar inner layer. Recent specimen of *Arctica islandica* (AG3).

G – Crowded growth lines, which entirely mask the fine complex crossed lamellar fabric of the inner layer. Fossil specimen of *Arctica islandica* (ACG225-1).

H – Aligned porosity along the earlier-deposited side of the prisms composing the growth line (white arrows), which represent a local enrichment in organic matrix. Fossil specimen of *Arctica islandica* (ACG253-2).

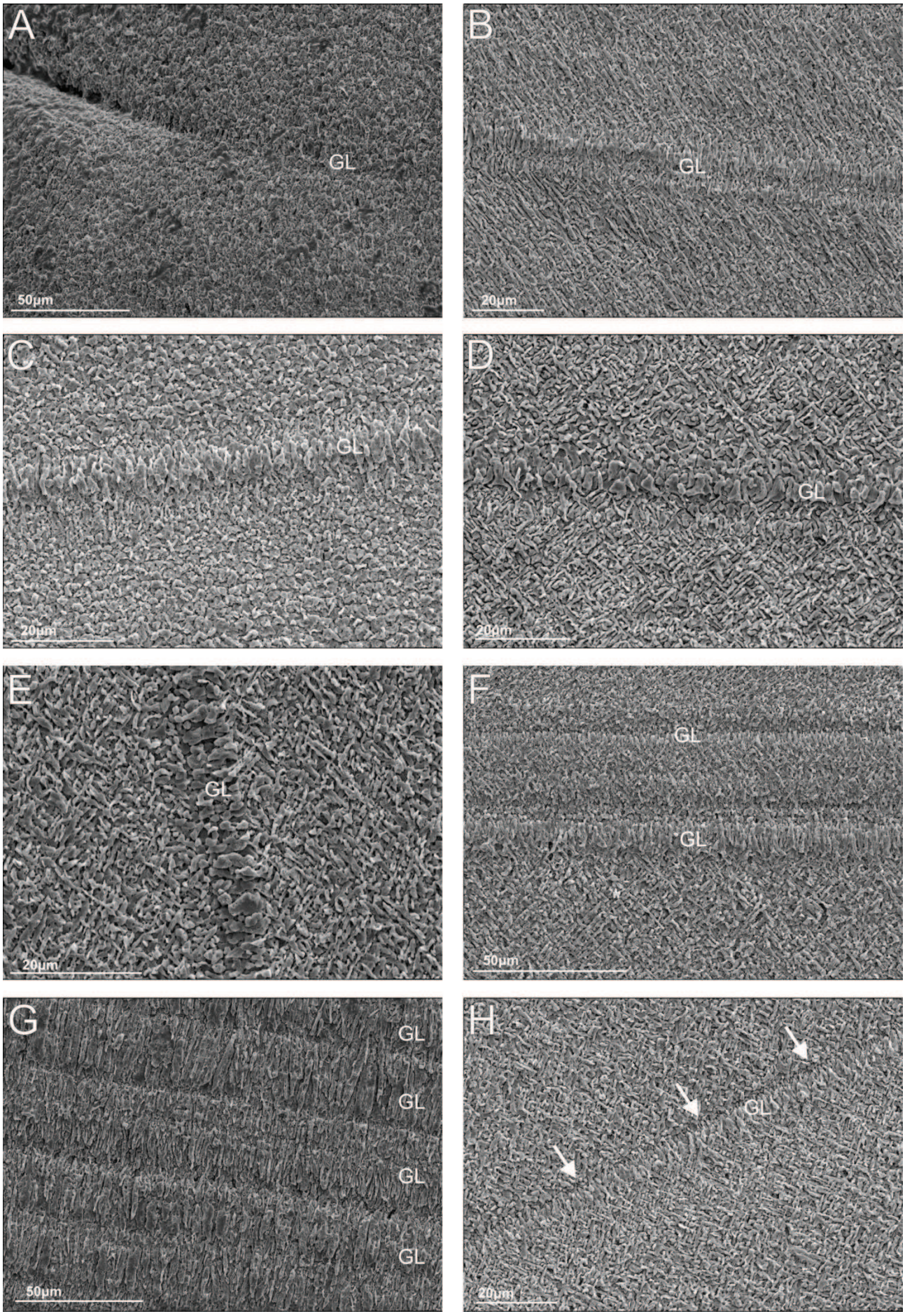
A
GL
50µm
B
GL
20µm
C
GL
20µm
D
GL
20µm
E
GL
20µm
F
GL
GL
50µm
G
GL
GL
GL
GL
50µm
H
GL
20µm

PLATE 16

Scanning electron microscope images showing the ultrastructure of shells of *Arctica islandica;* IS: inner shell surface; ISP: irregular simple prisms.

A – Irregular prismatic layer in the inner part of the hinge plate, probably representing the attachment site for the pedal retractor muscles. Fossil specimen of *Arctica islandica* (ACG224-1).

B – Spherulitic fabric occurring in the umbonal region. Fossil specimen of *Arctica islandica* (ACG254-1).

C – Spherulitic fabric occurring in the umbonal region. Recent specimen of *Arctica islandica* (AG3).

D – Detail of the spherulitic fabric represented in fig. C. Recent specimen of *Arctica islandica* (AG3).

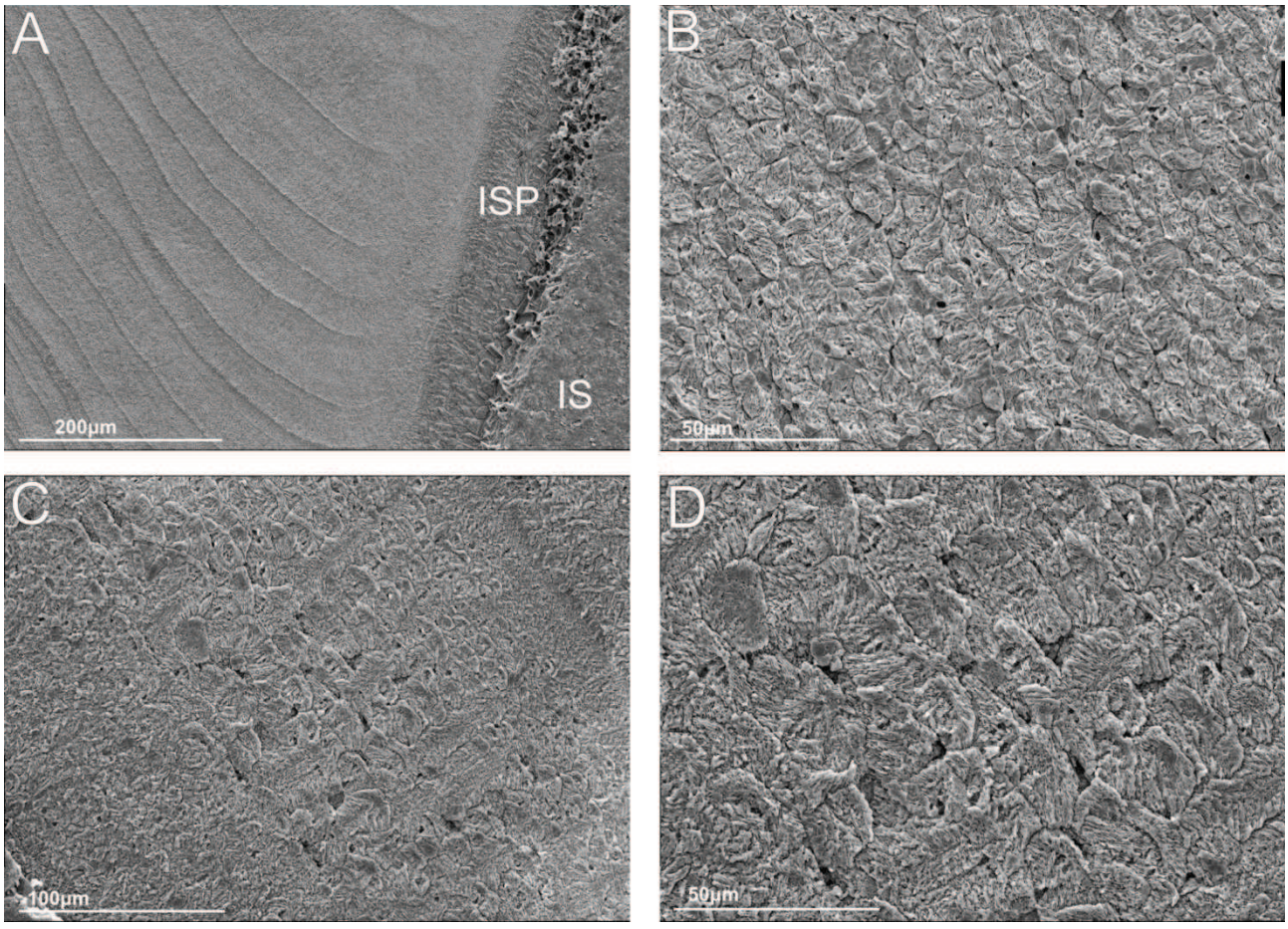

Appendix A.1

In each bed I select the larger and the smaller specimens, measuring height (H), length (L) and height/length ratio (H/L) using a caliper (to the nearest 0.1mm). All measurements are in mm.

TABLE 1: *Glycymeris glycymeris* (Linnaeus, 1758)

Right valves

Specimen	Height	Length	H/L ratio
ACG14-24	63.4	67.2	0.95
ACG27bis-7	48.6	49.8	0.98
ACG243-1	47.3	46.0	1.02

Left valves

Specimen	Height	Length	H/L ratio
ACG14-1	52.9	53.7	0.98
ACG14-3	61.6	66.4	0.93
ACG14-5	60.6	60.8	0.99
ACG27bis-8	72.5	71.0	1.02
ACG35-1	45.7	46.7	0.98
ACG241-14	48.8	50.9	0.96

TABLE 2: *Glycymeris inflata* (Brocchi, 1814)

Articulated specimens

Specimen	Height	Length	H/L ratio
ACG10-4	57.9	56.0	1.03
ACG14-25	61.0	58.8	1.04
ACG24-33	76.4	70.0	1.09

Left valves

Specimen	Height	Length	H/L ratio
ACG29bis-29	63.0	62.7	1.01
ACG14-6	58.6	55.4	1.06
ACG29bis-3	69.2	62.9	1.10

Right valves

Specimen	Height	Length	H/L ratio
ACG9-3	46.7	45.5	1.03
ACG29bis-1	70.0	66.0	1.06

TABLE 3: *Glycymeris insubrica* (Brocchi, 1814)

Articulated specimens

Specimen	Height	Length	H/L ratio
ACG29-2	31.3	31.9	0.98
ACG46-1	12.6	13.2	0.95
ACG46-2	18.1	>17.0	
ACG49-3	58.8	64.4	0.91
ACG91-3	35.0	38.3	0.91
ACG91-10	16.4	17.3	0.95
ACG94-13	9.5	10.3	0.92
ACG197-1	46.0	46.2	0.99
ACG198-5	41.2	44.8	0.92
ACG198-6	39.0	43.3	0.90
ACG200-6	45.7	48.4	0.94
ACG200-7	43.8	47.2	0.93
ACG202-1	23.7	26.3	0.90
ACG204-1	43.0	46.7	0.92
ACG210-1	58.3	62.0	0.94
ACG252-2	47.6	53.2	0.89
ACG256-2	39.9	40.2	0.99
ACG256-3	48.0	48.7	0.99
ACG256-4	20.0	21.3	0.94
ACG256bis-1	42.4	46.7	0.91
ACG256bis-2	50.0	50.6	0.99
ACG258-2	35.5	35.8	0.99
ACG259-4	61.2	62.6	0.98
ACG261-1	50.8	51.9	0.98
ACG261-2	14.7	15.8	0.93
ACG261bis-1	45.0	47.2	0.95
ACG261bis-2	>50.0	60.0	
ACG261bis-3	14.2	13.1	1.08
ACG262-1	46.8	46.5	1.01
ACG262-2	34.0	36.4	0.93
ACG262-3	34.7	37.4	0.93
ACG263-1	49.5	52.1	0.95
ACG263-4	32.4	34.0	0.95
ACG265-4	14.0	15.0	0.93

Right valves

Specimen	Height	Length	H/L ratio
ACG29bis-4	56.3	57.0	0.99
ACG29bis-13	22.6	22.7	0.99
ACG30-5	7.3	7.4	0.99
ACG31-1	51.4	51.5	1.00
ACG42-2	42.4	45.7	0.93
ACG42bis-2	46.5	51.3	0.91
ACG43-1	43.7	46.5	0.94
ACG60-1	45.4	49.0	0.93
ACG66-5	26.0	28.9	0.90
ACG89-1	43.3	47.0	0.93
ACG89-3	30.4	35.0	0.87
ACG90-3	36.3	41.6	0.87
ACG91-2	29.0	31.6	0.92
ACG91-5	28.7	31.8	0.90
ACG92-1	34.9	38.7	0.90
ACG92-2	25.5	27.8	0.92
ACG93-4	19.0	20.0	0.95
ACG93-7	38.0	42.0	0.90
ACG94-1	39.5	43.5	0.91
ACG95-1	16.2	17.7	0.91
ACG96-3	28.6	30.7	0.93
ACG96-4	21.4	23.4	0.91
ACG97bis-1	28.6	31.9	0.90
ACG97-3	26.4	29.8	0.88
ACG97-10	21.4	23.3	0.92
ACG98-1	33.0	36.7	0.90
ACG98-2	36.6	42.0	0.87
ACG99-1	28.0	30.8	0.91
ACG197-4	39.0	41.7	0.93
ACG198-3	19.8	22.3	0.89
ACG200-15	47.0	50.0	0.94
ACG204-7	10.0	10.4	0.96
ACG252-6	12.0	13.0	0.92
ACG258-3	51.7	52.5	0.98
ACG258-4	24.7	27.3	0.90
ACG260-2	50.7	52.7	0.96
ACG262-4	11.3	11.7	0.97
ACG264-1	43.3	47.2	0.92
ACG264-5	20.9	22.0	0.95
ACG265-1	46.5	43.8	1.06
ACG267-1	47.3	46.4	1.02
ACG267-2	27.7	32.4	0.85

Left valves

Specimen	Height	Length	H/L ratio
ACG9-2	37.3	37.2	1.00
ACG13-2	26.5	29.6	0.89
ACG29bis-12	>41.5	50.7	
ACG29bis-14	30.4	33.4	0.91
ACG29bis-17	16.0	16.1	0.99
ACG49-1	40.6	>42.0	
ACG66-4	16.4	17.5	0.94
ACG66-6	48.3	50.7	0.95
ACG68-1	47.3	51.7	0.91
ACG83-1	42.5	45.6	0.93
ACG90-1	33.6	35.9	0.94
ACG90-12	21.7	23.5	0.92
ACG91-1	35.5	37.7	0.94
ACG91-4	28.0	31.0	0.90
ACG92-3	27.7	31.3	0.88
ACG93-1	42.0	46.7	0.90
ACG93-2	38.0	42.0	0.90
ACG93-13	15.8	17.0	0.93
ACG94-2	37.9	37.3	1.02
ACG94-5	16.0	17.2	0.93
ACG96-1	>31.0	34.7	
ACG96-2	27.7	29.8	0.93
ACG97-4	25.5	29.0	0.88
ACG97-11	37.3	39.4	0.95
ACG97-12	12.5	14.4	0.87
ACG98-3	13.4	14.3	0.94
ACG197-5	26.0	29.5	0.88
ACG197-11	19.0	20.4	0.93
ACG199-1	34.0	37.3	0.91
ACG203-3	12.6	13.2	0.95
ACG204-3	49.3	50.6	0.97
ACG204-4	31.4	34.4	0.91
ACG204-6	4.4	5.0	0.88
ACG205-3	23.0	25.4	0.90
ACG252-3	50.4	56.8	0.89
ACG252-4	45.6	50.7	0.89
ACG259-1	61.5	64.8	0.95
ACG259-3	25.0	27.6	0.91
ACG259-5	16.7	18.3	0.91
ACG260-1	42.6	45.4	0.94
ACG263-5	17.0	18.0	0.94
ACG264-3	35.7	41.0	0.87
ACG266-1	33.8	33.8	1.00
ACG267-3	19.4	21.0	0.92

TABLE 4: *Glycymeris* sp. ind.

Right valves

Specimen	Height	Length	H/L ratio
AC14-7	64.6	62.5	1.03
ACG24-4	73.0	69.0	1.06

Left valve

Specimen	Height	Length	H/L ratio
ACG76-25	>65.0	75.0	

TABLE 5: *Aequipecten opercularis* (Linnaeus, 1758)

Articulated specimens

Specimen	Height	Length	H/L ratio
ACG132-4	35.7	33.0	1.08
ACG133-1	35.6	35.0	1.02

Right valves

Specimen	Height	Length	H/L ratio
ACG2-2	33.3	31.8	1.05
ACG2-4	31.6	>31.0	
ACG4-10	43.2	42.0	1.03
ACG4-13	24.4	23.3	1.05
ACG6-5	37.0	38.7	0.96
ACG9-6	37.4	36.7	1.02
ACG11-1	34.7	33.8	1.03
ACG12-5	14.5	15.8	0.92
ACG13-3	40.4	38.8	1.04
ACG13-8	>26.0	>24.0	
ACG24-7	47.4	51.2	0.93
ACG25-8	35.8	35.5	1.01
ACG25-18	15.4	14.0	1.10
ACG26-1	40.0	38.9	1.03
ACG26-3	30.7	29.4	1.04
ACG27-6	30.2	29.0	1.04
ACG27bis-3	46.7	44.0	1.06
ACG27bis-5	31.5	31.7	0.99
ACG30-7	10.0	9.3	1.07
ACG32-2	20.0	18.6	1.07
ACG37-8	13.1	12.0	1.09
ACG41-3	44.7	47.0	0.95
ACG41-29	18.3	17.7	1.03
ACG41bis-2	44.3	43.7	1.01
ACG41bis-6	19.3	18.5	1.04
ACG42-7	47.6	47.4	1.00
ACG42-19	20.2	19.7	1.02
ACG42bis-10	50.5	50.3	1.00
ACG42bis-20	18.6	17.5	1.06
ACG43-3	25.3	24.4	1.04
ACG52-1B	18.3	16.6	1.10
ACG53-3	17.0	15.3	1.11
ACG54-4	19.0	18.0	1.05
ACG54-5	11.3	10.6	1.07
ACG57-2	32.8	32.9	1.00
ACG57-4	32.6	30.9	1.05
ACG59-2	40.6	38.0	1.07
ACG59-8	25.5	24.4	1.04
ACG60-3	35.7	34.0	1.05
ACG66-13	27.8	26.9	1.03
ACG68-2	44.2	44.7	0.99
ACG70-1	42.7	43.8	0.97
ACG70-3	51.7	52.7	0.98
ACG76-4	47.7	50.0	0.95
ACG76-12	50.4	50.2	1.00
ACG76-21	32.9	31.8	1.03
ACG80-1	31.4	29.9	1.05
ACG80-2	38.9	38.8	1.00
ACG81-1	41.6	41.0	1.01
ACG81-2	39.8	38.9	1.02
ACG82-2	32.0	30.6	1.05
ACG84-2	42.8	42.4	1.01
ACG84-5	28.8	27.7	1.04
ACG85-1	45.8	47.7	0.96
ACG89-8	38.9	37.7	1.03
ACG90-6	34.0	32.0	1.06
ACG90-10	34.4	32.6	1.05
ACG91-8	33.0	30.8	1.07
ACG91bis-1	43.7	46.5	0.94
ACG91bis-3	18.4	17.0	1.08
ACG92-4	57.0	57.6	0.99
ACG92-8	19.0	17.0	1.12
ACG93-4	25.5	23.6	1.08
ACG93-10	25.5	25.0	1.02
ACG94-10	28.3	27.7	1.02
ACG97-7	30.6	29.5	1.04
ACG97-8	27.0	26.6	1.01
ACG100-4	16.5	14.6	1.13
ACG101-1	22.6	22.0	1.03
ACG102-3	11.2	10.0	1.12
ACG103-2	36.0	34.5	1.04
ACG103-3	31.0	29.9	1.04
ACG104-2	35.3	36.0	0.98
ACG132-3	31.4	30.0	1.05
ACG194-2	41.0	40.0	1.02
ACG194-7	8.5	7.4	1.15
ACG195-5	36.0	37.0	0.97
ACG195-7	9.4	8.5	1.10
ACG197-6	54.0	56.8	0.95

ACG197-10	44.6	47.5	0.94
ACG198-4	35.0	35.0	1.00
ACG199-2	36.5	37.0	0.99
ACG200-1	45.0	44.9	1.00
ACG200-4	49.0	48.6	1.01
ACG201-1	41.0	40.0	1.02
ACG207-4	23.6	23.0	1.03
ACG208-2	>32.0	39.4	
ACG215-1	43.0	41.2	1.04
ACG215-3	72.0	75.0	0.96
ACG217-6	23.3	22.4	1.04
ACG220-4	24.7	23.7	1.04
ACG222-1	47.0	48.8	0.96
ACG222-6	15.5	14.5	1.07
ACG223-2	39.2	37.4	1.05
ACG223-5	19.7	18.6	1.06
ACG234-4	34.4	33.4	1.03
ACG240-3	15.6	14.6	1.07

Left valves

Specimen	Height	Length	H/L ratio
ACG6-6	27.5	>24.0	
ACG12-1	42.8	42.3	1.01
ACG13-10	>14.4	14.2	
ACG25-5	40.3	38.3	1.05
ACG25-13	9.4	8.8	1.07
ACG26-7	11.1	9.9	1.12
ACG27-7	19.0	17.2	1.10
ACG27bis-1	43.8	44.0	0.99
ACG29bis-16	14.7	14.0	1.05
ACG29bis-18	33.3	31.7	1.05
ACG30-2	12.0	11.0	1.09
ACG33-1	>35.0	>33.0	
ACG34-1	39.0	38.8	1.00
ACG34-2	27.2	25.6	1.06
ACG37-8	13.0	12.0	1.08
ACG41-2	39.2	38.3	1.02
ACG41-8	9.4	8.5	1.10
ACG41-31	10.3	9.4	1.10
ACG41bis-1	36.2	36.6	0.99
ACG42-11	24.4	23.2	1.05
ACG42-16	20.0	18.7	1.07
ACG42-17	10.0	8.5	1.18
ACG42bis-4	39.5	38.3	1.03
ACG42bis-13	19.5	18.7	1.04
ACG51-1	38.9	40.9	0.95
ACG51-3	25.8	>25.0	
ACG51bis-12	16.0	14.7	1.09
ACG52-1	15.9	14.4	1.10
ACG55-2	18.3	17.0	1.08
ACG55-3	12.5	11.2	1.12
ACG56-10	10.7	9.4	1.14
ACG57-1	39.8	39.0	1.02
ACG59-4	28.5	27.0	1.05
ACG60-6	22.3	21.3	1.05
ACG61-1	47.0	48.0	0.98
ACG66-8	35.9	34.2	1.05
ACG66-9	41.4	40.8	1.01
ACG76-15	49.4	51.3	0.96
ACG76-17	36.8	37.7	0.98
ACG82-1	31.8	30.5	1.04
ACG82-5	21.6	21.0	1.03
ACG89-5	53.6	54.6	0.98
ACG89-10	24.7	23.0	1.07
ACG90-11	50.0	48.8	1.02
ACG90-20	21.0	18.6	1.13
ACG91-6	49.5	49.7	1.00
ACG91-9	21.0	20.0	1.05
ACG92-5	42.0	41.6	1.01
ACG92-7	30.6	30.0	1.02
ACG93-9	25.8	24.0	1.07
ACG94-9	28.9	28.6	1.01
ACG97-6	39.7	38.6	1.03
ACG101-4	13.6	12.4	1.10
ACG103-4	32.3	31.3	1.03
ACG103-6	11.0	9.6	1.15
ACG104-4	25.8	25.0	1.03
ACG104-5	10.0	8.7	1.15
ACG133-3	28.6	27.7	1.03
ACG133-4	>41.0	>49.0	
ACG194-5	34.4	33.5	1.03
ACG195-4	34.0	32.4	1.05
ACG195-6	43.4	42.5	1.02
ACG197-11	25.7	25.0	1.03
ACG198-1	38.6	37.2	1.04
ACG198-7	12.0	11.0	1.09
ACG199-4	59.0	56.4	1.05
ACG199-5	51.3	51.7	0.99
ACG200-2	46.0	43.6	1.05

ACG201-3	27.5	26.5	1.04
ACG207-3	31.0	31.8	0.97
ACG217-2	51.0	51.0	1.00
ACG217-3	55.4	58.4	0.95
ACG222-2	63.0	64.3	0.98
ACG235-2	60.0	61.0	0.98
ACG235-5	23.7	23.0	1.03
ACG236-3	49.3	48.4	1.03
ACG236-6	25.0	22.6	1.10
ACG237-4	59.6	56.3	1.06
ACG238-3	42.7	44.2	0.97
ACG238-4	44.7	43.7	1.02
ACG238-5	18.0	17.0	1.06
ACG239-2	30.8	28.0	1.10
ACG239-4	26.6	25.0	1.06

TABLE 6: *Aequipecten scabrella* (Lamarck, 1819)

Right valves

Specimen	Height	Length	H/L ratio
ACG1-1	45.0	>47.3	
ACG2-5	37.4	38.9	0.96
ACG3-4	38.8	42.2	0.92
ACG3-7	25.8	25.4	1.02
ACG4-7	44.7	45.8	0.98
ACG4-11	20.8	20.0	1.04
ACG5-3	33.4	36.5	0.91
ACG5-4	>23.0	>24.3	
ACG6-2	25.3	26.2	0.97
ACG8-2	27.9	>27.3	
ACG12-4	24.2	23.7	1.02
ACG13-11	10.7	10.0	1.07
ACG66-11	32.5	33.4	0.97

Left valves

Specimen	Height	Length	H/L ratio
ACG1-2	27.7	>25.0	
ACG2-6	38.6	42.0	0.92
ACG3-3	32.0	31.3	1.02
ACG4-2	39.4	42.9	0.92
ACG4-12	15.3	14.4	1.06
ACG5-2	28.6	29.8	0.96
ACG6-4	22.0	>19.0	
ACG6-8	45.5	48.5	0.94
ACG12-2	30.8	31.6	0.97
ACG12-6	16.7	16.5	1.01

TABLE 7: *Arctica islandica* (Linnaeus, 1767)

Articulated specimens

Specimen	Height	Length	H/L ratio
ACG253-2	68.6	79.8	0.86
ACG254-4	64.0	78.0	0.82
ACG254-6	79.0	80.0	0.99

Right valves

Specimen	Height	Length	H/L ratio
ACG86-4	55.0	60.0	0.92
ACG86-5	72.0		
ACG200-9	62.4	62.9	0.99
ACG200-12	78.0	>81.0	
ACG202-3	67.3		
ACG215-5	84.5	91.5	0.92
ACG215-8	79.2	88.2	0.90
ACG215-10	67.0	>65.0	
ACG216-1	82.4	>57.0	
ACG216-3	59.7	65.0	0.92
ACG217-5	65.0	71.7	0.90
ACG220-2	50.4	50.8	0.99
ACG220-3	51.4	53.8	0.95
ACG224-1	90.0	91.0	0.99
ACG253-3	57.8	59.4	0.97
ACG253-4	41.0	44.0	0.93

Left valves

Specimen	Height	Length	H/L ratio
ACG78-1	83.0	>76.2	
ACG78-2	71.0	70.0	1.01
ACG200-14	56.1	62.2	0.90
ACG213bis-2	82.6		
ACG215-7	74.6	78.3	0.95
ACG215-9	90.7	92.4	0.98
ACG226-2	55.3	>54.0	
ACG229-1	66.4		
ACG254-2	70.4	70.0	1.00

Acknowledgments

First, I would like to deeply thank my supervisor Prof. Lucia Angiolini, who have accompanied me in this journey in the Pleistocene bivalves world! Thanks for yours teachings, for your motivation, for being always present when needed and for all the opportunities you gave to me. Thanks for having been not only a supervisor but also a friend, supporting me in these three years. Thanks Lucia!

Warm thanks to the British Geological Survey of Keyworth, UK, which has trusted in the Arda project, financing the geochemical and isotope analysis here undertaken.
I am very grateful to Prof. Mike Stephenson and Prof. Melanie Leng for their constant support, their kindness and their useful and precious advices on this thesis. Thanks to Dr. Jan Hennissen for his efficiency and his patience. Thanks to Hilary Sloane and Chris Kendrick for the isotope analysis and to Prof. Randy Parrish and Dr. Nick Roberts for the Uranium-Lead dating.
Thanks to Dr. Matthew Pound from Northumbria University for the pollen analysis.

Dr. Gianluca Raineri from Riserva Geologica del Piacenziano and Dr. Carlo Francou from Museo Geologico di Castell'Arquato are thanked for giving me the permission and thus the possibility to study the beautiful Arda section. Many thanks to Gianluca Raineri: with your wide knowledge of the succession and of the mollusks in general you have been a precious source of information.

Many thanks to Dr. Fabrizio Felletti for his kindness, his useful suggestions on this thesis and for his enthusiasm and constant interest in what I was doing, even when talking about fossils!
Thanks to all the people who, with their knowledge, gave an important contribute for this thesis: Dr. Fabrizio Felletti and Christian Frigerio for the sedimentological analysis; Dr. Cinzia Bottini, Prof. Elisabetta Erba and Prof. Isabella Raffi for the nannofossil biostratigraphy; Prof. Flavio Jadoul for the cathodoluminescence analysis; Dr. Monica Dapiaggi and Giorgia Confalonieri for the analyses at X-Ray Powder Diffractometer.
Thanks to Curzio Malinverno for the numerous sections he made for this thesis and to Agostino Rizzi for making the numerous hours passed at SEM less boring. Thanks also to Dr. Elena Ferrari for helping me with the preparation of chemical solutions.

A great thank goes to the wonderful Ufficio 70: Giulia, Irene and Alessia. We began and finished together this Ph.D. adventure, sharing happy and sad times, but always supporting each other. This three years with you have been fantastic!
A big thank to my irreplaceable travel companion Claudio, for your big patience in helping me with computer matters, for your long conversations and for having instill in me a bit of your calm!

I extend my thanks to my lunch friends, Cinzia, Francesca, Cristina C., Dario, Silvia and Andrea, and to my intra- and extra-university friends: Cristina L., Meri, Marianna and Elisa. Thanks for the funny moments we spent together.

I deeply thank my parents who constantly trusted in me and encouraged in every moment of this Ph.D. Thanks to my grandmother; even if she didn't understand what I was doing, she always gave a particular care for me.

Finally, my biggest thank is for Claudio, for his enormous patience, his technical help, for the hundreds of photos he made for me and for his useful critiques on this thesis. You have shared with me all my ups and downs; thanks for always being with me!

References

Adams, H. & Adams, A. (1853–1858), The genera of Recent Mollusca, arranged according to their organization, London, v.1, 256 pp & 257-484, v. 2: 66 pp. J. Van Voorst.

Almera, J. & Bofill, A. (1898), Moluscos fosiles recogidos en los terrenos pliocenicos de Cataluna, *Boletin de la Com. Del Mapa Geol. De Espana IV*, I-XII + 223 pp.

Altaba, C.R., Forés, M. & Monserrat, S. (2006), Long-term environmental record in *Glycymeris inflata,* a relic of old-growth soft bottoms in the Mediterranean. In Malchus, N. & Pons, J.M. (2006), Abstracts and Posters of the "International Congress on Bivalvia" at the Universitat Autònoma de Barcelona, Spain, 22-27 July 2006.

Anderson, H.J. (1959), Die muschelfauna des nord-westdeutschen Untermiozan, *Palaeontographica,* 61-179.

Andrés, I. (1982), Estudio malacologico (Clase Bivalvia) del Plioceno marino de Bonares (Huelva). Tesis doctoral. Universidad de Salamanca.

Andrés, I. (1989), Estudio sistematico de los bivalvos Palaeotaxodonta y Pteriomorphia (Arcoida, Mytiloida) del Plioceno de Bonares (Huelva, Espana), *Studia geologica Salmanticensia, 26,* 317-353.

Anfossi, G. & Brambilla, G. (1980), La fauna pleistocenica del Colle di S. Colombano al Lambro (Lombardia). I Lamellibranchi, *Estratto da atti Dell'Instituto Geologico della Università di Pavia, 29,* 49-68.

Angiolini, L., Darbyshire, D.P.F., Stephenson, M.H., Leng, M.J., Brewer, T.S., Berra, F. & Jadoul, F. (2008), Lower Permian brachiopods from Oman: their potential as climatic proxies, *Earth and Environmental Science Transactions of the Royal Society of Edinburgh, 98(3-4),* 327-344.

Angiolini, L., Stephenson, M.H., Leng, M.J., Jadoul, F., Millward, D., Aldridge, A., Andrews, J.E., Chenery, S. & Williams, G. (2012), Heterogeneity, cyclicity and diagenesis in a Mississippian brachiopod shell of palaeoequatorial Britain, *Terra Nova, 24,* 16-26.

Arduini, V. (1895), Conchiglie plioceniche del bacino di Albenga, *Atti Società Ligure di Scienze Naturali, 6,* 159-209.

Artegiani, A., Bregant, D., Paschini, E., Pinardi, N., Raicich, F. & Russo, A. (1997), The Adriatic Sea General Circulation. Part I: Air–Sea Interactions and Water Mass Structure, *Journal of physical oceanography, 27,* 1492-1514.

Azzaroli, A. (1995), The ‘‘*Elephant-Equus’’* and the ‘‘End-Villafranchian’’ Events in Eurasia. In: Vrba, E.S., Denton, G.H., Partridge, T.C., Burckle, L.H. (Eds.), *Paleoclimate and Evolution, with Emphasis on Human Origins. Yale University Press, New Haven,* 311 – 318.

Backman, J., Raffi, I., Rio, D., Fornaciari, E. & Pälike, H. (2012), Biozonation and biochronology of Miocene through Pleistocene calcareous nannofossils from low and middle latitudes, *Newsletters on Stratigraphy, 45(3),* 221-244.

Barbieri, F. (1967), The Foraminifera in the Pliocene section Vernasca-Castell'Arquato including the «Piacenzian stratotype» (Piacenza Province). Il Pliocene del subappennino piacentino-parmense-reggiano., *Mem. Soc. It. Sc. Nat. Mus. Civ. St. Nat. Milano, 15, (3),* 145-163.

Barbin, V. (2000), Cathodoluminescence of carbonate shells: biochemical vs. diagenetic process. In: Pagel, M., Barbin, V., Blanc, P, Ohnenstetter, D. (eds) *Cathodoluminescence in geosciences. Springer-Verlag, Berlin,* p 303–329.

Bates, C.C. (1953), Rational theory of delta formation, *Bulletin of American Association of Petroleum Geology, 37(9),* 2119–2162.

Becker, J., Hilgen, F.J., Lourens, L.J., Reichart, G.-J., van der Laan, E. & Kouwenhofen T.J. (2005), Late Pliocene climate variability on Milankovitch to millennial time scales: A high-resolution study of MIS100 from the Mediterranean, *Palaeogeogr. Palaeoclimatol. Palaeoecol., 228*, 338–360.

Becker, J., Lourens, L.J., & Raymo, M.E. (2006), High-frequency climate linkages between the North Atlantic and the Mediterranean during marine oxygen isotope stage 100 (MIS100). *Paleoceanography, 21(3).*

Bellardi, L. & Sacco, F. (1872-1904), I Molluschi dei terreni terziarii del Piemonte e della Liguria. *Mem. Reale Accademia delle Scienze di Torino.* C.Claudsen Ed., Torino, 30 Vol.

Benigni, C. & Corselli, C. (1982), Paleocomunità a molluschi bentonici del Pliocene di Volpedo (Alessandria), *Rivista Italiana di Paleontologia e Stratigrafia 87,* 637–702.

Berthou, P., Blanchard, M., Noël, P. & Vergnaud-Grazzini, C. (1986), Stable isotope analysis of shells for age determination in four bivalve species from the Normand-Breton Gulf (western English Channel). *International Council for the Exploration of the Sea Shellfish Committed, report 1986/K, 16.*

Bertini, A. (2001), Pliocene climatic cycles and altitudinal forest development from 2.7 Ma in the Northern Apennines (Italy): evidence from the pollen record of the Stirone Section (5.1 to 2.2Ma), *Geobios 34,* 253– 265.

Bertini, A. (2003), Early to Middle Pleistocene changes of the Italian flora and vegetation in the light of a chronostratigraphic framework, *Il Quaternario, 16(1),* 19-36.

Beurlen, K. (1944) Beitrage zur Stammesgeschichte der Muscheln. *Bayer Akademie der Wissenschaften, Sitzungsber., 1-2,* 133-145.

Bieler, R. & Mikkelsen, P.M. (2006), Bivalvia – a look at the branches, *Zoological Journal of the Linnean Society, 148,* 332pp.

Böhm, F., Joachimski, M.M., Dullo, W.C., Eisenhauer, A., Lehnert, H., Reitner, J. & Worheide, G. (2000), Oxygen isotope fractionation in marine aragonite of coralline sponges, *Geochimica et Cosmochimica Acta, 64:* 1695-1703.

Bonadonna, F.P. (1968), Studi sul Pleistocene del Lazio. V. La biostratigrafia di Monte Mario e la "fauna malacologica mariana" di Cerulli Irelli. *Memorie della Società Geologica italiana, VIII (2),* 261-321.

Bongo, F. (1914), I fossili tortoniani del Rio di Bocca d'Asino presso Stazzano (Serravalle Scrivia), *Bollettino della Società Geologica Italiana, 33 (2),* 395-484.

Boni, A. (1933), Il Miocene del Monte Valassa, *Atti R. Accademia Nazionale dei Lincei, ser. VI, Rend. Clas. Sc. fis. mat. e nat., XV (12),* 981-986.

Boni, A. & Sacchi Vialli, G. (1962), Studi biostratigrafici sui Pettinidi di località neogeniche e quaternarie dell'Italia nord-occidentale (Parte prima). *Atti Ist. Geol. Univ. Pavia XIII,* 65-119.

Bonnefille, R. (1995), A reassessment of the Plio-Pleistocene pollen record of East Africa. In: Vrba, E.S., Denton, G.H., Partridge, T.C., Burckle, L.H. (Eds.), *Paleoclimate and Evolution, with Emphasis on Human Origins. Yale University Press, New Haven,* 299–310.

Borghi, M. & Vecchi, G. (2005), La malacofauna Plio-Pleistocenica del Torrente Stirone (Pr). Cerithiidae – Turritellidae, *Parva Naturalia, 7,* 3-46.

Born, I. (1778), Index rerum naturalium Musei Cæsarei Vindobonensis. Pars 1, Testacea. XLII+458pp Kraus, Vienna.

Borson, S. (1820-1825), Saggio di orittografia Piemontese. *Memorie della Reale Accademia delle Scienze di Torino* XXV, 180-229; XXVI, 297-364; XXIX, 251-318.

Brand, U., Logan, A., Bitner, M.A., Griesshaber, E., Azmy, K. & Buhl, D. (2011), What is the ideal proxy of Palaeozoic seawater chemistry?, *Memoirs of the Association of Australasian Palaeontologists, 41, 9.*

Brocas, W.M., Reynolds, D.J., Butler, P.G., Richardson, C.A., Scourse, J.D., Ridgway, I.D. & Ramsay, K. (2013), The dog cockle, *Glycymeris glycymeris* (L.), a new annually-resolved sclerochronological archive for the Irish Sea, *Palaeogeography, Palaeoclimatology, Palaeoecology, 373,* 133-140.

Brocchi, G.B. (1814), Conchiologia fossile subappennina. 2 vol. of 712 pp. Stamperia Reale, Milano.

Bronn, H.G. (1831), Italiens Tertiär-Gebilde und deren organische Einschlüsse. Heidelberg, XII+176 pp.

Buccheri, G. (1970), Una malacofauna calabriana del territorio di Sciacca (Sicilia sud-occidentale), *Geologica Romana, IX,* 239-274.

Bukry, D., (1973), Low Latitude Coccolith Biostratigraphic Zonation. In: Edgar, N.T., Saunders, J.B., et al. (Eds.), *Initial Reports DSDP, 15*, US Govt. Printing Office, Washington, 685–703.

Bukry, D., (1975), Coccolith and silicoflagellate stratigraphy, northwestern Pacific Ocean, Deep Sea Drilling Project Leg 32. In: Larson, R. L., Moberly, R., et al., *Initial Reports DSDP, 32,* Washington, U.S. Govt. Printing Office, 677–701.

Bukry, D. (1978), Biostratigraphy of Cenozoic marine sediments by calcareous nannofossils, *Micropaleontology, 24,* 44–60.

Buonanni, P.F. (1681), Ricreatione dell'occhio e della mente nell'osservatione delle Chiocciole, Roma, 16+384.

Bušelić, I., Peharda, M., Reynolds, D.J., Butler, P.G., González, A.R., Ezgeta-Balić, D., Vilibić, I., Grbec, B., Hollyman, P. & Richardson, C.A. (2015), *Glycymeris bimaculata* (Poli, 1795) — A new sclerochronological archive for the Mediterranean?, *Journal of Sea Research, 95,* 139-148.

Butler, P.G., Wanamaker Jr., A.D., Scourse, J.D., Richardson, C.A. & Reynolds, D.J. (2011), Long-term stability of ^{13}C with respect to biological age in the aragonite shell of mature specimens of the bivalve mollusk *Arctica islandica, Palaeogeography, Palaeoclimatology, Palaeoecology*, *302(1),* 21-30.

Butler, P.G., Wanamaker Jr., A.D., Scourse, J.D., Richardson, C.A. & Reynolds, D.J. (2013), Variability of marine climate on the North Icelandic Shelf in a 1357-year proxy archive based on growth increments in the bivalve *Arctica islandica, Palaeogeography, Palaeoclimatology, Palaeoecology, 373,* 141-151.

Cacho, I., Grimalt, J.O., Sierro, F.J., Shackleton, N. & Canals M. (2000), Evidence for enhanced Mediterranean thermohaline circulation during rapid climatic coolings, *Earth Planet. Sci. Lett., 183,* 417– 429.

Calabrese, L. & Di Dio, G. (2009), Note Illustrative della Carta Geologica d'Italia alla scala 1: 50.000, foglio 180 "Salsomaggiore Terme". Servizio Geologico d'Italia-Regione Emilia Romagna, Roma.

Capotondi, L. (2011), Isotopi stabili dell'ossigeno e del carbonio: principi e applicazioni. ISPRA

Caprotti, E. (1972), I Bivalvi dello stratotipo Piacenziano (Castell'Arquato, Piacenza), *Natura, 63 (1),* 47-86.

Caprotti, E. (1976), Malacofauna dello stratotipo Piacenziano (Pliocene di Castell'Arquato), *Conchiglie, 12 (1-2),* 1-56.

Cargnelli, L.M., Griesbach, S.J., Packer, D.B. & Weissberger, E. (1999), Ocean quahog, *Arctica islandica,* life history and habitat characteristics. NOAA Technical Memorandum NMFS-NE-148. 1–12.

Carré, M., Bentaleb, I., Fontugne, M. & Lavallee, D. (2005), Strong El Niño events during the early Holocene: stable isotope evidence from Peruvian sea shells, *The Holocene 15,* 42–47.

Carter, J.G. (1990), Skeletal biomineralization: patterns, processes and evolutionary trends. V. of 832 pp. Van Nostrand Reinhold, New York.

Cavallo, O. & Repetto, G. (1992), Conchiglie fossili del Roero. Atlante iconografico, *Associazione Naturalistica Piemontese e Amici del Museo "Federico Eusebio",* Alba, 251 p.

Cerulli Irelli, S. (1907-1916), Fauna malacologica mariana, *Palaeont. Italiana,* XIII-XVIII, XX, XII, XIV, 501 pp.

Chauvaud, L., Thébault, J., Clavier, J., Lorrain, A. & Strand, O. (2011), What's hiding behind ontogenetic δ13C variations in mollusk shells? New insights from the great scallop *Pecten maximus, Estuaries and Coasts, 34,* 211–220.

Chave, K.E. (1954), Aspects of the biogeochemistry of magnesium 1. Calcareous marine organisms. *The Journal of Geology*, *62,* 266-283.

Checa, A.G., Esteban-Delgado, F.J. & Rodriguez-Navarro, A.B. (2007), Crystallographic structure of the foliated calcite of bivalves, *Journal of Structural Biology, 157,* 393–402.

Ciangherotti, A.D., Crispino, P. & Esu, D. (1997), Paleoecology of the non-marine molluscs of the Pleistocene Stirone River sequence (Emilia, Northern Italy). *Boll. Soc. Paleont. It., 36,* 303-310.

Cigala Fulgosi, F. (1976), *Dicerorhinus hemitoechus* (Falconer) del post-Villafranchiano fluvio lacustre del T. Stirone (Salsomaggiore, Parma). *Boll. Soc. Paleont. It., 15(1),* 59–72.

Clark, P.U., Archer, D., Pollard, D., Blum, J.D., Rial, J.A., Brovkin, V., Mix, A.C., Pisias, N.G. & Roy, M. (2006), The middle Pleistocene transition: characteristics, mechanisms, and implications for long-term changes in atmospheric pCO^2, *Quaternary Science Reviews, 25(23),* 3150-3184.

Cocconi, G. (1873), Enumerazione sistematica dei molluschi miocenici e pliocenici delle provincie di Parma e di Piacenza, *Memoire della Accademia delle Scienze dell'Instituto di Bologna, serie 3, 3,* 409-776, 11 pls.

Cohen, A.L. & McCartney, M.S. (1996), Seasonally resolved records of surface ocean conditions in brain coral from Bermuda, *Proceedings from the Atlantic Climate Variability meeting*, 16-23.

Compagnoni, B. (1966), Nuovi dati sulla malacofauna del Macco di Palo (Roma), *Geologica Romana,* 165-176.

Conato, V., Malatesta, A. & Valletta, M. (1967), Calabriano ad *Arctica islandica* sulla costa meridionale d'Abruzzo, *Quaternaria, 9,* 261-266.

Coplen, T.B., Kendall, C. & Hopple, J. (1983), Comparison of stable isotope reference samples, *Nature, 302,* 236-238.

Cossignani, T., Cossignani, V., di Nisio, A. & Passamonti, M. (1992), Atlante delle conchiglie del Medio Adriatico, *L'Informatore Piceno,* 118 pp.

Cowper Reed, F.R. (1935.), Notes on the Neogene faunas from Cyprus, *Ann. and Mag. Nat. Hist., serie 10, XVI,* 489-524.

Cox, L.R. & 24 authors (1969-1971), Bivalvia. In Moore, R. (Ed.), Treatise on Invertebrate Paleontology, Part N, Mollusca 6, Bivalvia. *The Geological Society of America and the University of Kansas, 1-3,* 1-952.

Crippa, G. (2013), The shell ultrastructure of the genus Glycymeris Da Costa, 1778: a comparison between fossil and recent specimens, *Rivista Italiana di Paleontologia e Stratigrafia, 119 (3),* 387-399.

Crippa, G. & Raineri, G., The Lower Pleistocene invertebrate fauna of the Arda River: systematics and biostratigraphic and palaeoclimatic significance, submitted to *Rivista Italiana di Paleontologia e Stratigrafia*, 2014.

Da Costa, E.M. (1778), Historia Naturalis Testaceorum Britanniae, Millan, White, Elmsley & Robson, London, XII + 254 + VIII pp.

Dahlgren, T.G., Weinberg, J.R. & Halanych, K.M. (2000), Phylogeography of the ocean quahog (*Arctica islandica*): influences of paleoclimate on genetic diversity and species range, *Marine biology, 137,* 487-495.

Dall, W.H., (1902), Synopsis of the family Veneridae and of the North American species, *Same, Proc., 26,* p. 335-412.

Dall, W.H. (1895), Contributions to the Tertiary fauna of Florida, with especial reference to the Miocene Silex-beds of Tampa and the Pliocene beds of the Caloosahatchie River. Part III, A new classification of the Pelecypoda. *Wagner Free Institute of Science of Philadelphia, Transactions, 3(3),* 483–570.

Dall, W.H. (1908), The mollusca and the brachiopoda. Harvard University, *Museum of Comparative Zoology, Bulletin, 43 (6),* 205-487.

Dalloni, M. (1915), Recherches sur la période néogène dans l'Algérie occidentale, *Bull. Soc. Geol. Fr., IVe ser., 15,* 428-457.

Dauphin, Y. & Denis, A. (2000), Structure and composition of the aragonitic crossed lamellar layers in six species of Bivalvia and Gastropoda, Comparative Biochemistry and Physiology, Part A, 126: 367–377.

de Menocal, P.B. (1995), Plio-Pleistocene, African climate, *Science, 270,* 53–59.

Denton, G.H, Alley, R.B, Comer, G.C. & Broecker, W.S. (2005), The role of seasonality in abrupt climate change, *Quaternary Science Reviews, 24,* 1159–1182.

De Stefani, C. (1902), Molluschi pliocenici di Viterbo, *Atti della Società Toscana di Scienze Naturali, Memorie XVIII,* 22-33.

De Stefani, C. & Pantanelli, D. (1878), Molluschi pliocenici dei dintorni di Siena, *Bullettino della Società Malacologica Italiana, 4,* 113–160.

Dettman, DL, Reische, AK & Lohmann, KC (1999), Controls on the stable isotope composition of seasonal growth bands in aragonitic fresh-water bivalves (unionidae), *Geochimica et Cosmochimica Acta, 63,* 1049-1057.

Dodd, J. R. & Schopf, T.J.M. (1972), Approaches to biogeochemistry. In: T.J.M. Schopf (ed) Models in Paleobiology, *Freeman, Cooper and Co., San Francisco*, 46-60.

Dodd, J.R., & Stanton, R.J. (1990), Paleoecology: concepts and applications. John Wiley & Sons.

Domenech, R. (1983), Els Bivalves del Plioce de l'Empordà. Sistematica i Paleoecologia. Tesi doctoral. Universitat de Barcelona.

Domenech, R. (1986), Nuculoida, Arcoida i Mytiloida (Mollusca: Bivalvia) Del Pliocè de l'Empordà, *Butlletí de la Institució Catalana d'Història Natural (Secció de Geologia, 4) 53,* 117-141.

Dominici, S. (2001), Taphonomy and paleoecology of shallow marine macrofossil assemblages in a collisional setting (late Pliocene–early Pleistocene, western Emilia, Italy), *PALAIOS, 16,* 336–353.

Dominici, S. (2004), Quantitative Taphonomy in Sandstones from an Ancient Fan Delta System (Lower Pleistocene, Western Emilia, Italy), *PALAIOS, 19,* p. 193–205.

Dubertret, L., Vautrin, H. & Keller, A. (1937), Stratigraphie du Pliocene et du Quaternaire de la region de Lattaquié. Contribution a l'étude geologique de la Cote Libano-Syrienne. *Haut Comm. De la Rep. Fr. en Syrie et au Liban. Notes et Mem., II,* 93-110.

Dunca, E., Schöne, B.R. & Mutvei, H. (2005), Freshwater bivalves tell of past climates: but how clearly do shells from polluted rivers speak, *Palaeogeogr. Palaeoclimatol. Palaeoecol., 228,* 43–57.

Dunca, E., Mutvei, H., Göransson, P., Mörth, C.-M., Schöne, B.R., Whitehouse, M.J., Elfman, M. & Baden, S.P. (2009), Using ocean quahog (*Arctica islandica*) shells to reconstruct palaeoenvironment in Öresund, Kattegat and Skaggerak, *Sweden. Int. J. Earth Sci., 98,* 3–17.

Dwyer, G.S., Cronin, T.M., Baker, P.A., Raymo, M.E., Buzas, J.S. & Correge, T. (1995), North Atlantic deepwater temperature change during late Pliocene and late Quaternary climatic cycles, *Science, 270,* 1347–1351.

Elorza, J. & Garcia-Garmilla, F. (1996), Petrological and geochemical evidence for diagenesis of inoceramid bivalve shells in the Plentzia Formation (Upper Cretaceous , Basque- Cantabrian Region , northern Spain), *Cretaceous Research, 17,* 479 – 503.

Emiliani, C. (1966), Paleotemperature analysis of Caribbean cores P6304-8 and P6304-9 and a generalized temperature curve for the past 425,000 years, *The Journal of Geology, 74,* 109-124.

Epstein, S., Buchsbaum, R., Lowenstam, H.A. & Urey, H.C. (1953), Revised carbonate – water isotopic temperature scale, *Bulletin of the Geological Society of America, 64,* 1315-1326.

Erunal Erentoz, L. (1958), Mollusques du Néogène des bassins de Karaman, Adana et Hatay (Turquie), *Publ. Inst. Et. et Rech. Miner. Turq., ser. C, no. 4*, 232 pp.

Erunal Erentoz, L. & Oztemur, C. (1964), Apercu general sur la stratigraphie du Néogène de la Turquie et observations sur les limites inferieure et supérieure. Cursillos y Conferencias del Inst. "Luca Mallada", *Mem. De la II Reun. Del Comité del Neog. Medit. IX,* 259-266.

Esteban-Delgado, F.J., Harper, E.M., Checa, A.G. & Rodriguez-Navarro, A.B. (2008), Origin and Expansion of Foliated Microstructure in Pteriomorph Bivalves, *Biol. Bull., 214,* 153–165

Faraone, A. (1986), Malacofaune Plio-Pleistoceniche umbre: le associazioni di Città della Pieve e Monteleone d'Orvieto, *Geologica Romana, 25,* 9-24.

Feigl, F. (1937), Qualitative analysis by spot tests, Nordemann Publishing Company, New York, 400p.

Festa, A. (1950), Ulteriori notizie sulla fauna pliocenica del Genovesato, *Annali Museo Civico di Storia Naturale, Genova LXIV,* 85-100.

Fischer, P. (1880-1887), Manual de Conchyliologie et de Paléontologie Conchyliologique. Paris, Savy XXIV + 1369 pp.

Fontannes, F. (1879-1882), Les mollusques pliocenes de la vallée du Rhone et du Roussillon. F. Savy, Paris, 2 vol, 278-322.

Friedberg W. (1934-1954), Mollusca Miocenica Poloniae (Mieczaki miocenskie ziem Polskich), I, 628 pp.; II, 283 pp.

Fusco, F. (2010), *Picea+Tsuga* pollen record as a mirror of oxygen isotope signal? An insight into the Italian long pollen series from Pliocene to Early Pleistocene, *Quaternary International, 225(1),* 58-74.

Garilli, V. (2011), Mediterranean Quaternary interglacial molluscan assemblages: Palaeobiogeographical and palaeoceanographical responses to climate change, *Palaeogeography, Palaeoclimatology, Palaeoecology, 312(1),* 98-114.

Ghinassi, M., Magi, M., Sagri, M. & Singer, B.S. (2004), Arid climate 2.5 Ma in the Plio-Pleistocene Valdarno Basin (Northern Apennines, Italy), *Palaeogeography, Palaeoclimatology, Palaeoecology, 207(1),* 37-57.

Gibson, R.N., Barnes, M. & Atkinson, R. (2001), Molluscs as archives of environmental change, *Oceanogr. Mar. Biol. Annu. Rev, 39,* 103-164.

Gignoux, M. (1913), Les formations marines pliocènes et quaternaires de l'Italie du Sud et de la Sicile. *Ann. Univ. Lyon I (36),* 393 pp.

Gillikin, D.P. (2005), Geochemistry of Marine Bivalve Shells: the potential for paleoenvironmental reconstruction. Unpublished PhD thesis, Bruxelles University.

Gillikin, D.P., De Ridder, F., Ulens, H., Elskens, M., Keppens, E., Baeyens, W. & Dehairs, F. (2005), Assessing the reproducibility and reliability of estuarine bivalve shells (*Saxidomus giganteus*) for sea surface temperature reconstruction: Implications for paleoclimate studies. *Palaeogeography, Palaeoclimatology, Palaeoecology*, *228(1),* 70-85.

Gillikin, D.P., Lorrain, A., Bouillon, S., Willenz, P. & Dehairs, F. (2006), Stable carbon isotope composition of *Mytilus edulis* shells: Relation to metabolism, salinity, $\delta^{13}C_{DIC}$, and phytoplankton, *J. Organic Geochemistry, 37,* 1371–1382.

Gillikin, D.P., Lorrain, A., Meng, L. & Dehairs, F. (2007), A large metabolic carbon contribution to the delta C-13 record in marine aragonitic bivalve shells, *Geochimica et Cosmochimica Acta, 71,* 2936–2946.

Gillikin, D.P., Hutchinson, K. & Kumai, Y. (2009), Ontogenic increase of metabolic carbon in freshwater mussel shells (*Pyganodon cataracta*), *Journal of Geophysical Research: Biogeosciences, 114* (G1).

Glibert, M. & van de Poel, L. (1965-1970), Les Bivalvia fossiles du cénozoïque étranger, *Mémoires de l'Institut Royal des Sciences Naturelles de Belgique (2e série) 77,* 105 pp., *78,* 112 pp.

Gofas, S., Le Renard, J. & Bouchet, P. (2001), Mollusca. In: Costello, M. J. et al. (ed.) (2001). European register of marine species: a check-list of the marine species in Europe and a bibliography of guides to their identification. *Collection Patrimoines Naturels, 50,* 180-213.

Goldfuss, G.A. (1837), Petrefacta Germianiae, Abbildungen und Beschreibungen der Petrefacten Deutschlands und der angrenzenden Länder 6. Lieferung,Teil II, 3, 141-224.

Gómez Alba, J. (1988), Guia de campo de los fósiles de España y de Europa. Omega ed., Barcelona, 925 pp.

Goodwin, D.H., Flessa, K.W., Schöne, B.R & Dettman, D.L. (2001), Cross calibration of daily growth increments, stable isotope variation, and temperature in the Gulf of California bivalve mollusk *Chione cortezi*: implications for paleoenvironmental analysis, *Palaios, 16,* 387–398.

Goodwin, D., Schöne, B. & Dettman, D. (2003), Resolution and fidelity of oxygen isotopes as paleotemperature proxies in bivalve mollusc shells: models and observations, *Palaios, 18,* 110–125.

Gosling, E.M. (1992), Systematics and geographic distribution of *Mytilus*. In The mussel *Mytilus*: ecology, physiology, genetics and culture, (ed. E.M. Gosling), pp. 1-20. Amsterdam: Elsevier Science Publ.

Greco, A. (1970), La malacofauna pliocenica di contrada Cerausi presso Serradifalco (Caltanissetta), *Geol. Rom., IX,* 275-314.

Gröcke, D.R., & Gillikin, D. P. (2008), Advances in mollusc sclerochronology and sclerochemistry: tools for understanding climate and environment, *Geo-Marine Letters*, *28* (5-6), 265-268.

Grossman, E. L. (1984), Stabel isotope fractionation in live benthic foraminifera from the southern California borderland, *Palaeogeogr. Palaeoclimatol. Palaeoecol., 47,* 301-327.

Grossman, E.L. & Ku, T.L. (1986), Oxygen and carbon isotope fractionation in biogenic aragonite - temperature effects*, Chemical Geology, 59,* 59-74.

Grossman, E.L. (1987), Stable isotopes in modern benthic foraminifera: a study of vital effect, *Journal of foraminiferal Research, 17,* 48-61.

Grossman, E.L., Mii, H.S. & Yancey, T.E. (1993), Stable isotopes in Late Pennsylvanian brachiopods from the United States : implications for Carboniferous paleoceanography, *Geological Society of America, Bulletin 105,* 1284 – 1296.

Gunderson, K.L., Kodama, K.P., Anastasio, D.J. & Pazzaglia, F.J. (2013), Rock-magnetic cyclostratigraphy for the Late Pliocene–Early Pleistocene Stirone section, Northern Apennine mountain front, Italy, *Geological Society, London, Special Publications, 373(1),* 309-323.

Harper, E.M. (2000), Are calcitic layers an effective adaptation against shell dissolution in the Bivalvia? *J. Zool., 251,* 179-186

Hayward, P.J. & Ryland, J.S. (1990), The Marine Fauna of the British Isles and North-West Europe. Clarendon Press, Oxford, UK.

Herbert, T.D., Ng, G. & Peterson, L.C. (2015), Evolution of Mediterranean sea surface temperatures 3.5–1.5Ma: Regional and hemispheric influence, *Earth and Planetary Science Letters, 409,* 307–318.

Hickson, J.A., Johnson, A.L., Heaton, T.H. & Balson, P.S. (1999), The shell of the Queen Scallop *Aequipecten opercularis* (L.) as a promising tool for palaeoenvironmental reconstruction: evidence and reasons for equilibrium stable-isotope incorporation, *Palaeogeography, Palaeoclimatology, Palaeoecology, 154(4),* 325-337.

Hickson, J.A. & Johnson, A.L.A., Heaton, T.H.E. & Balson, P.S. (2000), Late Holocene environment of the southern North Sea from the stable isotopic composition of queen scallop shells, *Palaeontol. Electronica*, *3*(11).

Hornibrook, N. de B. (1992), New Zealand Cenozoic marine paleoclimates: a review based on the distribution of shallow water and terrestrial biota. In: Tschi, R., Ingle, J.C. (Eds.), *Pacific Neogene. University of Tokyo Press, Tokyo,* 83– 106.

Imbesi, M. (1951), Nuove osservazioni e ricerche presso i giacimenti fossiliferi di Ravagnese (Reggio Calabria), *Atti della Società Toscana di Scienze Naturali, Memorie 58,* 121-136.

Irie, T. & Iwasa Y. (2005), Optimal growth pattern of defensive organs: the diversity of shell growth among mollusks, *Am Nat, 165*.

Ivany, L., Wilkinson, B. & Jones, D. (2003), Using stable isotopic data to resolve rate and duration of growth throughout ontogeny: an example from the surf clam, *Spisula solidissima*, *Palaios, 18,* 126–137.

Ivany, L.C., Wilkinson, B.H., Lohmann, K.C., Johnson, E.R., McElroy, B.J. & Cohen G.J. (2004), Intra-annual isotopic variation in *Venericardia* bivalves: Implications for early Eocene temperature, seasonality, and salinity on the US Gulf Coast, *Journal of Sedimentary Research, 74(1),* 7-19.

Ivany, L.C. & Runnegar, B. (2010), Early Permian seasonality from bivalve δ18O and implications for the oxygen isotopic composition of seawater. *Geology*, *38*(11), 1027-1030.

Jiménez, A.P., Aguirre, J. & Rivas, P. (2009), Taxonomic study of scallops (Pectinidae: Mollusca, Bivalvia) from Pliocene deposits (Almería, SE Spain), *Revista Española de Paleontología, 24 (1)*, 1-30.

Jeffreys, J.G. (1864), British Conchology, vol. 2 Van Voorst, London. 479pp.

Jeffreys, J.G. (1878-1885), On the mollusca procured during the H.M.S. "Lightning" and "Porcupine" expedition, *Proceedings of the Zoological Society of London*: Part 1-9.

Johnson, A.L., Hickson, J.A., Bird, A., Schöne, B.R., Balson, P.S., Heaton, T.H. & Williams, M. (2009), Comparative sclerochronology of modern and mid-Pliocene (c. 3.5 Ma) *Aequipecten opercularis* (Mollusca, Bivalvia): an insight into past and future climate change in the north-east Atlantic region, *Palaeogeography, Palaeoclimatology, Palaeoecology, 284(3),* 164-179.

Jones, D.S. (1980), Annual cycle of shell growth increment formation in two continental shelf bivalves and its paleoecologic significance, *Paleobiology 6,* 331–340.

Karney, G.B., Butler, P.G., Scourse, J.D., Richardson, C.A., Lau, K.H., Czernuszka, J.T. & Grovenor, C.R.M. (2011), Identification of growth increments in the shell of the bivalve mollusc *Arctica islandica* using backscattered electron imaging, *Journal ofMicroscopy, 241*, pp. 29–36

Keller, N., Del Piero, D. & Longinelli, A. (2002), Isotopic composition, growth rates and biological behaviour of *Chamelea gallina* and *Callista chione* from the Gulf of Trieste (Italy), *Marine Biology 140,* 9-15.

Kennett, J.P. (1982), Marine Geology. Prentice-Hall, New Jersey, 813 pp.

Kennish, M.J. & Olsson, R.K. (1975), Effects of thermal discharges on the microstructural growth of *Mercenaria mercenaria, Environmental Geology*, *1,* 41–64.

Keyser, D. (1980), Auftreten und konstanz von poren und borsten auf der schale von *Podocopa* (Ostracoda, Crustacea), *Verhandlungen des naturwissenschaftlichen Vereins, 23*, 175-193.

Killingley, J.S. & Berger, W.H. (1979), Stable isotopes in a mollusc shell: Detection of upwelling Events, *Science, 205,* 186–188.

Kim, J.K., Khim, B.-K., Woo, K.S. & Yoon, S.H. (2010), Records of palaeo-seawater conditionfrom oxygen-isotope profiles of early Pleistocene fossil molluscs from the Seoguipo Formation (Korea), *Lethaia, 43,* 170–181.

Klepal, W. & Barnes, H. (1975), A historical and scanning electron microscopical study of the formation of the wall plates in *Chthamalus depressus* (Poli), *Journal of experimental marine ecology, 20,* 183-198.

Knudsen, J. (1970), The systematics and biology of abyssal and hadal Bivalvia, Galathea Report, Vol. 11. Copenhagen: Danish Science Press.

Kobayashi, I. & Samata, T. (2006), Bivalve shell structure and organic matrix, *Materials Science and Engineering C, 26,* 692–698.

Kouchinsky, A. (2000), Shell microstructures in Early Cambrian molluscs, *Acta Palaeontologica Polonica, 45 (2),* 119-150.

Krantz, D.E., Williams, D.F. & Jones, D.S. (1987), Ecological and paleoenvironmental information using stable isotope profiles from living and fossil mollusks, *Palaeogeography, Palaeoclimatology, Palaeoecology, 58,* 249-266.

Kukla, G., Collins, B.P. & Bender, M.L. (1979), Radiometric age of the *Arctica islandica* boundary in Italy: 2 my. *Ann. Géol. Pays Hellén., T. hors sèrie*, 699-709.

Kukla, G. & An, J. (1989), Loess stratigraphy in Central China, *Palaeogeogr. Palaeoclimatol. Palaeoecol., 72,* 203– 225.

Lamarck, J.B. (1805), Suite des mémoires Sur les fossiles des environs de Paris. *Ann. Mus. Paris, 6,* 214-221, 337-345.

Lamarck, J.B. de (1809), Philosophie Zoologique, ou exposition des considérations relative à l'histoire naturelle des animaux; à la diversité de leur organisation et des facultés qu'ils en obtiennent; aux causes physiques qui maintiennent en eux la vie et donnent lieu aux mouvements qui'ils exécutent; enfin, à celles qui produisent, les unes le sentiment, et les autres l'intelligence de ceux qui en sont doués. V. 1 of 1- 422 pp., V. 2 of 1-473 pp. Paris.

Lamarck, J.B. de (1819), Histoire naturelle des animaux sans vertèbres, A. Berlin, Paris, 6, 343 pp.

Landers, W.S. (1976), Reproduction and early development of the ocean quahog, *Arctica islandica*, in the laboratory, *Nautilus, 90,* 88–92.

La Perna R. (2006), Life habit and ontogeny of the unusual arcid bivalve *Ambrogia mytiloides* (Brocchi, 1814), *Lethaia, 39,* 245-252.

La Perna, R. & D'Abramo, M. (2009), Morphometric and systematic study on three *Acanthocardia* species from the Mediterranean Pleistocene (Mollusca, Bivalvia, Cardiidae), *Geodiversitas, 31(3*), 669-682.

Lawrence, K., Sosdian, S., White, H. & Rosenthal, Y. (2010), North Atlantic climate evolution through the Plio-Pleistocene climate transitions, *Earth Planet. Sci. Lett., 300*, 329–342.

Lecointre, G. (1952), Recherches sur le Néogène et le Quaternaire marins des la cote atlantique du Maroc. *Protect. Rep. Fr. Maroc. Serv. Geol., Notes et Mem., 99*, 174 pp.

Lécuyer, C., Reynard, B. & Martineau, F. (2004), Stable isotope fractionation between mollusc shells and marine waters from Martinique Island, *Chemical Geology*, *213*(4), 293-305.

Linnaeus, C. (1758), Systema Naturae per Regna tria naturae, secundum classes, ordines, genera, species cum characteribus, differentiis, synonymis, locis. Editio decima, reformata. Tomus 1, 824 pp. Laurentii Salvii, Holmiae.

Linnaeus, C. (1767), Systema Naturae per Regna tria naturae, secundum classes, ordines, genera, species cum characteribus, differentiis, synonymis, locis. Editio duodecima, reformata. Tomus 1, pars 2, 533-1327 pp. Laurentii Salvii, Holmiae.

Lisiecki, L.E. & Raymo, M.E. (2005), A Pliocene-Pleistocene stack of 57 globally distributed benthic δ18O records, *Paleoceanography, 20(1),* p. 522–533.

Lona, F. & Bertoldi, R. (1972), Rinvenimento di *Arctica (Cyprina) islandica* in una serie continua plio-pleistocenica presso Castell'Arquato (Piacenza) in connessione con sequenze pollinologiche. *L'Ateneo Parmense, 8,* 35-44.

Loosanoff, V.L. (1953), Reproductive cycle in *Cyprina islandica, Bull. Mar. biol. Lab*., Woodshole, *104*, 146-155.

Lorrain, A., Paulet, Y.M., Chauvaud, L., Dunbar, R., Mucciarone, D. & Fontugne, M. (2004), $\delta^{13}C$ variation in scallop shells: increasing metabolic carbon contribution with body size?, *Geochimica et Cosmochimica Acta, 68,* 3509–3519.

Lourens, L.J. (2004), Revised tuning of Ocean Drilling Program Site 964 and KC01B (Mediterranean) and implications for the $\delta^{18}O$, tephra, calcareous nannofossil, and geomagnetic reversal chronologies of the past 1.1 Myr, *Paleoceanography, 19 (3),* PA3010.

Lourens, L.J., Antonarakou, A., Hilgen, F.J., Van Hoof, A.A.M., Vergnaud-Grazzini, C. & Zachariasse, W.J. (1996), Evaluation of the Plio-Pleistocene astronomical timescale, *Paleoceanography, 11 (4),* p. 391.

Lowenstam, H.A. (1954a), Factors affecting the aragonite: calcite ratios in carbonate-secreting marine organisms, *The Journal of Geology, 62,* 284-322.

Lowenstam, H.A. (1954b), Environmental relations of modification compositions of certain carbonate secreting marine invertebrates, *Proceedings of the National Academy of Sciences of the United States of America, 40(1),* 39.

Lozano Francisco, M.C., Vera Pelaez, J.L. & Guerra Merchan, A. (1993), Arcoida (Mollusca, Bivalvia) del Plioceno de la provincia de Málaga, España, *Treballs del Museu de Geologia de Barcelona, 3,* 157-188.

Lutz, R.A., Goodsell, J.G., Mann, R. & Castagna, M. (1981), Experimental culture of the ocean quahog, *Arctica islandica*, *J. World Aquacult. Soc., 12,* 196–205.

Lutz, R.A., Mann, R., Goodsell, J. & Castagna, M. (1982), Larval and early post-larval development of *Arctica islandica, J. Mar. Biol. Assoc.*, *62,* 745–769.

Lutz, R.A. & Rhoads, D.C. (1977), Anaerobiosis and a theorie of growth line formation, *Science, 198,* 1222-1227.

MacFadden, B.J., Labs-Hochstein, J., Quitmyer, I. & Jones, D.S. (2004), Incremental growth and diagenesis of skeletal parts of the lamnoid shark *Otodus obliquus* from the early Eocene (Ypres) of Morocco, *Palaeogeography, Palaeoclimatology, Palaeoecology, 206,* 179-192.

Malatesta, A. (1957), Terreni, faune ed industrie quaternarie nell'Arcipelago delle Egadi, *Quaternaria IV,* 165-190.

Malatesta, A. (1960-1963), Malacofauna pleistocenica di Grammichele (Sicilia), *Mem. Serv. Descr. Carta Geologica d'Italia, 12,* 1-392.

Malatesta, A. (1974), Malacofauna pliocenica umbra, *Memoria per servire alla descrizione della Carta Geologica d'Italia, 13,* 1-490.

Malatesta, A. & Nicosia, M.L. (1955), I fossili del Pliocene e Pleistocene di Agrigento della collezione Lomi, *Bollettino del Servizio Geologico Italiano, 77,* 173-180.

Malatesta, A. & Zarlenga, F. (1986), Northern guests in the Pleistocene Mediterranean Sea, *Geologica Romana, 25,* 91-154.

Mann, R. & Wolf, C.C. (1983), Swimming behaviour of larvae of the ocean quahog *Arctica islandica* in response to pressure and temperature, *Mar. Ecol. Prog. Ser. 13*, 211–218.

Marasti, R. (1973), La fauna tortoniana del T. Stirone (limite Parmense-Piacentino), *Bollettino della Società Paleontologica Italiana 12, (1),* 76-120.

Marasti, R. & Raffi, S. (1980), La diversità tassonomica dei bivalvi del Pliocene mediterraneo, Centro Grafico dell' Università di Parma, 1-30.

Marchitto, T.M., Jones, G.A., Goodfriend, G.A. & Weidman, C.R. (2000), Precise Temporal Correlation of Holocene Mollusk Shells Using Sclerochronology, *Quaternary Research, 53,* 236-246.

Marin, F., Le Roy, N. & Marie, B. (2012), The formation and mineralization of mollusk shell, *Frontiers in Bioscience, S4,* 1099-1125.

Martinell, J. & Domenech, R. (1982), El Plioceno marino de la margen derecha del rio Fluvia (Alt Emporda, Girona), *Estudios Geologicos, 38,* 379-384.

Martinetto, E., Monegato, G., Irace, A., Vaiani, S. C. & Vassio, E. (2014), Pliocene and Early Pleistocene carpological records of terrestrial plants from the southern border of the Po Plain (northern Italy), *Review of Palaeobotany and Palynology*. doi:10.1016/j.revpalbo.2014.10.007.

Martinez-Garcia, A., Rosell-Mele, A., McClymont, E.L., Gersonde, R. & Haug, G.H. (2010), Subpolar link to the emergence of the modern Equatorial Pacific Cold Tongue, *Science, 328,* 1550–1553.

Martini, E. (1971), Standard Tertiary and Quaternary calcareous nannoplankton zonation. In: Farinacci, A. (Ed.), Proceedings 2nd International Conference Planktonic Microfossils, Rome, 2, 739–785.

Martini, I.P., Broofield, M.E. & Sadura, S. (2001), Principles of Glacial Geomorphology and Geology. Prentice-Hall, London. 381 pp.

Mayer, C. (1868), Catalogue systématique et descriptif des fossiles des terrains Tertiaires qui se trouvent au Musée Fédéral de Zurich. 3eme Cahier. Mollusques, Famille des Arcidés. Schabelitz, Zurich, 124 pp.

Mayer, C. (1876), La verité sur la mer glaciale au pied des Alpes, *Bull. Soc. Geol. Fr., ser. III, IV,* 199-222.

McClymont, E.L. & Rossel-Mele, A. (2005), Links between the onset of modern Walker circulation and the mid-Pleistocene climate transition, *Geology, 33*, 389–392.

McConnaughey, T.A. (1989a), ^{13}C and ^{18}O isotopic disequilibrium in biological carbonates: I. Patterns, *Geochimica et Cosmochimica Acta, 53(1),* 151-162.

McConnaughey, T.A. (1989b), ^{13}C and ^{18}O isotopic disequilibrium in biological carbonates: II. In vitro simulation of kinetic isotope effects, *Geochimica et Cosmochimica Acta, 53(1),* 163-171.

McConnaughey, T.A., Burdett, J., Whelan, J.F. & Paull, C.K. (1997), Carbon isotopes in biological carbonates: respiration and photosynthesis, *Geochimica et Cosmochimica Acta, 61,* 611–622.

McConnaughey, T. A. & Gillikin, D. P. (2008), Carbon isotopes in mollusk shell carbonates, *Geo-Marine Letters*, *28*(5-6), 287-299.

McCrea, J.M. (1950), On the isotopic chemistry of carbonates and a paleotemperature scale, *The Journal of Chemical Physics, 18(6),* 849-857.

Meli, R. (1879), Note geologiche sui dintorni di Civitavecchia, *Atti R. Acc. Lincei, ser. 3,* V, 1-13.

Meli R. (1884), Cenni geologici sulle coste d'Anzio e di Nettuno ed elenco dei molluschi pliocenici ivi raccolti, *Ann. Ist. Tecn. Di Roma, IX,* 31 pp.

Mii, H.S. & Grossman, E.L. (1994), Late Pennsylvanian seasonality reflected in the ^{18}O and elemental composition of a brachiopod shell, *Geology, 22,* 661–664.

Monegatti, P. & Raffi, S. (2001), Taxonomic diversity and stratigraphic distribution of Mediterranean Pliocene bivalves, *Palaeogeography, Palaeoclimatology, Palaeoecology, 165(3),* 171-193.

Monegatti, P., Raffi, S., Roveri, M. & Taviani, M. (2001), One day trip in the outcrops of Castell'Arquato Plio–Pleistocene Basin: from the Badlands of Monte Giogo to the Stirone River: Paleobiogeography and Paleoecology 2001 International Conference, Excursion Guidebook, Università di Parma, Parma, 26 p.

Mook, W.G. & Vogel, J.C. (1968), Isotopic equilibrium between shells and their environment, *Science, 159,* 874-875.

Moroni, M.A. (1955), La macrofauna saheliana del Messiniano inferiore della Repubblica di S. Marino, *Giornale di Geologia, serie 2, 25,* 81–162.

Morton, B. (1980), Swimming in *Amusium pleuronectes* (Bivalvia: Pectinidae), *Journal of Zoology, 190,* 375–404.

Mulder, T., Syvitski, J.P.M., Migeon, S., Faugéres, J.C. & Savoye, B. (2003), Marine hyperpycnal flows: Initiation, behavior and related deposits: A review, *Marine and Petroleum Geology, 20,* 861–882.

Mulder, T. & Alexander, J. (2001), The physical character of subaqueous sedimentary density flows and their deposits, *Sedimentology, 48,* 269–299.

Mutti, E., Tinterri, R., Benevelli, G., Di Biase, D. & Cavanna, G. (2003), Deltaic, mixed and turbidite sedimentation of ancient foreland basins, *Marine and Petroleum Geology, 20,* 733–755.

Mutti, E., Tinterri, R., Di Biase, D., Fava, L., Mavilla, N., Angella, S. & Calabrese, L. (2000), Delta-front facies associations of ancient flood-dominated fluvio-deltaic systems, *Revista Societa` Geologica de España, 13,* 165–190.

Muttoni, G., Ravazzi, C., Breda, M., Pini, R., Laj, C., Kissel, C., Mazaud A. & Garzanti, E. (2007), Magnetostratigraphic dating of an intensification of glacial activity in the southern Italian Alps during Marine Isotope Stage 22, *Quaternary Research, 67(1),* 161-173.

Neumayr, M. (1884), Zur Morphologie des bivalve schlosses, *K.K. Akad. Wiss. Wien, Nat. Math. Cl., 88 (1),* 385-418.

Newell, N.D. (1969), Order Arcoida Stoliczka, 1871. In: Moore R. (ed.) - Treatise on invertebrate paleontology, Part N, Mollusca 6, Vol. 1. Bivalvia. Geological Society of America & University of Kansas, N248–N270.

Newton, R.B. (1891), Systematic list of the F. E. Edwards collection of British Oligocene and Eocene mollusca in the British Museum (Natural History), with references to the type-specimens from similar horizons contained in other collections belonging to the Geological Department of the Museum. London, British Museum, XXVIII + 365 pp.

Nicol, D. (1951), Recent species of the veneroid pelecypod *Arctica*, J. *Wash. Acad. Sci., 41,* 102–106.

Nicol, D. & Jones D.S. (1984), Review of *Postligata*, a Late Cretaceous pelecypod, *Tulane Studies in Geology and Paleontology, 18,* 67–69.

Nicosia, M.L. (1957), Lamellibranchi di Altavilla Milicia nel foglio 250 "Bagheria" (Isola di Sicilia), *Bollettino del Servizio Geologico Italiano, 79*

Nordsieck, F. (1969), Die europäischen Meeresmuscheln. Vom Eismeer bis Kapverden, Mittelmeer und Schwarzes Meer. Gustav Fischer, Stuttgart XIII + 256 pp.

Nyst, P.H. & Westendorp, G.D. (1839), Nouvelles recherches sur les coquilles de la province d'Anvers, *Bulletin de l'Acadèmie des Sciences de Bruxelles, 4,* 1-14.

Oberling, J.J. (1964), Observations on some structural features of the Pelecypod Shell. *Mitteilungen der Naturforschenden Gesellschaft in Bern*, *20:* 1-60.

Okada, H. & Bukry, D. (1980), Supplementary modification and introduction of code numbers to the low-latitude coccolith biostratigraphic zonation (Bukry 1973, 1975), *Marine Micropaleontology, 5,* 321–325.

Oliver P.G. & Holmes A.M. (2006), The Arcoidea (Mollusca: Bivalvia): a review of the current phenetic based systematics, *Zoological Journal of the Linnean Society, 148,* 237–251.

O'Neil, J.R., Clayton, R.N. & Mayeda, T.K. (1969), Oxygen isotope fractionation in divalent metal carbonates, *Journal of Chemical Physics, 51*, 5547-5558.

Owen, G. & Williams, A. (1969), The caecum of articulate Brachiopoda, *Proceedings of the Royal Society of London B, 172,* 187-201.

Palla, P. (1966), Lamellibranchi pliocenici della Bassa Val d'Elsa (Toscana occidentale), *Rivista Italiana di Paleontologia, 72, (2),* 397-458.

Palmer, A.R. (1983), Relative cost of producing skeletal organic matrix versus calcification: evidence from marine gastropods, *Marine Biology, 75*, 287– 292.

Palmer, R.A. (1992), Calcification in marine molluscs: how costly it is? *Proc. Nati. Acad. Sci. USA, 89*, pp. 1379-1382.

Palombo, M.R. (2007), What is the boundary for the Quaternary period and Pleistocene epoch? The contribution of turnover patterns in large mammalian complexes from north-western Mediterranean to debate, *Quaternaire, 18(1),* 35-53.

Papani, G. & Pelosio, G. 1962 (1963), La serie plio-pleistocenica del Torrente Stirone (Parmense Occidentale), *Bollettino della Società Geologica Italiana, 81 (3),* 293-325.

Parenzan, P. (1974), Carta d'idenlita delle conchiglie del Mediterraneo, 2 (Bivalvi), *Bios Taras,* Taranto, 546 pp.

Pareto, M. (1865), Sur les subdivisions que l'on pourrait établir dans le terrains Tertiaires de l'Apennin septentrional, *Bull. Soc. Geol. France, 22,* 210-277.

Parona, C.E. (1878), Il Pliocene dell'Oltrepò Pavese: osservazioni stratigrafiche e paleontologiche, *Atti Società italiana di Scienze naturali, 21,* 662-672 pp.

Parsons-Hubbard, K., Kyi, E., Hobart, K. & Hoffman, C. (2014), The role of microboring organisms in the degradation of shell carbonate. 4th International Palaeontological Congress, Mendoza, Argentina. 28 September-3 October 2014.

Peharda, M., Crnčević, M., Bušelić, I., Richardson, C.A. & Ezgeta-Balić, D. (2012), Growth and longevity of *Glycymeris nummaria* (Linnaeus, 1758) from the eastern Adriatic, Croatia, *J. Shellfish Res., 31,* 947–950.

Pelosio, G. & Raffi, S. (1974), Osservazioni su *Arctica islandica* ed altri lamellibranchi del Calabriano dell'Emilia occidentale, *Ateneo Parmense, acta nat., 10,* 347-367.

Pelosio, G. & Raffi, S. (1977), Preliminary remarks on mollusc assemblages of the Stirone river Pleistocene series (Parma Province, Northern Italy). X INQUA Congress, Birmingham, p. 1–19.

Pérés, J.M. & Picard, J. (1958), Manuel de bionomie benthique de la mer Méditerranée, *Recueil des Travaux de la Station Marine d'Endoume, 23 (14),* 5-122.

Pérès, J.M. & Picard, J. (1964), Nouveau manuel de bionomie bentique de la Méditerranée, *Rec. Trav. St. Mar. Endoume, 31,* 1-137.

Pesce, G.L. & Rapetti, C.A. (1971), Malacofauna pliocenica d'Abruzzo. Bivalvi del circondario di S. Eusanio del Sangro (Chieti), *Estratto degli Annali della Università degli studi dell'Aquila, anno V.*

Plesi, G. (1997), L'appennino settentrionale: processi e tempi di formazione di una catena montuosa, Dip. Di Scienze della Terra, Univ. Degli Studi di Pisa.

Poli, G.S. (1791-1827), Testacea utriusque Siciliae eorumque historia et anatome. Vol. I-III, Regio typographeio, Parmae.

Popov, S.V. (1992), Mikrostruktura rakoviny nekotrych grupp dvust vorcatych molljuskov, *Trudy Paleontologiceskogo Instituta, Rossijskaja Akademija Nauk, 245,* 1-46.

Popp, B.N., Anderson, T.F. & Sandberg, P.A. (1986), Brachiopods as indicators of original isotopic compositions in some Paleozoic limestones, *Geological Society of America, Bulletin 97,* 1262 – 1269 .

Raffi, S. (1970), I Pettinidi del Pliocene e Calabriano dell'Emilia occidentale (Piacentino e Parmense), *Bollettino della Società Paleontologica Italiana, 9 (2),* 97-135.

Raffi, S. (1986), The significance of marine boreal molluscs in the Early Pleistocene faunas of the Mediterranean area, Spano, C., 1989, *Palaeogeogr., Palaeoclimatol., Palaeoecol., 52,* 267–289.

Raffi, S., Stanley, S.M. & Marasti, R. (1985), Biogeographic pattern and Plio-Pleistocene extinction of Bivalvia in the Mediterranean and southern North Sea, *Paleobiology, 11(4),* 368–388.

Raffi, S., Rio, D., Sprovieri, R., Valleri, G., Monegatti, P., Raffi, I. & Barrier, P. (1989), New stratigraphic data on the Piacenzian stratotype, *Boll. Soc. Geol. It., 108,* 183-196.

Raffi, I., Backman, J., Rio, D. & Shackleton, N.J. (1993), Plio-Pleistocene nannofossil biostratigraphy and calibration to oxygen isotope stratigraphies from Deep Sea Drilling Project Site 607 and Ocean Drilling Program Site 677, *Paleoceanography, 8,* 387–408.

Rafinesque, C.S. (1815), Analyse de la Nature, ou tableau de l'univers et de corp organisés. Palermo: C.S. Rafinesque, from the Press of Jean Barravecchia.

Raineri, G. (2007), Riserva natural geologica del Piacenziano: appunti per un'escursione, *Parchi e Riserve dell'Emilia-Romagna,* 52pp.

Ramsay, K., Kaiser, M.J., Richardson, C.A., Veale, L.O. & Brand, A.R. (2000), Can shell scars on dog cockles (*Glycymeris glycymeris* L.) be used as an indicator of fishing disturbance? *Journal of Sea Research, 43,* 167–176.

Raymo, M.E., Hodell, D. & Jansen, E. (1992), Response of deep ocean circulation to initiation of Northern Hemisphere glaciation (3– 2Ma), *Paleoceanography, 7*, 645–672.

Reindl, S. & Haszprunar, G. (1996), Fine structure of caeca and mantle of arcoid and limopsoid bivalves (Mollusca: Pteriomorpha), *The Veliger, 39 (2),* 101-116.

Rhoads, D.C. & Lutz, R.A. (1980), Skeletal Growth of Aquatic Organisms: Biological records of environmental change. Plenum Press.

Riedl, R. (1986), Fauna y Flora del Mediterráneo, Omega, Barcelona, 858 pp.

Rio, D., Sprovieri, R., Raffi, I. & Valleri, G. (1988), Biostratigrafia e paleoecologia della sezione stratotipica del Piacenziano, *Boll. Soc. Paleont. It., 27, (2),* 213-238.

Risso, A. (1826), Histoire naturelle des principales productions de l'Europe Méridionale et particulièrement de celles des environs de Nice et des Alpes Maritimes, *Paris, F.G. Levrault 4,* 1-439.

Röding, P.F. (1798), Museum Boltenianum sive Catalogus cimeliorum e tribus regnis naturae quae olim collegerat Joa. Fried. Bolten M.D.p.d. Pars secunda continens Conchylia sive Testacea univalvia, bivalvia et multivalvia VIII+119 pp.

Rogalla, N.S. & Amler, M.R.W. (2007), Statistic approach on taphonomic phenomena in shells of *Glycymeris glycymeris* (Bivalvia: Glycymerididae) and its significance in the fossil record, *Palaontologische Zeitschrift, 81 (3),* 334-355.

Roger, J. (1940), Pectinides miocenes pliocenes er quaternarie de Syrie, *Haut-Comm. De la Rep. Francaise en Syrie et en Liban,* 325-352.

Ropes, J.W., Jones, D.S.,Murawski, S.A., Serchuk, F.M. & Jearld Jr., A. (1984), Documentation of annual growth lines in ocean quahogs, *Arctica islandica* Linné, *Fish. Bull., 82,* 1–19.

Rossi Ronchetti, C. (1951), I Tipi della «Conchiologia fossile subapennina» di G. Brocchi, *Rivista Italiana di Paleontologia, 57,* 2-63.

Royer, C., Thébault, J., Chauvaud, L. & Olivier, F. (2013), Structural analysis and paleoenvironmental potential of dog cockle shells (*Glycymeris glycymeris*) in Brittany, northwest France, *Palaeogeography, Palaeoclimatology, Palaeoecology*, *373*, 123-132.

Ruddiman, W., Raymo, M., Martinson, D., Clement, B. & Backman, J. (1989), Pleistocene evolution: Northern Hemisphere ice sheets and North Atlantic Ocean, *Paleoceanography, 4,* 353–412.

Ruggieri, G. (1949a), Il Pliocene superiore di Capocolle (Forlì), *Giornale di Geologia, serie 2, 20*, 19–38.

Ruggieri, G. (1949b), La malacofauna del Calabriano Romagnolo, *Giornale di Geologia, serie 2, 20,* 63–110.

Ruggieri, G. (1957a), Geologia e stratigrafia della sommità del terziario a Castrocaro, *Giornale di geologia, serie 2, 26,* 52 pp.

Ruggieri, G. (1957b), Molluschi pliocenici sopravvissuti nel Calabriano, *Atti della Societa Toscana di Scienze Naturali, serie A, 64,* 80–87, 1 pl.

Schaffer, F.X. (1910-1912), Das Miocän von Eggenburg. Die Fauna der ersten Mediterranstufe des Wiener Beckens und die geologischen Verhältnisse der Umgebung des Manhartsberges in Niederösterreich. Die Gastropoden der Miocänbildungen von Eggenburg, *Abhandlungen der K.K. Geologischen Reichsanstalt, 22 (1),* 3-126.

Schöne, B.R. (2008), The curse of physiology - challenges and opportunities in the interpretation of geochemical data from mollusk shells, *Geo-Marine Letters, 28(5-6),* 269-285.

Schöne, B.R. (2013), *Arctica islandica* (Bivalvia): A unique paleoenvironmental archive of the northern North Atlantic Ocean, *Global and Planetary Change, 111*, 199–225.

Schöne, B.R. & Fiebig, J. (2009), Seasonality in the North Sea during the Allerød and Late Medieval Climate Optimum using bivalve sclerochronology, *International Journal of Earth Sciences, 98(1),* 83-98.

Schöne, B.R., Flessa, K.W., Dettman, D.L., Goodwin, D.H. & Roopnarine, P.D. (2002), Sclerochronology and growth of the bivalve mollusks *Chione fluctifraga* and *C. cortezi* in the northern Gulf of California, Mexico, *Veliger, 45,* 45–5.

Schöne, B.R., Oschmann, W., Rössler, J., Castro, A., Houk, S., Kröncke, I., Dreyer, W., Janssen, R., Rumohr, H. & Dunca, E. (2003), North Atlantic oscillation dynamics recorded in shells of a long-lived bivalve mollusk, *Geology, 31,* 1037–1040.

Schöne, B.R., Castro, A.D.F., Fiebig, J., Houk, S.D., Oschmann, W. & Kröncke, I. (2004), Sea surface water temperatures over the period 1884-1983 reconstructed from oxygen isotope ratios of a bivalve mollusk shell (*Artica islandica*, southern North Sea), *Palaeogeography, Palaeoclimatology, Palaeoecology, 212,* 215- 232.

Schöne, B.R., Fiebig, J., Pfeiffer, M., Gleβ, R., Hickson, J., Johnson, A.L.A., Dreyer, W. & Oschmann, W. (2005a), Climate records from a bivalved Methuselah (*Arctica islandica*, Mollusca; Iceland), *Palaeogeography, Palaeoclimatology, Palaeoecology, 228(1),* 130-148.

Schöne, B.R., Dunca, E., Fiebig, J. & Pfeiffer, M. (2005b), Mutvei's solution: an ideal agent for resolving microgrowth structures of biogenic carbonates, *Palaeogeography, Palaeoclimatology, Palaeoecology, 228,* 149–166

Schöne, B.R., Pfeiffer, M., Pohlmann, T. & Siegismund, F. (2005c), A seasonally resolved bottom water temperature record for the period of AD 1866–2002 based on shells of *Arctica islandica* (Mollusca, North Sea), *Int. J. Climatol., 25,* 947–962.

Schöne, B.R., Rodland, D.L., Wehrmann, A., Heidel, B., Oschmann, W., Zhang, Z., Fiebig, J. & Beck, L. (2007), Combined sclerochronologic and oxygen isotope analysis of gastropod shells (*Gibbula cineraria*, North Sea): life-history traits and utility as a high-resolution environmental archive for kelp forests, *Marine Biology, 150(6),* 1237-1252.

Schöne, B.R., Wanamaker Jr., A.D., Fiebig, J., Thébault, J. & Kreutz, K.J. (2011a). Annually resolved δ^{13}Cshell chronologies of long-lived bivalve mollusks (*Arctica islandica*) reveal oceanic carbon dynamics in the temperate North Atlantic during recent centuries, *Palaeogeogr. Palaeoclimatol. Palaeoecol., 302,* 31–42.

Schöne, B.R., Zhang, Z., Radermacher, P., Thébault, J., Jacob, D.E., Nunn, E.V. & Maurer, A.-F., (2011b). Sr/Ca and Mg/Ca ratios of ontogenetically old, long-lived bivalve shells (*Arctica islandica*) and their function as paleotemperature proxies, *Palaeogeography, Palaeoclimatology, Palaeoecology, 302,* 52–64.

Schöne, B.R., Radermacher, P., Zhang, Z. & Jacob, D.E. (2013), Crystal fabrics and element impurities (Sr/Ca, Mg/Ca, and Ba/Ca) in shells of *Arctica islandica* - Implications for paleoclimate reconstructions, *Palaeogeography, Palaeoclimatology, Palaeoecology, 373,* 50–59.

Schrag, D.P., Adkins, J.F., McIntyre, K., Alexander, J.L., Hodell, D.A., Charles, C.D. & McManus, J.F. (2002), The oxygen isotopic composition of sea water during the Last Glacial Maximum, *Quaternary Science Reviews,21,* 331–342.

Schumacher, C. F. (1817), Essai d'un nouveau système des habitations des vers testacés. pp. [1-3], 1-287, Pl. I-XXII, Copenhague.

Schumm, S. A., (1977), The fluvial system: New York, John Wiley and Sons, 338 p.

Schumm, S. A., (1981), Evolution and response of the fluvial system: Sedimentologic implications, *SEPM Special Publication, 31,* p. 19–29.

Scourse, J., Richardson, C., Forsythe, G., Harris, I., Heinemeier, J., Fraser, N., Briffa K. & Jones, P. (2006), First cross-matched floating chronology from the marine fossil record: data from growth lines of the long-lived bivalve mollusc *Arctica islandica*, *The Holocene, 16(7),* 967-974.

Seed, R. (1992), Systematics evolution and distribution of mussels belonging to the genus *Mytilus*: an overview, *American Malacological Bulletin, 9*, 123-137.

Seed, R. (1995), Speciation and geographical distribution within the genus *Mytilus, Bulletin of the Malacological Society of London, 24,* 4.

Seguenza, G. (1873-1877), Studi stratigrafici sulla formazione pliocenica dell'Italia meridionale, *Boll. R. Com. Geol. It. IV, V, VI, VII, VIII, estr.,* 299 pp.

Shackleton, N.J. & Opdyke N.D. (1973), Oxygen isotope and paleomagnetic stratigraphy of Equatorial Pacific core V28-238: oxygen isotope temperatures and ice volumes on a 104 and 106 years scale, *Quat. Res., 3*, 39-55.

Shackleton, N.J. & Opdyke, N.D. (1976), Oxygen-isotope and paleomagnetic stratigraphy of Pacific core V28-239 late Pliocene to latest Pleistocene, *Geological Society of America Memoirs*, *145*, 449-464.

Shackleton, N.J., Backmann, J., Zimmermann, H., Kent, D.V., Hall, M.A., Roberts, D.J. & Baldauf, J. (1984), Oxygen isotope calibration of the onset of ice-rafting and history of glaciation in the North Atlantic region, *Nature, 307,* 620–623.

Shackleton, N.J., Hall, M.A. & Pate, D. (1995), Pliocene stable isotope stratigraphy of Site 846. *Proceedings, Ocean Drilling Program, Sc. Results, 138*, 337–355.

Shibata, M. (1979), Tubules found in the arcoid shell, *VENUS, Jap. Jour. Malac*., *38 (1),* 48-60.

Signor, P. W. & Lipps, J. H. (1982), Sampling bias, gradual extinction patterns and catastrophes in the fossil record, *Geological Society of America Special Papers, 190,* 291-296.

Sirna, G. (1978), Problemi di nomenclatura: la priorità di *Glycymeris insubricus* (Brocchi), *Conchiglie, 14 (9-10),* 181-184.

Skibinski, D.O.F., Ahmad, M. & Beardmore, J.A. (1978), Genetic evidence for naturally occurring hybrids between *Mytilus edulis* and *Mytilus galloprovincialis, Evolution, 32(2),* 354-364.

Sosdian, S. & Rosenthal, Y. (2009), Deep-sea temperature and ice volume changes across the Pliocene–Pleistocene climate transitions, *Science, 325,* 306–310.

Squires, R.L. (2010), Northeast Pacific Upper Cretaceous and Paleocene Glycymeridid bivalves, *J. Paleont., 84(5),* 895–917.

Srivastava, R., Ramesh, R., Prakash, S., Anilkumar, N. & Sudhakar, M. (2007), Oxygen isotope and salinity variations in the Indian sector of the Southern Ocean, *Geophys. Res. Lett., 34.*

Stemmer, K., Nehrke, G. & Brey, T. (2013), Elevated CO^2 Levels do not Affect the Shell Structure of the Bivalve *Arctica islandica* from the Western Baltic, *PLoS ONE 8(7),* e70106.

Stewart, R.B. (1930), Gabb's California Cretaceous and Tertiary type lamellibranchs, *Academy of Natural Sciences of Philadelphia, Special Publication, 3*, 1–314.

Steyer, S., Laurin, M., Castanet, J. & de Riclès, A. (2004), First histological and sclerochronological data on temnospondyl growth: palaeoecological and palaeoclimatological implications, *Palaeogeography, Palaeoclimatology, Palaeoecology, 206,* 193- 201.

Stoliczka, F. (1870-71), Cretaceous fauna of southern India, v. 3, The Pelecypoda, with a review of all known genera of this class, fossil and recent, *Geological Survey of India, Palaeontologica Indica, ser. 6, 3,* 537 pp.

Strom, A., Francis, R.C., Mantua, N.J., Miles, E.L. & Peterson, D.L. (2004), North Pacific climate recorded in growth rings of geoduck clams: a new tool for paleoenvironmental reconstruction, *Geophysical Research Letters, 31(6).*

Suzuki, S. & Uozumi, S. (1981), Organic components of prismatic layers in molluscan shells, *Jour. Fac. Sci. , Hokkaido Univ., 20 (1),* 7-20.

Tanabe, K. (1988), Age and growth rate determinations of an intertidal bivalve, *Phacosoma japonicum*, using internal shell increments, *Lethaia, 21*, 231–241.

Tanaka, N., Monaghan, M.C. & Rye, D.M. (1986), Contribution of metabolic carbon to mollusk and barnacle shell carbonate, *Nature, 320,* 520–523.

Tarutani, T., Clayton, R.N. & Mayeda, T. (1969), The effect of polymorphism and magnesium substitution on oxygen isotope fractionation between calcium carbonate and water, *Geochimica et Cosmochimica Acta, 33,* 987-996.

Tavani, G. (1938-1939), Fossili del Miocene della Cirenaica, *Palaeont. Ital. 38*, 127-187, *39*, 17-76.

Taviani, M., Roveri, M., Impiccini, R. & Vigliotti, L. (1997), Segnalazione di Quaternario marino nella Val Chero (Appennino piacentino), *Bollettino Società Palaeontologica Italiana, 36*, 331-338.

Tebble, N. (1966), British Bivalve seashells, Royal Scottish Museum by Her Majesty' s Stationery Office, Edinburgh, 212 pp.

Thébault, J., Chauvaud, L., L'Helguen, S., Clavier, J., Barats, A., Jacquet, S., Pécheyran, C. & Amouroux, D. (2009a). Barium and molybdenum records in bivalve shells: geochemical proxies for phytoplankton dynamics in coastal environments? *Limnology and Oceanography, 54,* 1002–1014.

Thébault, J., Schöne, B., Hallmann, N., Barth, M. & Nunn, E. (2009b), Investigation of Li/Ca variations in aragonitic shells of the ocean quahog *Arctica islandica*, (northeast Iceland), *Geochemistry Geophysics Geosystems, 10,* Q12008.

Thomas, R.D.K. (1976), Constraints of ligament growth, form and function on evolution in the Arcoida (Mollusca: Bivalvia), *Paleobiology, 2,* 64–83.

Thompson, I., Jones, D.S. & Dreibelbis, D. (1980), Annual internal growth banding and life history of the Ocean Quahog *Arctica islandica* (Mollusca: Bivalvia), *Mar Biol, 57*, 25–34.

Thunell, R. (1979), Pliocene - Pleistocene paleotemperatures and paleosalinity history of the Mediterranean Sea, results from Deep Sea Drilling Project Sites125 and 132, *Mar. Micropaleontol., 4,* 173.

Thunell, R., Williams, D., Tappa, E., Rio, D. & Raffi I. (1990), Pliocene-Pleistocene stable isotope record for ocean drilling program site 653, Thyrrenian basin: implications for the paleoenvironmental history of the Mediterranean Sea, *Proc. Of the Ocean Drilling Program, Scientific results, 107,* 387-399.

Thunell, R., Rio, D., Sprovieri, R. & Vergnaud-Grazzini, C. (1991), An overview of the post-Messinian paleoenvironmental history of the western Mediterranean, *Paleoceanography, 6,* 143–164.

Tiedemann, R., Sarnthein, M. & Shackleton, N. J. (1994), Astronomic timescale for the Pliocene Atlantic δ18O and dust flux records of Ocean Drilling Program site 659, *Paleoceanography, 9(4),* 619-638.

Tinterri, R. (2007), The Lower Eocene Roda Sandstone (South-Central Pyrenees): an Example of a Flood-Dominated River-Delta System in a Tectonically Controlled Basin. *Rivista Italiana di Paleontologia e Stratigrafia, 113 (2),* 223-255.

Tinterri, R., Muzzi Magalhaes, P. & Tagliaferri, A. (2012), Foredeep turbidites of the Miocene Marnoso-arenacea Formation (Northern Apennines), *Geol. F. Trips., 4(2.1),* 133p.

Tschudin, P.E. (2001), Shell morphology, shell texture and species discrimination of Caribbean *Tucetona* (Bivalvia, Glycymeridae), *Journal of paleontology*, *75 (3),* 658-679.

Ugolini, R. (1906), Monografia dei Pettinidi neogenici della Sardegna, Parte I: Generi *Chlamys*, *Hinnites, Inaequipecten*, *Palaeont. It., 12,* 155-206.

Urey, H.C., Lowenstam, H.A., Epstein, S. & McKinney, C.R. (1951), Measurement of paleotemperatures and temperatures of the upper Cretaceous of England, Denmark and the southeastern United States, *Bull Geol Soc Am, 62,* 399–416.

Van Couvering, J.A. (1997), The Pleistocene boundary and the beginning of the Quaternary. *Cambridge University Press*, 296 pp.

Veizer, J., Ala, D., Azmy, K., Bruckschen, P., Buhl, D., Bruhn, F., Carden, G.A.F., Diener, A., Ebneth, S., Godderis, Y., Jasper, T., Korte, C., Pawellek, F., Podlaha, O.G. & Strauss, H. (1999). $^{87}Sr/^{86}Sr$, $\delta^{13}C$ and $\delta^{18}O$ evolution of Phanerozoic seawater, *Chemical Geology, 161(1),* 59-88.

Venzo, S. (1933-1935), Fossili del Neogene Trentino, Veronese e Bresciano, *Palaeont. It., 34,* 31-84; *35*, 201-255.

Venzo, S. & Pelosio, G. (1963), La malacofauna tortoniana del Colle di Vigoleno (Preappennino piacentino), *Palaeontographia Italica, 58,* 43–213.

Verri, A. (188), Azione delle forze nell'assetto delle Valli con Appendice sulla distribuzione dei fossili nella Valdichiana e nell'Umbria interna settentrionale, *Bollettino della Società Geologica Italiana, 5,* 416–454.

Wahl, M., Jormalainen, V., Eriksson, B.K., Coyer, J.A. & others (2011), Stress ecology in *Fucus*: abiotic, biotic and genetic interactions, *Adv Mar Biol, 59*, 37−105.

Waller, T.R. (1969), The evolution of the *Argopecten gibbus* stock (Mollusca: Bivalvia), with Emphasis on the Tertiary and Quaternary species of Eastern Nord American, *Journal of Paleontology, 43,* 125 pp.

Waller, T.R. (1980), Scanning electron microscopy of shell and mantle in the order Arcoida (Mollusca: Bivalvia), *Smithsonian contributions to zoology, 313*, 1-58.

Waller, T.R. (1984), The ctenolium of scallop shells: functional morphology and evolution of a key family-level character in the Pectinacea (Mollusca: Bivalvia), *Malacologia, 25,* 203–219.

Waller, T.R. (1991), Evolutionary relationships among commercial scallops (Mollusca: Bivalvia: Pectinidae). In: Shumway SE, ed. Scallops - biology, ecology and aquaculture. *Amsterdam: Elsevier Science,* 1–73.

Wanamaker Jr., A.D., Heinemeier, J., Scourse, J.D., Richardson, C.A., Butler, P.G., Eiríksson, J. & Knudsen, K.L. (2008), Very-long lived molluscs confirm 17th century AD tephra-based radiocarbon reservoir ages for north Icelandic shelf waters, *Radiocarbon, 50,* 399–412.

Wanamaker Jr, A.D., Baker, A., Butler, P.G., Richardson, C.A., Scourse, J.D., Ridgway, I. & Reynolds, D.J. (2009), A novel method for imaging internal growth patterns in marine mollusks: A fluorescence case study on the aragonitic shell of the marine bivalve *Arctica islandica* (Linnaeus), *Limnology and Oceanography: Methods, 7,* 673-681.

Wang, P., Tian, J. & Lourens, L. J. (2010), Obscuring of long eccentricity cyclicity in Pleistocene oceanic carbon isotope records, *Earth and Planetary Science Letters, 290,* 3–4, 319-330.

Warnke, D.A., Allen, C.P., Muller, D.W., Hodell, D.A. & Brunner, C.A. (1992), Miocene– Pliocene Antarctic glacial evolution: a synthesis of ice-rafted debris, stable isotopes, and planktonic foraminiferal indicators, ODP Leg114. In: Kennet, J.P., Wranke, A.D. (Eds.), *The Antarctic Paleoenvironment: A Perspective on Global Change. Pt1. Antarctic Research Series, 56,* 311–325.

Wilkinson, B.H. & Ivany, L.C. (2002), Paleoclimatic inference from stable isotope profiles of accretionary biogenic hardparts - a quantitative approach to the evaluation of incomplete data, *Palaeogeography, Palaeoclimatology, Palaeoecology, 185,* 95- 114.

Witbaard, R. (1997) Tree of the sea. The use of internal growth lines in the shell of *Arctica islandica* (Bivalvia, Mollusca) for the retrospective assessment of marine environmental change. PhD thesis Rijksuniversiteit Groningen (157 pp.).

WoRMS (2014), World Register of Marine Species. Available from http://www.marinespecies.org

Zachariasse, W., Gudjonsson, L., Hilgen, F., Langereis, C., Lourens, L., Verhallen, P. & Zijderveld, J. (1990), Late Gauss to early Matuyama invasions of *Neogloboquadrina atlantica* in the Mediterranean and associated record of climatic change, *Paleoceanography, 5,* 239–252.

Zamarreño, I., De Porta, J. & Vazquez, A. (1996), The shell microstructure, mineralogy and isotopic composition of *Amussiopecten baranensis* (Pectinidae, Bivalvia) from the Miocene of Spain: a valuable palaeoenvironmental tool, *GEOBIOS, 29,* 6, 707-724.

Zavala, C., Ponce, J., Drittanti, D., Arcuri, M., Freije, H. & Asensio, M. (2006), Ancient lacustrine hyperpycnites: A depositional model from a case study in the Rayoso Formation (Cretaceous) of west-central Argentina, *Journal of Sedimentary Research, 76*, 41–59.

Zavala, C., Arcuri, M., Di Meglio, M., Gamero Diaz, H. & Contreras, C. (2011), A genetic facies tract for the analysis of sustained hyperpycnal flow deposits, in: Slatt, R.M. & Zavala, C., eds., Sediment transfer from shelf to deep water - Revisiting the delivery system, *AAPG Studies in Geology, 61,* p. 31–51.

Zavatarelli, M., Raicich, F., Bregant, D., Russo, A. & Artegiani, A. (1998), Climatological biogeochemical characteristics of the Adriatic Sea, *Journal of Marine Systems, 18(1),* 227-263.

Zhou, G.T. & Zheng, Y.F. (2003), An experimental study of oxygen isotope fractionation between inorganically precipitated aragonite and water at low temperatures. *Geochimica et Cosmochimica Acta, 67,* 387-399.